STABLE ISOTOPIC EVIDENCE FOR FLUID MIXING IN THE TERTIARY ALKALIC-TYPE EPITHERMAL Au-Te DEPOSIT, CRIPPLE CREEK, CO

by
Amber N. McIntosh

Submitted as partial fulfillment of the
Requirements for the Degree of
Master of Science in Geology
May 15, 2004

Department of Earth and Environmental Science
New Mexico Institute of Mining and Technology
Socorro, NM

ABSTRACT

The Au-Te deposit at Cripple Creek, CO is the largest alkalic-type epithermal deposit of the North American Cordillera and a historical world-class producer of gold. The Tertiary Cripple Creek volcanic-subvolcanic complex intrudes a suite of Precambrian metamorphic and plutonic rocks that comprise the basement lithologies in the region. Intrusions hosting mineralization range in composition from phonolite to lamprophyre and become successively more mafic with time. Lamprophyre emplacement was followed by hydrothermal brecciation, gold mineralization, and intense potassium metasomatism extending several km outside the diatreme. Structurally controlled gold mineralization is manifested by high-grade, epithermal Au-telluride (± quartz ± fluorite ± carbonate ± adularia ± pyrite ± trace barite/celestite and base metal sulfide minerals) veins with halos of K-metasomatism containing disseminated gold, mineralized hydrothermal breccias, and low-grade bulk-tonnage deposits.

Past research has documented consistent characteristics for the mineralizing fluids at Cripple Creek. Mineralization took place at relatively low temperatures (125-225°C) and salinities (< 5 wt. %), and like other alkalic-type deposits, Cripple Creek has heavy $\delta^{18}O$ values (3 - 9‰) for vein minerals and calculated fluid values, which are consistent with a magmatic source for mineralizing fluids. Most studies on the Cripple Creek District to date acknowledge a minor shift in the stable isotope data to lighter $\delta^{18}O$ values during later stages of mineralization, suggesting that mixing with meteoric fluid may

have been a factor; however, convincing data to support the presence of meteoric fluid is lacking.

In an attempt to further explore the role of meteoric fluid, this study presents a stable isotope survey encompassing ore related and barren carbonate (± quartz ± fluorite ± carbonate ± pyrite ± trace barite/celestite and base metal sulfide) veins from the entire district. Measured $\delta^{18}O$ and $\delta^{13}C$ mineral values for carbonates range from –7.4 to 23.0‰ and –8.6 to 5.5‰, respectively. Fluid inclusion temperatures collected from this study (T_H = 108 to 321°C) were applied to published fractionation factors to calculate fluids with $\delta^{18}O_{H2O}$ values of –15.8 to 12.1‰ and $\delta^{13}C_{HCO3-}$ values of –11.8 to 14.4‰, documenting a much broader range of fluid compositions than previous research. $\delta^{34}S_{H2S}$ values from vein pyrites (–14.5 to –1.1‰) and calculated fluids (-15.4 to -0.1‰) fall within a range of values reported in previous studies, and overlap the range of values typically seen in alkalic-type deposits.

New stable isotope and fluid inclusion data from carbonates represent a broader spatial and temporal view of the district than previous research, which has focused on ore-stage mineralization. When this data is examined at a district scale, geochemical and spatial trends emerge, suggesting mixing between magmatic and meteoric fluids. Spatially, the data are divided into broad zones with a central magmatic isotope signature, transitioning into more meteoric signatures towards the margins of the diatreme.

ACKNOWLEDGEMENTS

First and foremost I would like to thank The Cripple Creek and Victor Gold Mining Company and Anglo Gold North America for not only providing me with the funding to carry out this project, but also employing me as a junior mine geologist during two summer seasons at Cripple Creek. The opportunity to work in such an epic mining district doesn't come along every day, and I appreciate all the time I've been able to spend there. The historical aspect of living in an old mining town led to many adventures. A very special thanks to Marc Melker, who was assigned/tortured with the task of training the new summer intern: your patience through all the chip logging, high wall mapping, driving lessons, and spray paint accidents is much appreciated. You taught me most of what I know about the district and your thoughtful discussions through the course of my research have been a great help. I want to thank Eric Jensen, whose undying enthusiasm for all things geologic has always been an inspiration (and on most days, an endless source of entertainment) and kept me going through tough times. EJ inspired me long before I came to Cripple Creek and will no doubt continue to do so. I think the other grad students who followed in his footsteps would agree that when the going gets tough, pretend you're EJ. To all the other geologists: Julie Rosdeutscher, Reyna Abeyta, Alison Mote, Jeff Gaul, Doug and Michelle White, David Vardiman, Tim Brown, Gordon

Siebel, George Papic, Emery Roy, Fleetwood Koutz, Mike Ward, and Larry Pancoast, your knowledge, insight, and friendship made working in Cripple Creek one of the most memorable experiences of my life. I miss working with all of you!

Many people at New Mexico Tech contributed greatly to this project. I would like to thank my academic advisor, Andy Campbell, for his insight, thoughtful discussions, and being so generous with his time in the lab. The other members of my committee, Bill Chavez, Virgil Lueth, and Dave Norman, taught so many interesting classes and took me on as many adventurous ore deposit field trips (long live *The Thing*). If I wasn't an economic geologist already, you guys sure turned me into one! I am very appreciative of all the students that helped me run samples in the stable isotopes lab. Working in that dungeon we call the fluid inclusion lab wouldn't have been as fun without Amanda Rowe.

To my friends and fellow graduate students here at New Mexico Tech that have made Socorro home: Reyna Abeyta, Scott Lynch, Amanda Rowe, Jason Odette, Dylan Canales, Marisa Wolfe, Kathryn Fletcher, Erin Phillips, Joel Bensing, Lynne Kurilovitch, Mike Smith, Zach Hibdon, and Garrett Kramer, thanks for all the adventures.

Rob Sanders, my partner in crime, has been a tremendous help in offering intelligent insights from a non-economic geology point of view. Many late nights spent talking about geology have not been in vain. He also provided me with plenty of demolition-type remodeling projects to take my aggressions out on. Thanks, honey, the

house looks great! And of course I can't forget Bella, who is living proof that *"There are some simple truths and dogs know what they are" - Joseph Duemer*. I can only imagine this refers to a dog's ability to make people laugh, even on the worst days.

Finally I want to thank my parents Dave and Toni McIntosh, and my brother Jacy for *always* believing in me and encouraging me to follow my dreams. You guys instilled the adventurous spirit in me that makes that old adage *"you can be anything you want to be when you grow up"* ring true. I am the first in the family with a college education because you sacrificed so much for me to have that opportunity. I have no words to express my gratitude; I couldn't have done it without you.

TABLE OF CONTENTS

	Page
TITLE PAGE	i
ABSTRACT	
ACKNOWLEDGEMENTS	ii
LIST OF TABLES	4
LIST OF FIGURES	5
LIST OF SYMBOLS	6
LIST OF APPENDICES	8
INTRODUCTION	9
REGIONAL GEOLOGY	11
DISTRICT GEOLOGY: CRIPPLE CREEK DIATREME COMPLEX	17
PREVIOUS WORK AND SCOPE OF PRESENT STUDY	23
METHODS	28
Sample Selection	28
Sample Descriptions	30
RESULTS	35
Fluid Inclusion Microthermometry	35
Stable Isotopes	39
Oxygen and Carbon Isotopes	39
Sulfur Isotopes	39
Calculated Fluid Values	39
X-ray Diffraction Data	47
DISCUSSION	49
Fluid Inclusions	49
Varying Degrees of Fill	49

Depth of Mineralization 50
Transition from Epithermal to Porphyry-Style Mineralization 51
Stable Isotopes 52
Oxygen and Carbon Isotopes 52
Origin of Hydrothermal Calcite 55
Sulfur Isotopes 57
Variation in Isotopes 59

EXPLORATION 63

CONCLUSIONS 71

APPENDIX A: AGE DATING 72

APPENDIX B: PREVIOUS WORK 74
Early Studies 74
Silberman, 1992 75
Wild Horse 75
Portland 76
Cresson 76
Altman (Gold Star Pit) 76
1996 SEG Guidebook: Pontius 79
1996 SEG Guidebook: Beaty et al 79
1996 SEG Guidebook: Thompson 82
The Ajax Mine 82
Hydrothermal Breccias 84
1996 SEG Guidebook: Seibel 85
Thompson, 1998 88
Jensen, 1998 89
Rosdeutscher, 1998 89
Kelley et al, 1998 91
Mote, 2000 94
Jensen and Barton, 2000 95

APPENDIX C: FLUID INCLUSION DATA COMPILED FROM PREVIOUS STUDIES 98

APPENDIX D: STABLE ISOTOPE DATA COPILED FROM PREVIOUS STUDIES 99

APPENDIX E: METHODS 106

Fluid Inclusion Microthermometry 106
Stable Isotopes 106
Oxygen and Carbon Isotopes 107
Sulfur Isotopes 108
X-Ray Diffraction Data 108

APPENDIX F: SALINITIES (EQUIVALENT WEIGHT PERCENT NaCl) CORRESPONDING TO MEASURED FREEZING POINT DEPRESSIONS (DEGREES CELSIUS) 109

APPENDIX G: FLUID INCLUSION PRESENTATION (ON DISC) 110

APPENDIX H: SAMPLE LOCATIONS AND LITHOLOGIC DESCRIPTIONS OF CARBONATE SAMPLES ANALYZED 111

APPENDIX I: SAMPLE LOCATIONS AND LITHOLOGIC DESCRIPTIONS OF SULFIDE SAMPLES ANALYZED 115

APPENDIX J: CALCITE SAMPLE DESCRIPTIONS (ON DISC) 110

APPENDIX K: DOLOMITE SAMPLE DESCRIPTIONS (ON DISC) 110

APPENDIX L: ANKERITE SAMPLE DESCRIPTIONS (ON DISC) 110

APPENDIX M: RHODOCHROSITE SAMPLE DESCRIPTIONS (ON DISC) 110

APPENDIX N: X-RAY DIFFRACTION RESULTS 116

REFERENCES CITED 118

LIST OF TABLES

Table 1: Fluid Inclusion Data 36

Table 2: Stable Isotope Values for Minerals and Calculated Fluid Values 40

LIST OF FIGURES

Figure 1: Geologic Map of the Cripple Creek District and Legend 12

Figure 2: Cross Section Along A-A' 22

Figure 3: Sample Locations 29

Figures 4a-e: Photographs of Calcite Samples 31

Figures 5a-d: Photographs of Dolomite Samples 32

Figures 6a-c: Photographs of Ankerite Samples 33

Figures 7a-d: Photographs of Rhodochrosite Samples 34

Figure 8: Histogram of Fluid Inclusion Homogenization Temperatures 38

Figure 9: Homogenization Temperature vs. Salinity 38

Figure 10: $\delta^{18}O$ vs. $\delta^{13}C$ Mineral Values 43

Figure 11: Histogram of $\delta^{34}S$ Mineral Values 44

Figure 12: $\delta^{18}O$ vs. $\delta^{13}C$ Fluid Values 45

Figure 13: Histogram of Calculated $\delta^{34}S$ Fluid Values 46

Figure 14: Compilation Histogram of $\delta^{34}S$ Mineral Values 58

Figure 15: Sulfur vs. Oxygen Fluid Values 60

Figure 16: Sulfur vs. Depth 61

Figures 17a-b: Diagrams Comparing Hydrothermal Plumbing 64

Figures 18a-c: Maps showing Carbon and Oxygen Mineral and Fluid Values 67

LIST OF SYMBOLS

The following list of symbols is used throughout the thesis to refer to rock types. If a symbol is followed by a "d" it refers to a dike of the same lithology. The list starts with the youngest rocks, T refers to Tertiary and Y or X refers to Precambrian lithologies.

Thbx - Hydrothermal Breccia
Late stage breccia pipes consisting of angular to rounded, heterolithic clasts in a rock flour matrix. Typically associated with pervasive argillic alteration.

Tlh – Hornblende-bearing - Lamprophyre Dike
Dark green to greenish-black, fine-to medium-grained porphyry with hornblende, pyroxene and olivine phenocrysts in an analcime matrix with minor amounts of orthoclase, magnetite, and apatite.

Tlb – Biotite-bearing - Lamprophyre Dike
Dark green, fine-to medium-grained porphyry with biotite phenocrysts in a fine-grained groundmass consisting of analcime, alkali feldspar, biotite, hornblende and minor magnetite.

Tlbx - Lamprophyre Breccia
Late-stage lamprophyric breccia pipe consisting of both matrix and clast supported heterolithic breccia with abundant dark-green lamprophyre clasts and variable late carbonate alteration.

Ttd – Phonotephrite
Dark gray, fine-grained to porphyritic dikes and sills with variable trachytic texture. Groundmass composed of fine-grained plagioclase, orthoclase, analcime, pyroxene, and olivine as well as minor hornblende and magnetite.

Tsy – Tephriphonolite
Gray, medium-to fine-grained intrusive composed of orthoclase, plagioclase, pyroxene and minor hornblende and analcime, commonly occurring as small- to medium-sized stocks.

Tph - Phonolite
Gray, brown, or pink, aphanitic phonolite composed of fine-grained orthoclase,

nepheline, minor aegerine-augite, and analcime.

Tphk – Feldspar-bearing Plagioclase Phonolite
Light to medium gray porphyry with subhedral to euhedral, medium-to coarse-grained phenocrysts of alkali feldspar with minor amounts of feldspathoids, glassy apatite and pyroxenes.

Tphh - Hornblende\Pyroxene-bearing Plagioclase Phonolite
Gray, medium-grained porphyry with euhedral to subhedral hornblende, aegerine-augite, and alkali feldspar phenocrysts.

Tphb – Biotite-bearing Plagioclase Phonolite
Gray, fine-grained porphyry with euhedral biotite and alkali feldspar phenocrysts.

Tbx1L - Cripple Creek Lapilli Breccia
Generally massive, structureless, matrix supported breccia that is poorly sorted, typical of diatremal crater fill breccia. Clasts are sub-angular to sub-rounded and primarily composed of various phonolite units with occasional Precambrian fragments. Commonly shows varying degrees of hydrothermal alteration.

Tbx2 - Cripple Creek Breccia-Bedded
Variably stratified volcaniclastic breccia with matrix and clast compositions much the same as Tbx1L. Locally occurs in thinly bedded base surge deposits.

Ypp - Pikes Peak Granite
Massive, pink to reddish tan, medium-to coarse-grained, biotite-hornblende-microcline granite.

Ycc - Cripple Creek Quartz Monzonite
Massive, pink, medium-grained, biotite-muscovite-quartz monzonite.

Xgd - Granodiorite
Massive to foliated, medium-to coarse-grained, hornblende-biotite granodiorite. Locally occurs as augen gneiss. Includes diabase dikes and schistose lenses.

Xgnb - Biotite Gneiss
Strongly foliated, biotite-quartz-plagioclase gneiss to schist, which is locally migmatitic.

LIST OF APPENDICES

APPENDIX A: AGE DATING 72

APPENDIX B: PREVIOUS WORK 74

APPENDIX C: FLUID INCLUSION DATA COMPILED FROM PREVIOUS STUDIES 98

APPENDIX D: STABLE ISOTOPE DATA COPILED FROM PREVIOUS STUDIES 99

APPENDIX E: METHODS 106

APPENDIX F: SALINITIES (EQUIVALENT WEIGHT PERCENT NaCl) CORRESPONDING TO MEASURED FREEZING POINT DEPRESSIONS (DEGREES CELSIUS) 109

APPENDIX G: FLUID INCLUSION PRESENTATION (ON DISC) 110

APPENDIX H: SAMPLE LOCATIONS AND LITHOLOGIC DESCRIPTIONS OF CARBONATE SAMPLES ANALYZED 111

APPENDIX I: SAMPLE LOCATIONS AND LITHOLOGIC DESCRIPTIONS OF SULFIDE SAMPLES ANALYZED 115

APPENDIX J: CALCITE SAMPLE DESCRIPTIONS (ON DISC) 110

APPENDIX K: DOLOMITE SAMPLE DESCRIPTIONS (ON DISC) 110

APPENDIX L: ANKERITE SAMPLE DESCRIPTIONS (ON DISC) 110

APPENDIX M: RHODOCHROSITE SAMPLE DESCRIPTIONS (ON DISC) 110

APPENDIX N: X-RAY DIFFRACTION RESULTS 116

This Thesis is accepted on behalf of the faculty
of the Institute by the following committee:

Andrew Campbell

Academic Adviser

Andrew Campbell

Research Advisor

David L. Noon

Committee Member

Committee Member

Virgil W.

Committee Member

5-5-2004

Date

I release this document to New Mexico Institute of Mining and Technology

Vincent McIntosh 5-5-2004

Students Signature Date

INTRODUCTION

The Au-Te deposit at Cripple Creek, CO is the largest alkalic-type epithermal deposit of the North American Cordillera and a historical world-class producer of gold. Numerous stable isotope and fluid inclusion studies have been conducted in the district in an effort to understand the hydrothermal system responsible for producing such a rich deposit. Fluid characteristics used to infer fluid sources and processes responsible for precipitating gold are popular topics of investigation.

Past research has documented consistent characteristics for the mineralizing fluids at Cripple Creek. Mineralization took place at relatively low temperatures (125-225°C) and salinities (< 5 wt. %), and like other alkalic-type deposits, Cripple Creek has heavy $\delta^{18}O$ values (3 - 9‰) for vein minerals and calculated fluid values, which is consistent with a magmatic source for mineralizing fluids (Jensen, 2003). This is an unusual characteristic relative to other, "classic" epithermal deposits that are dominated by meteoric fluids (O'Neil et al, 1973; O'Neil and Silberman, 1974; Taylor, 1973, 1974b; Bethke and Rye, 1979; Casedevall and Ohmoto, 1977; Criss and Taylor, 1983). However, Cripple Creek is still considered an epithermal system on the basis of low temperature (<300°C), shallow (<1-2 km) mineralization (Jensen and Barton, 2000). Because the term "alkalic" implies a genetic relationship between alkalic-type epithermal gold deposits and alkalic magmatism (Richards, 1995), a transition into Cu-Au porphyry-style mineralization that occurs at higher temperatures (>300°C) and greater depths (>1km) may be a more accurate model for Cripple Creek (Jensen and Barton, 2000). Although the intrusive phase directly responsible for mineralization has yet to be identified, evidence to suggest this transition is seen in high temperature mineralization and

alteration, such as biotite-stable alteration assemblages, overprinted by lower temperature, epithermal-style mineralization (Jensen and Barton, 2000). Zones of hydrothermal biotite alteration in Cripple Creek are restricted to the deepest levels of the Ajax and Portland mines in the southern part of the diatreme, but in the northern part, zones of biotite alteration are seen at much higher levels in the vicinity of the Mollie Kathleen mine, Moffat Tunnel, and Globe and Ironclad Hills (Jensen, 2003; see Figure 2). The presence of high temperature biotite alteration seems to fit with the high volume of magmatic fluids documented in this system, suggesting that Cripple Creek may be nearing the transition between epithermal and porphyry-style mineralization.

Most studies on the Cripple Creek District to date acknowledge a minor shift in the stable isotope data to lighter $\delta^{18}O$ values during later stages of mineralization, suggesting that mixing with meteoric fluid may have been a factor; however, convincing data to support the presence of meteoric fluid is lacking.

In an attempt to further explore the role of meteoric fluid, this study presents a stable isotope survey encompassing ore-stage and barren carbonate (± quartz ± fluorite ± carbonate ± pyrite ± trace barite/celestite and base metal sulfide) veins from the entire district. O and C isotopes from carbonates, and S isotopes from sulfides are utilized in conjunction with fluid inclusion data to identify fluid sources and address fluid evolution, patterns of fluid flow, and examine the spatial scale of mixing zones between different end member fluids. Ultimately this data is used to assess the viability of applying a simplistic epithermal model for hydrothermal circulation to the Cripple Creek District in an exploration context.

REGIONAL GEOLOGY

The Tertiary Cripple Creek volcanic-subvolcanic complex in central Colorado intrudes a suite of Precambrian metamorphic and plutonic rocks that comprise the basement lithologies in the region (Figure 1). The oldest rocks in the Cripple Creek district are the biotite-muscovite schists and gneisses of the Idaho Springs Formation (Xgnb), that record the accretion of juvenile island arc terranes to the southern margin of the Archean Wyoming craton beginning around 1.8 Ga (Reed et al, 1987). The 1.7 Ga granodiorite (Xgd) present in the Cripple Creek district belongs to a group of late orogenic plutons that intruded the supracrustal rocks of 1.8 Ga (Selverstone et al, 1997). During and subsequent to accretion, northeast trending shear zones and petrotectonic provinces (Yavapai and Mazatzal) were established, and are interpreted to have repeatedly influenced younger tectonism and magmatism (Selverstone et al, 1997; Karlstrom and Humphreys, 1998). Similarly, Tweto and Sims (1963) suggested that north-northeast and north-northwest trending shear zones and faults were also established during the Precambrian. The prominent structural trends that acted as conduits for magmatism and mineralization within the Cripple Creek district coincide with regional trends established in the Precambrian.

A regional thermal and metamorphic event at ca. 1.4 Ga resulted in widespread plutonism in North America. In Colorado, granitic plutons were emplaced along northeast trending shear zones, and include the Cripple Creek Quartz Monzonite (Ycc) and Silver Plume magmatic suite (Selverstone et al, 1997; Karlstrom and Humphreys, 1998). The southwestern U.S. experienced extensional tectonism and magmatism (ca. 1.1 Ga) related to far field stress generated by Grenville collision to the southeast

Figure 1: Generalized Geologic Map of the Cripple Creek District (Legend, next 2 pages)

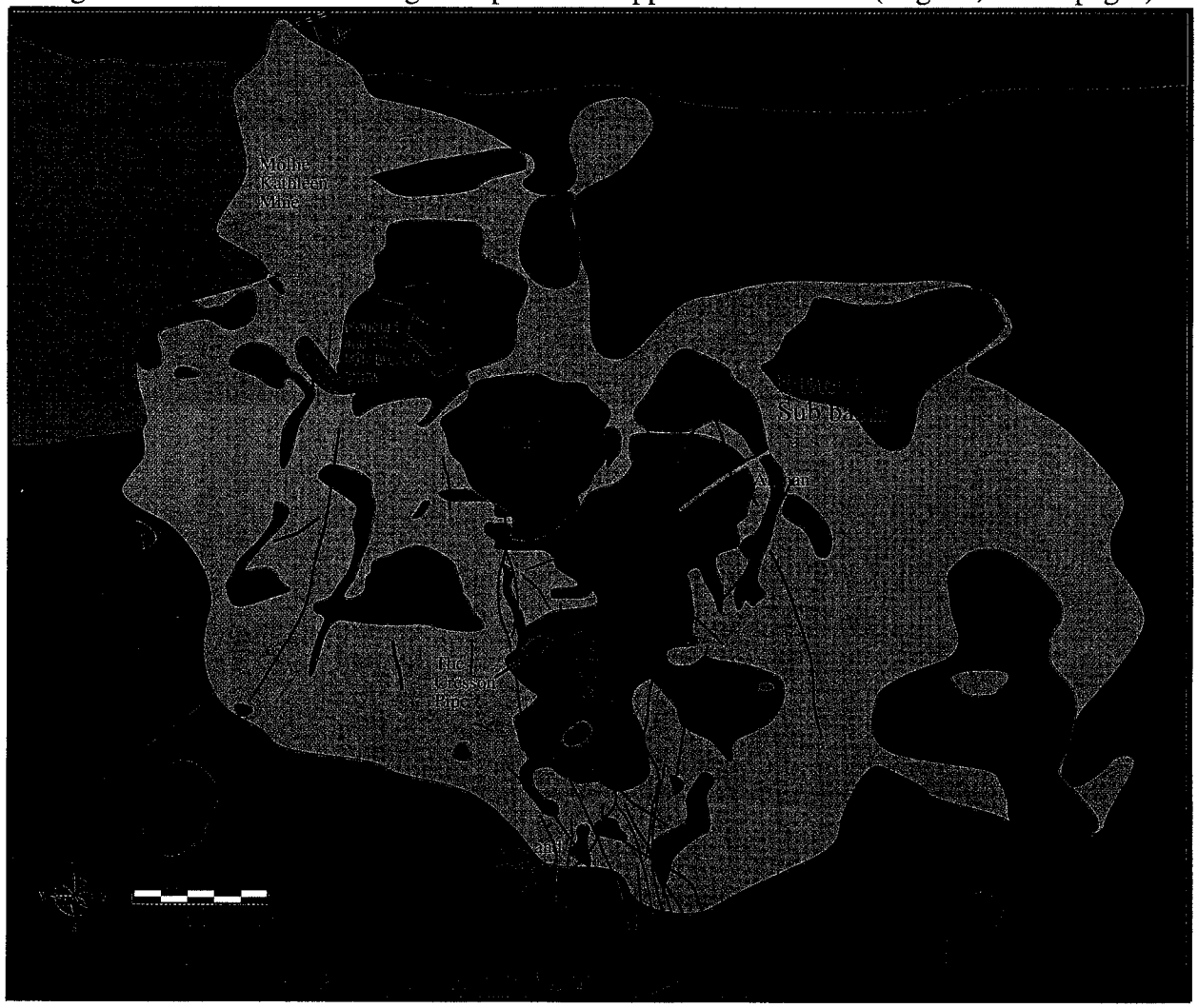

Figure 1: Map Legend of Symbols for Geologic Units

Thbx - Hydrothermal Breccia: Late stage breccia pipes consisting of angular to rounded, heterolithic clasts in a rock flour matrix. Typically associated with pervasive argillic alteration.

Tlh - Hornblende-bearing Lamprophyre Dike: Dark green to greenish-black, fine- to medium-grained porphyry with hornblende, pyroxene, and olivine phenocrysts in an analcime matrix with minor amounts of orthoclase, magnetite, and apatite.

Tlb - Biotite-bearing Lamprophyre Dike: Dark green, fine- to medium-grained porphyry with biotite phenocrysts in a fine-grained groundmass consisting of analcime, alkali feldspar, biotite, hornblende, and minor magnetite.

Tlbx - Lamprophyre Breccia: Late-stage lamprophyric breccia pipe consisting of both matrix and clast supported heterolithic breccia with abundant dark-green lamprophyre clasts and variable late carbonate alteration.

Ttd – Phonotephrite: Dark gray, fine-grained to porphyritic dikes and sills with variable trachytic texture. Groundmass composed of fine-grained plagioclase, orthoclase, analcime, pyroxene, and olivine as well as minor hornblende and magnetite.

Tsy – Tephriphonolite: Gray, medium-to fine-grained intrusive composed of orthoclase, plagioclase, pyroxene, and minor hornblende and analcime, commonly occurring as small- to medium-sized stocks.

Tph – Phonolite: Gray, brown, or pink, aphanitic phonolite composed of fine-grained orthoclase, nepheline, minor aegerine-augite, and analcime.

Tphk - Feldspar-bearing Plagioclase Phonolite: Light- to medium-gray, porphyry with subhedral to euhedral, medium- to coarse-grained phenocrysts of alkali feldspar with minor amounts of feldspathoids, glassy apatite, and pyroxenes.

Tphh - Hornblende\Pyroxene-bearing Plagioclase Phonolite: Gray, medium-grained porphyry with euhedral to subhedral hornblende, aegerine-augite, and alkali feldspar phenocrysts.

Tphb - Biotite-bearing Plagioclase Phonolite: Gray, fine-grained porphyry with euhedral biotite and alkali feldspar phenocrysts.

Figure 1: Map Legend of Symbols for Geologic Units

Tbx1L - Cripple Creek Lapilli Breccia: Generally massive, structureless, matrix supported breccia that is poorly sorted, typical of diatremal crater fill breccia. Clasts are sub-angular to sub-rounded and primarily composed of various phonolite units with occasional Precambrian fragments. Commonly shows varying degrees of hydrothermal alteration.

Tbx2 - Bedded Cripple Creek Breccia: Variably stratified volcaniclastic breccia with matrix and clast compositions much the same as Tbx1L. Locally occurs in thinly bedded base surge deposits.

Ypp - Pikes Peak Granite: Massive, pink to reddish tan, medium- to coarse-grained, biotite-hornblende-microcline granite.

Ycc - Cripple Creek Quartz Monzonite: Massive, pink, medium-grained, biotite-muscovite-quartz monzonite.

Xgd – Granodiorite: Massive to foliated, medium- to coarse-grained, hornblende- biotite granodiorite. Locally occurs as augen gneiss. Includes diabase dikes and schistose lenses.

Xgnb - Biotite Gneiss: Strongly foliated, biotite-quartz-plagioclase gneiss to schist, which is locally migmatitic.

(Karlstrom et al, 1999). At this time in central Colorado, a suite of plutonic rocks including the Pikes Peak Granite (Ypp) (1.04 to 1.08 Ga; Hedge, 1970; Unruh, unpublished data) were emplaced, and were accompanied by silicic volcanism (Sanders and Hawkins, 1999).

The oldest sedimentary rocks in contact with the Precambrian basement in the Pikes Peak region are Cambrian in age. The missing period of time in the sedimentary record has been termed the Great Unconformity (Powell, 1876) and is interpreted as a long-lived plateau across much of the western U.S. sometimes referred to as the trans-continental arch (Lochman-Balk, 1972). Sedimentation associated with low-energy fluvial and marine environments dominated Cambrian through Mississippian time. The sudden occurrence of Pennsylvanian-Permian coarse arkosic and conglomeratic sediments in the sedimentary record mark the onset of Ancestral Rocky Mountain tectonism in the western U.S. North-south trending uplifts and adjacent basins developed in response to the Ouachita-Marathon orogeny (Kluth and Coney, 1981) or a subduction zone off the southwest margin of the craton (Ye et al, 1996), and are interpreted to have reactivated existing faults established during the Precambrian (Kluth and Coney, 1981; Karlstrom and Humphreys, 1998; Timmons, 2001).

Following Ancestral Rocky Mountain deformation, the region remained near sea level as evidenced by marine regressions and transgressions recorded in the sedimentary sequence until the Laramide orogeny began in the late Cretaceous (Karlstrom and Humphreys, 1998). Laramide tectonism (75-45 Ma) involved crustal thickening and uplift (~1-2 km), and coeval magmatism (Tweto and Sims, 1963) along the north and northeast trending structures the Ancestral Rocky Mountains had exploited (Karlstrom

and Humphreys, 1998). Ore deposits associated with Laramide-age intrusions; define the Colorado Mineral Belt, a 400 km northeast-southwest trending zone in Colorado (Tweto and Sims, 1963). Cripple Creek is approximately 90 km east of the structural trend of the Colorado Mineral Belt.

From 55-37 Ma the Rockies experienced erosion and uplift resulting in an Eocene erosion surface approximately 6 km above sea level and still predominant today, although locally modified by Tertiary and younger volcanism (Karlstrom and Humphreys, 1998). Sometime between 40 and 32 Ma there was a transition between the compressional regime of active subduction (70-40 Ma) and the extension (beginning 32 Ma) causing the development of the Rio Grande rift (Kelley et al, 1998).

Between 40 and 35 Ma renewed volcanism formed the San Juan and Thirtynine Mile volcanic fields (Kelley et al, 1998). Volcanic tuffs and volcaniclastic sediments are present as clasts within the Cripple Creek breccia, and may have been initially deposited as early as 35 Ma providing an upper time constraint on Cripple Creek volcanism (Kelley et al, 1998). The Florissant Lakebeds, 15 km to the northwest, were deposited in a shallow valley on the Eocene erosion surface from 35 to 34 Ma (Chapin and Cather, 1994). Early Tertiary (32-27 Ma; Kelley et al, 1998) extension initiated the Rio Grande rift along north and northwest trending structures. Igneous activity in the Cripple Creek district (31.8-28.4 Ma; Jensen, 2003) occurred coincident with similar alkalic magmatism that parallels the Rio Grande rift from northern Colorado to Coahuila, Mexico (Jensen and Barton, 2000).

DISTRICT GEOLOGY: CRIPPLE CREEK DIATREME COMPLEX

The Cripple Creek diatreme complex covers approximately 18 square kilometers and forms a basin elongated along its NW-SE axis (Kelley et al, 1998). The orientation of the diatreme suggests its emplacement was controlled by preexisting northwest trending structures (Koschmann, 1949) that have been sporadically reactivated since their establishment in the Proterozoic.

The oldest and most common rock type in contact with the Precambrian basement in the diatreme is the Cripple Creek breccia. It is a heterolithic, matrix-supported breccia (Tbx1L) that also occurs as fine-grained, stratified volcaniclastic and lacustrine sediments (Tbx2) and massive basin fill. The breccia is composed of angular to subangular clasts of Precambrian metamorphic and igneous rocks, and Tertiary volcanic and sedimentary rocks in a matrix of quartz, microcline and rock fragments (0.5 to 2.0 mm in diameter; Thompson et al, 1985), and later dolomite and pyrite precipitated from circulating hydrothermal fluids (Lovering and Goddard, 1950). Near the margins of the diatreme Precambrian clasts become more prevalent as the breccia often grades into highly fractured Precambrian rock (Loughlin and Koschmann, 1935).

Carbonized tree trunks and plant matter can be found in the breccia to depths as great as 300 m (Lindgren and Ransome, 1906), and blocks of water lain sediments to depths of 1020 m (Koschmann, 1949). This suggests that the 1000 m (Thompson et al, 1985) of breccia accumulated as the basin subsided slowly and intermittently during its volcanic phase along steeply-dipping normal faults (average 65° to 80°) as evidenced by fault breccia, gouge and slickensides commonly found along the contact between the Cripple Creek breccia and the Precambrian rocks (Koschmann, 1949). Subsidence

culminated before the intrusion of alkaline igneous rocks, but repeated movements related to settling produced shear zones in the Cripple Creek breccia and adjacent Precambrian rocks that were subsequently exploited by the intrusions and later ore fluids (Koschmann, 1949).

The diatreme is divided into three sub basins defined by the presence of Precambrian ridges beneath the Cripple Creek breccia (Koschmann, 1949), two of which are presently exposed due to erosion (Granite Island and Schist Island). In the Eastern sub basin the Cripple Creek breccia is underlain by 200 feet of arkose and 400 feet of conglomerate, and is commonly interbedded with lacustrine deposits. The lacustrine deposits occur as thinly bedded sediments that occasionally have ripple marks, mud cracks, worm burrows, bird footprints, fossil leaves, and rain drop impressions (Koschmann, 1949; Thompson et al, 1985).

Following diatreme emplacement the Cripple Creek breccia was intruded by alkaline dikes, sills, and small stocks that became successively more mafic with time (Jensen and Barton, 2000). Alkaline intrusions and flows occur up to 15 km outside the diatreme where they cut or overlie Precambrian rocks, the Oligocene Tallahassee Creek Conglomerate, and Wall Mountain Tuff (Kelley et al, 1998). The maximum range over which emplacement of alkaline rocks occurred is 35.1 to 28.6 Ma (Kelley et al, 1998). Because pervasive hydrothermal alteration overprints the majority of the rocks within the district, the accuracy of age dates is problematic. Data reported here are after Jensen (2003; See Appendix A for further discussion of age dating).

The earliest intrusive phases are phonolites dated at ~31.8 Ma (Jensen, 2003). Tephriphonolite (Tsy) and phonotephrite (Ttd) were emplaced syn- to post-phonolite

time, and a second phase of phonolite emplacement occurred outside the complex at 30.9 Ma (Kelley et al, 1998). Lamprophyres (Tlbx, Tlb, Tlh) have been identified as the youngest intrusive stage on the basis of age dates (28.4 Ma; Jensen, 2003) and crosscutting relationships. Hydrothermal breccias (Thbx) formed later (Pontius, 1996) and contain clasts of all rock types present in the district.

Paragenesis has been carefully documented in several places in the district; however linking paragenetic stages between each locality is difficult, if not impossible. Below are paragenetic summaries for a few localities (discussed in greater detail, Appendix B).

Seibel (1991) and Thompson (1996) present a generalized paragenesis for hydrothermal breccia hosted mineralization at Ironclad and Globe Hill:

- *Stage 1:* adularia + quartz + apatite + pyrite/marcasite + fluorite + hematite
- *Stage 2:* celestite + sericite + dolomite + barite + galena + sphalerite + chalcopyrite + fluorite + pyrite + quartz + rutile
- *Stage 3:* Au-tellurides + pyrite + dolomite + quartz + sericite + native gold + Fe-Mn oxides

Dwelley (1984) and Thompson et al (1985) have documented the following paragenesis for veins of the Ajax Mine (minerals in parentheses reported by Thompson et al, 1985):

- *Stage 1:* adularia + quartz + fluorite + dolomite + pyrite + marcasite
- *Stage 2:* pyrite + marcasite + galena + sphalerite + chalcopyrite (+ quartz + pyrrhotite)

- *Stage 3:* sphalerite + quartz + fluorite + pyrite + rutile (+ hematite + sphalerite)
- *Stage 4:* quartz + pyrite + tellurides (+ rutile + acanthite)
- *Stage 5:* vug filling quartz + chalcedony + fluorite + dolomite

Jensen (2003) reviews paragenetic sequences presented in previous studies (also discussed in Appendix B), and points out ambiguities that can be problematic when trying to fit the data to a relative time scale. The term halo is used to refer to spatial zones *within* a vein. A very generalized paragenesis for veins is as follows (after Jensen, 2003):

- *Vein Margin (early):* ankerite + adularia + barite - celestite
- *Outer Halo:* quartz + fluorite + pyrite + tellurides ± barite - celestite + trace (sphalerite + galena + tetrahedrite)
- *Inner Halo:* quartz + fluorite + barite – celestite + carbonate (usually calcite) + pyrite + tellurides
- *Centerline (late):* chalcedony + calcite

It is important to note that most veins rarely show all stages of mineralization, and rarely are all phases present in each stage. No single mineral phase serves as an accurate indicator of mineralization. Tellurides are commonly accompanied by only a few gangue minerals, and they have been found in nearly all "stages" of mineralization, making it difficult to put Au-Te mineralization relative to barren carbonate + pyrite veins. Barren veins often are only distinguished from Au-Te veins on the basis of visible telluride minerals.

Gold mineralization is manifested by high-grade, epithermal Au-telluride (± quartz ± fluorite ± carbonate ± adularia ± pyrite ± trace barite/celestite and base metal

sulfide minerals) veins with halos of K-metasomatism containing disseminated gold, mineralized hydrothermal breccias, and low-grade bulk-tonnage deposits. Mineralization, which crosscuts all units in the district, is structurally controlled, with most veins exploiting northeast or northwest trending faults, fractures, shear zones, and lithologic contacts. Fluids were channeled along local structures from multiple source area breccia pipes (Figure 2). The most intense mineralization and hydrothermal alteration are observed at structural intersections, which likely saw a higher volume of fluid flow.

Figure 2: Schematic NNE-SSW Cross Section. See Figure 1 for Legend and A-A' Transect.

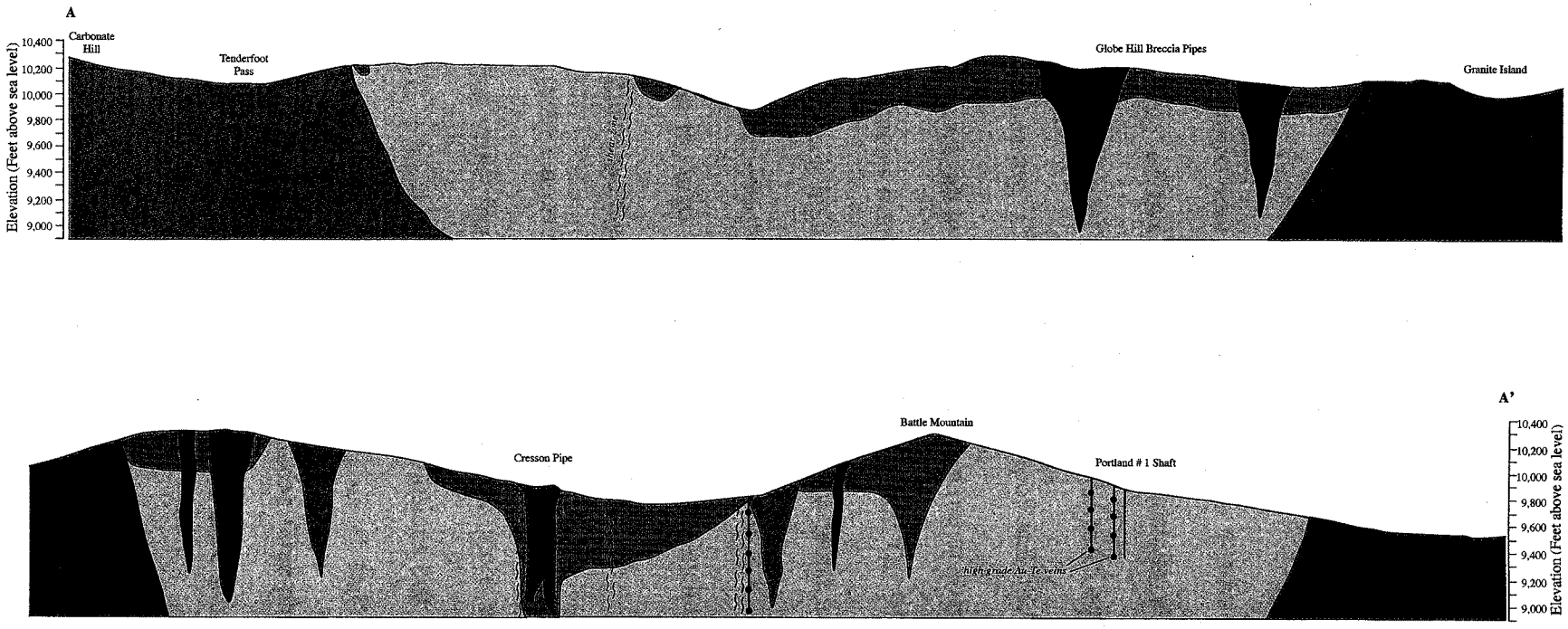

PREVIOUS WORK AND SCOPE OF PRESENT STUDY

Fluid inclusion and stable isotope data collected by previous researchers provide a framework in which to interpret data collected for the present study. Compilations of fluid inclusion and stable isotope data are presented in Appendices C and D, and are briefly summarized below.

Mote (2000) identified four types of inclusions in quartz-carbonate-sulfate-K-feldspar veins. A group of two-phase (L + V) inclusions with homogenization temperatures between 190° to 320°C, and salinities from 0.1 to 25 eq. wt. % NaCl are the most common. Halite-bearing, CO_2-bearing, and vapor-rich inclusions with higher homogenization temperatures (up to 640°C) and salinities (up to 40 eq. wt. % NaCl) were also observed in a few samples from certain intervals of the UGC 97-5 hole, however no evidence for high temperature, high salinity inclusions was found in UGC 97-5 samples in the present study, only two-phase inclusions were observed. It is important to note that Jensen (2003) states that the high temperature, high salinity inclusions are likely from Precambrian clasts within veins; this is further discussed below.

Rosdeutscher (1998) documented two groups of quartz inclusions in quartz-adularia-pyrite-kaolinite veins from Grassy Valley. The more abundant first group consists of two-phase (L + V), liquid-rich (~90% L) inclusions that homogenize between 228° and 432°C and have salinities from 3.3 to 6.6 eq. wt. % NaCl. The less abundant group 2 was observed in only two samples and contains three-phase (L + V + NaCl) inclusions that homogenize between 407° and 467°C and have salinities ≥ 26 eq. wt. % NaCl.

Thompson (1998, 1996, 1986, 1985) reports fluid inclusion data collected in a

number of different studies by his students (Burnett, 1995; Dwelley, 1994; Seibel, 1991; Nelson, 1989; Collins, 1979; and Lane, 1976). T_H and salinity ranges measured on veins of the Ajax mine are 200-510°C and 28-48 eq. wt. % NaCl for stage 1 quartz veins; 105-159°C and 7-9 eq. wt. % NaCl for stage 4 quartz; and <150°C and 1.4 - 3.5 for mineralized samples. Fluid inclusions from Globe Hill homogenized between 371 and 425°C for stage 1 quartz; and 198 and 211°C for stage 2 quartz, but salinities were not reported. Beaty et al (1996) measured fluid inclusions from quartz-Au telluride-fluorite veins in the vicinity of the Pharmacist vein system in the Altman area. Inclusions homogenized from 177 to 257°C, but no salinity data was obtained. Silberman (1992) documented fluids of 165-200°C and 4-6 eq. wt. % NaCl from quartz-telluride-fluorite veins in the Cresson diatreme.

The most recent study is Jensen's (2003) PhD dissertation. His thorough review and reevaluation of past studies, together with a wide spectrum of new data provide a very detailed account of the complex evolution of the Cripple Creek hydrothermal system. Generally, fluid inclusions in Tertiary veins are simple two phase, liquid + vapor inclusions, whereas Precambrian rocks contain high temperature inclusions with multiple daughter minerals. The presence of CO_2 is confined to Precambrian inclusions.

Jensen's (2003) oxygen isotope data from ore-stage veins show $\delta^{18}O$ fluid values that overlap magmatic fluid composition. Kelley et al (1998) used K-feldspar and biotite to calculate the composition of mineralizing fluids at the Ocean Wave mine. Fluid $\delta^{18}O$ values (2.4 and 4.2‰) approach the range for magmatic water, but they do not address what caused a shift toward lighter values.

Rosdeutscher's (1998) calculated δ18O and δD fluid values range from 3.5 to

8.7‰ and –84 to –38‰ from illite; and 7.8 to 10.3‰ and –88 to –62‰ from kaolinite. Calculated $\delta^{18}O$ fluid values for quartz are 12.2 to 15.4‰. The O and H isotopic values from illite and quartz suggest a magmatic origin for hydrothermal fluids.

Beaty et al (1996) studied stable isotopes of the Pharmacist vein system in the Altman area. The authors propose a model with altered phonolites adjacent to the vein having the lowest $\delta^{18}O$ values (7.1 to 14.3‰), "silicified rock from the upper levels of the hydrothermal system" (reported in their table 2 as quartz values) having intermediate values (~18‰), and the late stage vug quartz having the highest values (21 to 24‰) representing cooling of the ore fluid causing increased fractionation over time. These results are consistent with the Altman rocks being flooded with a large volume of $\delta^{18}O$-enriched ore fluid that mixed only locally at the margins of the deposit with $\delta^{18}O$-depleted meteoric water. Silberman (1992) examined stable isotope data from quartz ± telluride ± pyrite ± K-feldspar veins in Grassy Valley, Wild Horse, Portland, Altman, and Cresson. Silberman proposes a system in which magmatic waters ($\delta^{18}O$-enriched) move upward and mix with meteoric waters ($\delta^{18}O$-depleted) based on the fact that the data are not more consistent. If this was simply a cooling magmatic system, calculated fluid values for vein minerals should fall within a more restricted range. Mixing with meteoric water is suggested to cause the variation, and may be an important factor in triggering gold precipitation.

Numerous fluid inclusion and stable isotope studies have been conducted within the Cripple Creek District to date. In addition to the studies briefly summarized above, all are discussed in detail in Appendix B. The general consensus is that mineralization

took place at relatively low temperatures (125-225°C), and the mineralizing fluid had low salinity (< 5 wt. %) and heavy $\delta^{18}O$ values (3 - 9‰) consistent with a magmatically derived fluid (Jensen, 2003). Most studies acknowledge that there is enough variation in the data to suggest that mixing with meteoric water occurred at some point in the evolution of the hydrothermal system, however, convincing data to support this hypothesis is lacking.

Sulfur isotope data from ore-stage veins reported by Jensen (2003) shows the following: pyrite $\delta^{34}S_{mineral}$ values fall between –20 and 2‰, base metal sulfides (galena and sphalerite) are between –14 and -10‰, later paragenetic stages (stibnite and cinnabar) often have lighter $\delta^{34}S$ values than earlier pyrites, and sulfide from local sediments falls between –4 and -2‰. Sulfur isotope values throughout the district are quite variable, except along the western margin of the diatreme where sulfides have heavy $\delta^{34}S$ values. Rosdeutscher (1998) studied quartz-adularia-pyrite-kaolinite veins hosted largely in Proterozoic granodiorite to constrain an origin for the mineralizing fluid responsible for depositing the disseminated gold in the Grassy Valley area of the district. $\delta^{34}S$ values for 23 vein pyrites range from –10.4 to –3.9‰ with a mean of –5.3‰. These values fall within the same range reported by Jensen (2003). Thompson (1996) reports sulfur isotope data from galenas in the district are very light ($\delta^{34}S$ = -6.8 to –21.1‰) and in general show lightest values at shallower depths.

This study presents new stable isotope and fluid inclusion data from carbonates that represent a broader spatial and temporal view of the district than previous research, which has focused on ore-stage mineralization. When this data is examined at a district scale, a geochemical trend emerges, suggesting mixing between magmatic and exchanged

meteoric fluids. When examined spatially, the same data show a broad zone of magmatic values in the southern portion of the district, with lighter values away from the central magmatic zone. Difficulty in refining these zones may be due to the complexity of structural features within the district as well as multiple source areas for magmatic fluids. The lack of a clearly defined paragenetic sequence further complicates interpretation of this new data.

METHODS

Sample Selection

Intervals of drill core likely to have visible carbonate veins were identified based on whole rock C analyses obtained during assay. Favorable intervals were examined and sampled. The 77 carbonate veins chosen for analysis are generally massive and have a simple vein paragenesis: carbonates are dominant, with only minor amounts of pyrite and quartz being present, and if any, just trace amounts of fluorite, barite, and base metal sulfides. 22 samples of sedimentary dolomite found to react with hydrochloric acid were sampled from the Koschmann collection to investigate whether or not a "sedimentary" carbonate signature is a possible source for carbon. 3 samples of calcite replacing phenocryst sites in either volcaniclastic rocks or altered phonolites were sampled because they were found to react with hydrochloric acid. 4 fracture surfaces with calcite mineralization were also sampled. All samples were crushed, sieved, hand separated, and ground to a fine powder to obtain the cleanest samples possible for analysis.

Fluid inclusion microthermometry was conducted on carbonate veins to obtain temperature data for use in calculating stable isotopic values of the mineralizing fluids. 106 carbonate samples (Figure 3) taken from drill core, the Koschmann collection, and surface outcrop, as discussed above, were prepared and analyzed for O and C isotopes; sulfide mineral separates of pyrite, galena, and sphalerite from the same carbonate veins were analyzed for S isotopes.

The same powdered samples used for stable isotope analysis were used for X-ray Diffraction analysis of representative samples to confirm mineralogy. All methods are further described in Appendix E.

Figure 3: Sample Locations Plotted on Generalized Geologic Map, See Figure 1 for Legend

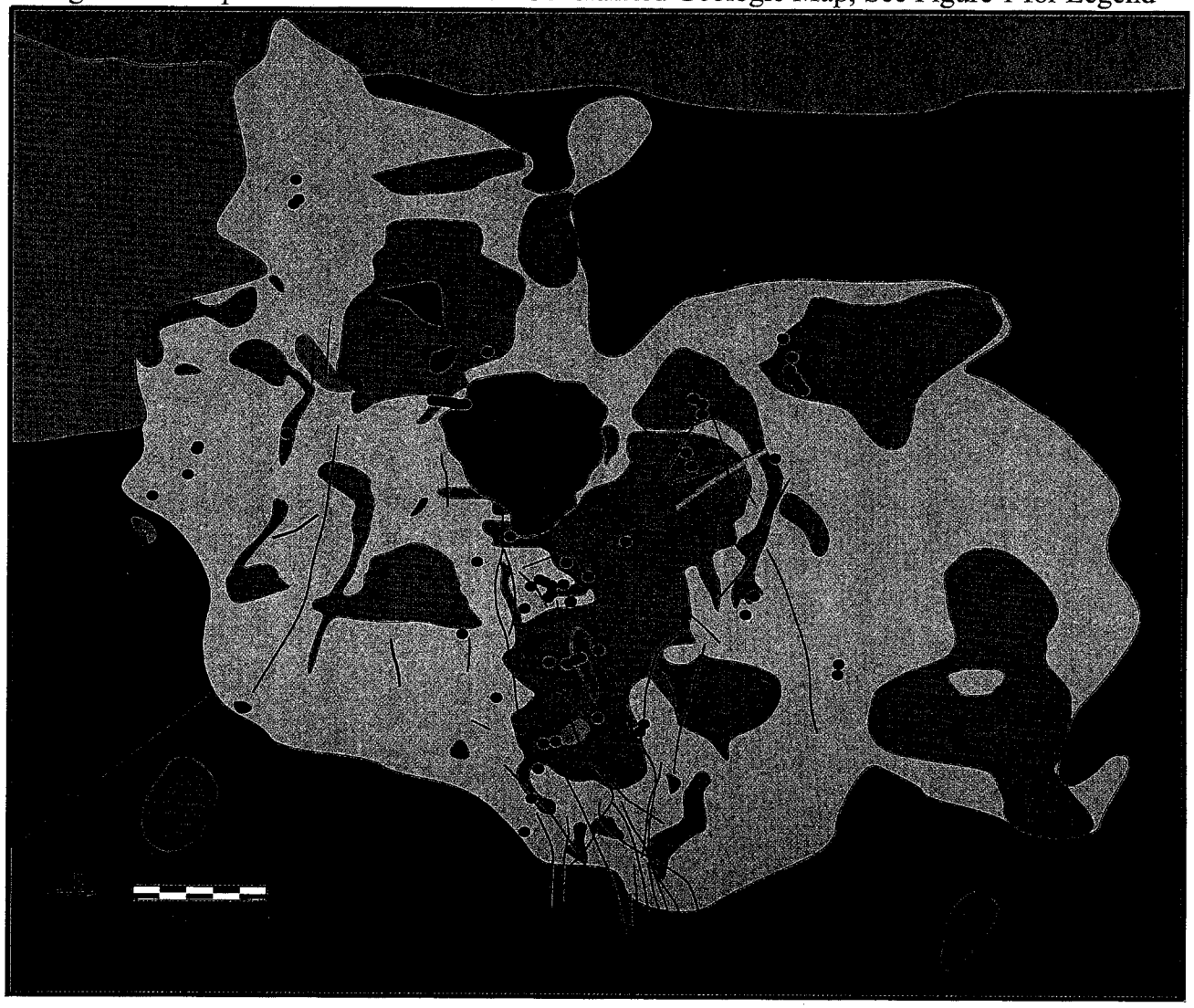

Sample Descriptions

Carbonates are divided into four groups based on mineralogy, discussed in further detail later. Each group is briefly described below. Calcite occurs in massive veins with minor amounts of pyrite and quartz, and if present at all, just trace amounts of fluorite, barite, and base metal sulfides (Figure 4a). Calcite can also occur along fracture surfaces (Figure 4b), in high-grade Au-Te veins (Figure 4c), replacing phenocryst sites in volcaniclastic rocks (Figure 4d), and as thin veins (Figure 4e).

Dolomite commonly occurs as open-space fill in breccias (Figure 5a), thin massive or euhedral veins (Figure 5b), and in lamprophyres (Figure 5c). Dolomitic sediments are common in the Eastern sub basin (Figure 5d).

Ankerite occurs along fracture surfaces (Figure 6a), as yellowish boxwork in vugs (Figure 6b), and in sugary textured veins with fluorite (Figure 6c).

Rhodochrosite can occur as euhedral veins with base metal rich zones (Figure 7a), thicker rhodochrosite veins with sphalerite along the edges (Figure 7b), and as rhodochrosite matrix breccias with sphalerite around the clasts (Figure 7c). Bright pink rhodochrosite veins occur with quartz and fluorite (Figure 7d).

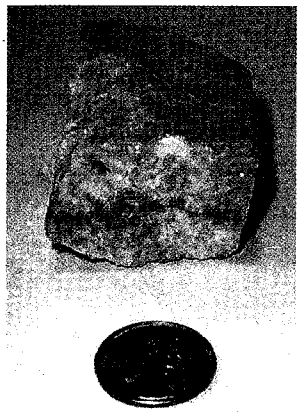

Figure 4a: Massive calcite veins. Base metal sulfides along center line (left). Host rock is granodiorite (right).

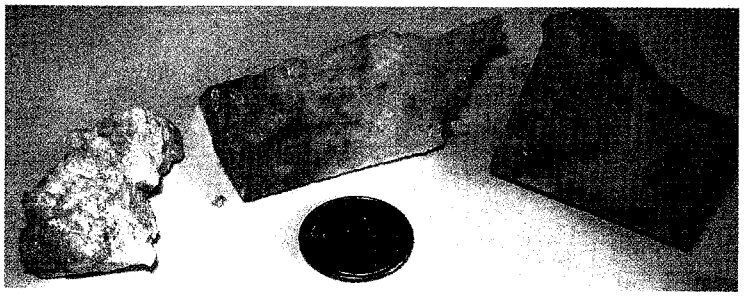

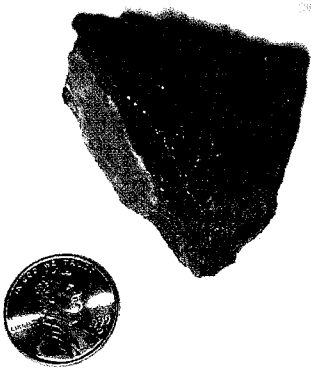

Figure 4b: Calcite along a fracture surface in a lamprophyre.

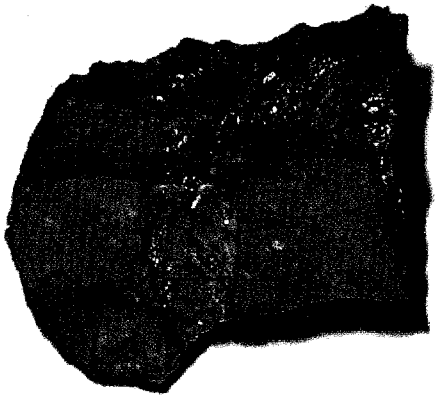

Figure 4d: Calcite replacing phenocryst sites in a volcaniclastic rock.

Figure 4c: High grade Au-Te vein with calcite and fluorite. Host rock is logged as "basalt".

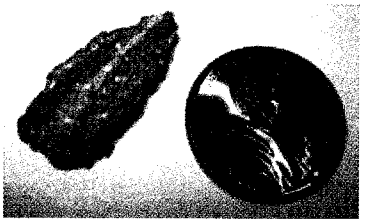

Figure 4e: Thin calcite veins in a phonotephrite (left) and an altered phonolite (right, with pyrite).

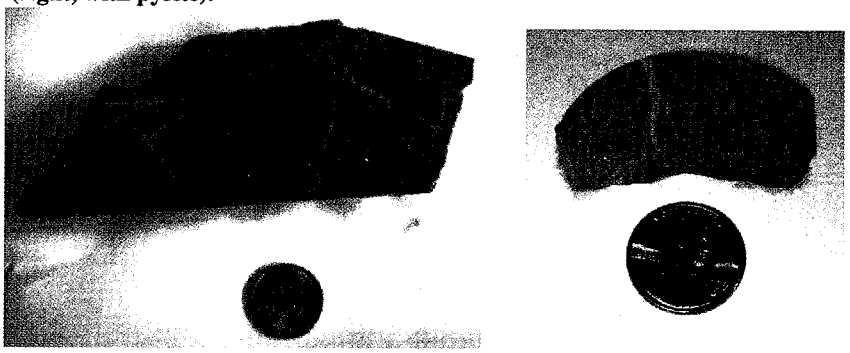

Figure 5a: Dolomite as open-space fill in phonolite breccia (Dante Collapse Breccia) with cinnabar.

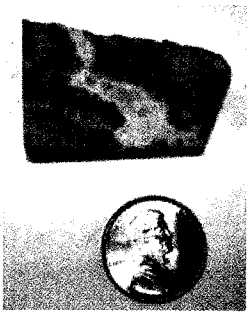

Figure 5b: (Top) Thin dolomite (edges) and calcite (center) vein in lamprophyre. (Bottom) Euhedral dolomite vein in granodiorite.

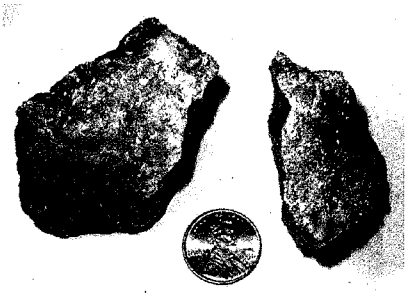

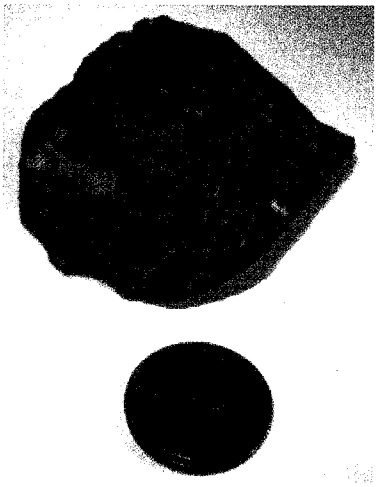

Figure 5c: Dolomite in lamprophyres. Note, same rock type, rock on the right is more altered that rock on the left.

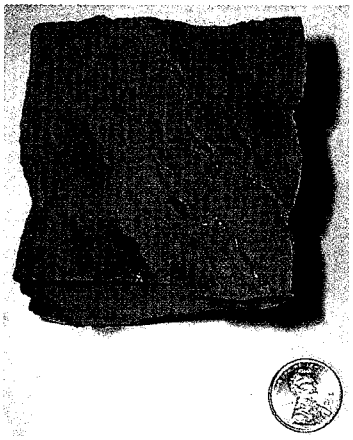

Figure 5d: Sedimentary dolomite from the Eastern sub basin.

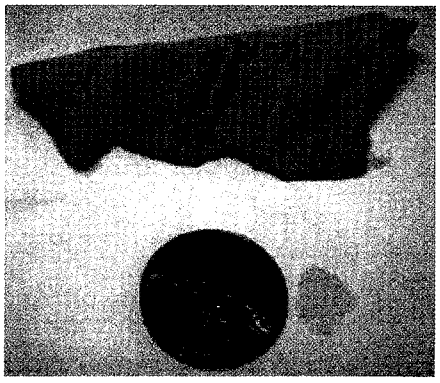

Figure 6a: Ankerite along a fracture surface in a lamprophyre breccia.

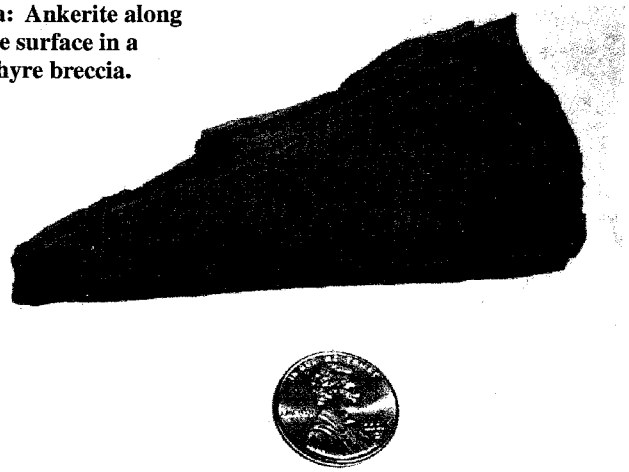

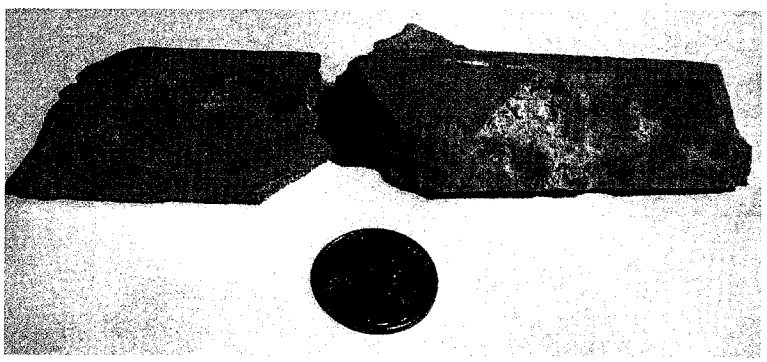

Figure 6b: Yellowish ankerite boxwork in a vug in phonolite.

Figure 6c: Sugary ankerite + fluorite vein in a hydrothermal breccia.

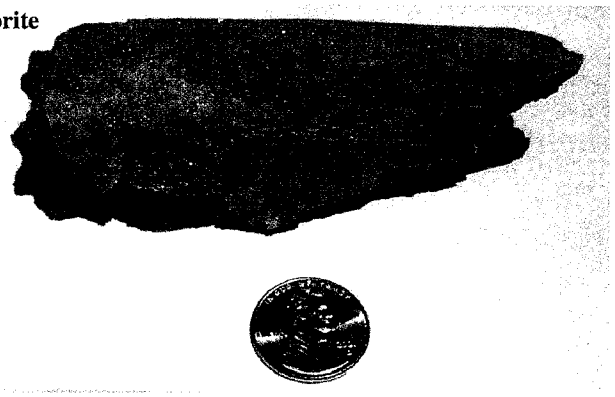

Figure 7a:
Euhedral rhodochrosite vein. Irridescence is from a base metal sulfide rich layer just below the surface.

Figure 7b:
Thick rhodochrosite vein with sphalerite on the edges.

Figure 7c: Rhodochrosite matrix breccia. Note, pyrite and sphalerite around phonolite clasts.

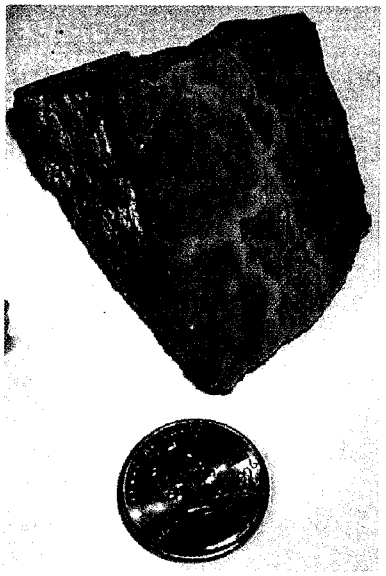

Figure 7d:
Pink rhodochrosite vein with quartz and fluorite.

RESULTS

Fluid Inclusion Microthermometry

Data were collected for 78 inclusions from massive carbonate veins. Thick sections were prepared for 6 calcite, 3 dolomite, 2 ankerite, and 2 rhodochrosite samples. Many more inclusions were observed, but due to the excellent cleavage and high internal pressures of carbonate inclusions, decrepitation or leakage of inclusions upon heating or freezing was common and made data collection difficult.

Primary, two-phase (liquid + vapor) inclusions are the most common type observed, with only a few measurable pseudosecondary inclusions present. Inclusions range in size from 2 to 43 μm, (average = 11 μm) and have degrees of fill from .55 to .95 (most = .90 - .95). Apparent daughter minerals were observed in a few inclusions, but they did not shrink upon heating and may have been imperfections within the mineral or accidentally trapped material. Variable liquid to vapor ratios were observed in primary inclusions in a few samples, but based on the scatter in measurements within each sample, the variation is attributed to leaking or necking off rather than boiling. Secondary veils of inclusions (too small to measure) in some samples also show variable liquid to vapor ratios, and because they are so abundant, may indicate boiling.

Salinities are estimated by the freezing point depression after Bodnar (1992; Appendix F). Photographs and data for each inclusion measured are presented in Appendix G, a PowerPoint presentation on disc. Homogenization temperatures and salinities range from 108°C to 321°C (average = 193°C) and 0 to 9.7 (average = 4.8) equivalent weight percent NaCl, respectively (Table 1 and Figures 8 and 9).

TABLE 1: FLUID INCLUSION DATA

SAMPLE	HOST MINERAL	TYPE	PHASES	F	SIZE (μ)	$T_{m\,ice}$	T_h	SALINITY	OBSERVATIONS
41-K-84	rhodochrosite	1, P/PS	L + V	.85	12	-4.1	253.4	6.59	Large inclusions slightly off fracture surfaces
	rhodochrosite	2, P/PS	L + V	.90	4		239.5		
AVERAGE				*.88*	*8*		*246.5*		
41-K-89 E	rhodochrosite	1, P	L + V	.90	6	-3.8	136.5	6.16	
	rhodochrosite	2, P	L + V	.90	12	-4.4	134.8	7.02	
	rhodochrosite	3, P	L + V	.85	12	-1	131.9	1.74	
	rhodochrosite	4, P	L + V	.80	6	-3.3		5.41	
	rhodochrosite	5, P	L + V	.95	7	-4.3	107.8	6.88	Bubble moves at room temp
	rhodochrosite	6, P	L + V	.90	6	-4.8	271.3	7.59	
	rhodochrosite	7, P	L + V	.90	13	-6.4	260.8	9.73	
	rhodochrosite	8, P	L + V	.85	12	-2.9		4.80	Decrepitated on second freeze
	rhodochrosite	9, P	L + V	.85	6	-4.4		7.02	Decrepitated on second freeze
	rhodochrosite	10, P	L + V	.80	13	-6.4		9.73	
AVERAGE				*.87*	*9*	*-4.2*	*173.9*	*6.61*	
AC 96-23 419'1"	dolomite	1, P	L + V	.90	8	-3.1	>192	5.11	Poor visibility
	dolomite	2, P	L + V	.95	6	-2.4	233.7	4.03	
AVERAGE				*.93*	*7*	*-2.8*	*233.7*	*4.57*	
CC 1954 1165'	ankerite	1, P	L + V	.95	14	-5	223.3	7.86	
	ankerite	2, P	L + V	.90	13	-4.9		7.73	
	ankerite	3, P	L + V	.90	12	-5.1	176.4	8.00	
	ankerite	4, P	L + V	.95	15	-5.6	184.1	8.68	
	ankerite	5, P	L + V	.90	7	-6.2	154.9	9.47	
AVERAGE				*.92*	*12*	*-5.4*	*184.7*	*8.35*	
CC 2236 1137'8"	ankerite	1,P	L + V	.90	8	-0.6	134.6	1.05	
	ankerite	2,P	L + V	.90	5	-3.3	214.4	5.41	
AVERAGE				*.90*	*7*	*-2.0*	*174.5*	*3.23*	
DOL-1	dolomite	1, P	L + V	.90	18	-3.2	209.8	5.26	
	dolomite	2, P	L + V	.95	13	-2	143.0	3.39	
	dolomite	3, P	L + V	.95	16	-2.6	151.0	4.34	
	dolomite	4, P	L + V	.95	6	0.3	147.5		
	dolomite	5, P	L + V	.95	4		122.4		
AVERAGE				*.94*	*11*		*154.7*	*4.33*	
LAMP-1	dolomite	1, P	L + V	.80	12	-1.7	>330	2.90	Bubble showed no change on heating, probably leaked
	dolomite	2, P	L + V	.55	10	-1.4	>330	2.41	Bubble showed no change on heating, probably leaked
	dolomite	3, P/PS	L + V + S?	.95	8	-2.3	169.7	3.87	Daughters? did not shrink on heating
	dolomite	4, P/PS	L + V	.95	8		138.1		Vapor bubble did not reappear when heating to 0°C, but came back by 46°C, probably leaked
	dolomite	5, P	L + V	.95	24		145.2		Vapor bubble did not reappear when heating to 0°C, but came back by 3.8°C, probably leaked
	dolomite	6, P	L + V	.95	8	-2.6		4.34	Poor visibility
	dolomite	7, P	L + V + S?	.95	8	-2.1	213.0	3.55	
	dolomite	8, P/PS	L + V + S?	.95	19	-2.2		3.71	Decrepitated on heating
AVERAGE				*.88*	*12*	*-2.05*	*166.5*	*3.46*	
UGC 97-5 1497'	calcite	1, P	L + V	.90	12	-0.5	202.2	0.88	
	calcite	2, P	L + V	.95	14	-1.6	148.7	2.74	
	calcite	3, P	L + V	.90	4	0	175.0	0.00	
AVERAGE				*.92*	*10*	*-0.7*	*175.3*	*1.21*	

Notes: P = primary; PS = pseudosecondary; L = liquid; V = vapor, S = solid; F = degree of fill; μ = microns; T_{mice} = melting temperature of ice (all temperatures reported in degrees C); T_h = homogenization temperature; Salinity reported in equivalent weight percent NaCl (Bodnar, 1992; Appendix F); T_e = eutectic temperature (hydrohalite); T_{mh} = melting temperature of hydrohalite

TABLE 1: FLUID INCLUSION DATA, PAGE 2

SAMPLE	HOST MINERAL	TYPE	PHASES	F	SIZE (μ)	$T_{m\,ice}$	T_h	SALINITY	OBSERVATIONS
UGC 97-5 1565'	calcite	1, P	L + V	.95					Bubble never reappeared during melting
	calcite	2, P	L + V	.85					Too small to see
	calcite	3, P	L + V	.90	20	-1.4		2.41	Too dark to see T_h
	calcite	4, P	L + V	.90	18	-1.4	171.1	2.41	
	calcite	5, P	L + V	.95	8	-4	182.7	6.45	
	calcite	6, P	L + V	.90	6	-5.8	247.0	8.95	Bubble moves at room temperature
	calcite	7, P	L + V	.85	6	-5.8	218.3	8.95	
	calcite	8, P	L + V	.95	8	-1.2		2.07	Tm ice repeated twice
	calcite	9, P	L + V	.90	6	-5.3	224.2	8.28	
	calcite	10, P	L + V	.95	10	-4.5	293.4	7.17	
	calcite	11, P	L + V	.90	6	-6.1	251.8	9.34	
	calcite	12, P	L + V	.85	6	-6	>207.0	9.21	Decrepitated at 207.0°C
	calcite	13, P	L + V	.90	20	-0.3		0.53	Poor visibility
AVERAGE				***.90***	***10***	***-3.8***	***226.9***	***5.98***	
UGC 97-5 1724'	calcite	1, P	L + V	.75	2	-5.5	184.5	8.55	Has hydrohalite, bubble moves at room temp
	calcite	2, P	L + V	.90	4	-5.5	187.4	8.55	Has hydrohalite
	calcite	3, P	L + V	.90	4	-5.3	182.5	8.28	Has hydrohalite, bubble moves at room temp
	calcite	4, P	L + V	.90	4	-5.3	182.5	8.28	Has hydrohalite, dark, bubble moves at room temp
AVERAGE				***.86***	***4***	***-5.4***	***184.2***	***8.42***	
UGC 97-5 1784'4"	calcite	1, P	L + V	.80	13	-3.1	311.0	2.24	
	calcite	2, P	L + V	.95	10	-2.2		3.71	Bubble moves at room temp
	calcite	3, P	L + V	.90	7	-3.1	203.9	5.11	Bubble moves slightly at room temp
	calcite	4, P	L + V	.90	10	-2.2		3.71	Bubble moves at room temp
	calcite	5, P	L + V	.80	14	-3.4	321.3	5.56	
AVERAGE				***.87***	***11***	***-2.8***	***278.7***	***4.07***	
UGC 97-5 2102'7"	calcite	1, P	L + V	.85	6	-4.3	216.2	6.78	
	calcite	2, P	L + V	.95	7	-1.1		1.91	Te = -20.9°C, Tmh = -19°C, heated to 500°C, bubble showed no chang
	calcite	3, P	L + V	.85	6	-4.5	161.6	7.17	
	calcite	4, P	L + V	.95	43	-0.1		0.18	Decrepitated on second freeze
	calcite	5, P	L + V	.90	20	-0.8		1.40	Decrepitated on heating
	calcite	6, P	L + V	.95	19	-1.8	>151.7	3.06	Bubble moved into dark area, poor visibility
	calcite	7, P	L + V	.95	15	-1.6		2.74	Decrepitated on second freeze
	calcite	8, P	L + V	.95	12	-0.5	134.5	0.88	
	calcite	9, P	L + V	.95	13	-1.6		2.74	Decrepitated on second freeze
AVERAGE				***.92***	***16***	***-1.8***	***170.8***	***2.98***	
UGC 97-5 2294'	calcite	1, P	L + V	.90	24	-0.2		0.35	Decrepitated on second freeze
	calcite	2, P	L + V	.80	10	-2.7	150.7	4.49	
	calcite	3, P	L + V	.90	13	-2.6		4.34	
	calcite	4, P	L + V	.85	14	-1.4	207.2	2.41	
	calcite	5, P	L + V	.90	8	-1.3	> 158	2.24	
	calcite	6, P	L + V	.90	19	-1.8		3.06	May have decrepitatied after second freeze ~-0.7°C
	calcite	7, P	L + V	.85	12	0	221.6	0	Decrepitated on heating~270°C
	calcite	8, P	L + V	.85	25	-2.4	>287	4.03	Decrepitated
	calcite	9, P	L + V	.90	6	-0.7		1.23	Poor visibility
	calcite	10, P	L + V			-1.9		3.23	Did not originally observe, but Tm was obvious
AVERAGE				***.87***	***15***	***-1.5***	***193.2***	***2.54***	

Stable Isotopes

Oxygen and Carbon Isotopes

Carbonates are separated into four different categories (calcite, dolomite, ankerite and rhodochrosite) based on fractionation factors that are used to calculate equilibrium fluids. Data is plotted according to these four categories and will be discussed following the same convention. Detailed sample descriptions and locations are presented in Appendix H.

The range of stable isotopic mineral values (Table 2) for each category are listed below and presented in Figure 10: calcite, $\delta^{18}O$ = 8.1 to 23.0‰, $\delta^{13}C$ = -6.3 to 5.5‰; dolomite, $\delta^{18}O$ = 7.0 to 16.9‰, $\delta^{13}C$ = -4.9 to -0.8‰; ankerite, $\delta^{18}O$ = -7.4 to 17.0‰, $\delta^{13}C$ = -8.6 to -1.4‰; rhodochrosite, $\delta^{18}O$ = 7.1 to 12.0‰, $\delta^{13}C$ = -6.9 to -4.0‰.

Sulfur Isotopes

The range of stable isotopic pyrite values (Table 2) is $\delta^{34}S$ = -14.5 to –1.1‰ (Figure 11). Only two galena samples and one sphalerite sample were analyzed and have values of –14.0, –14.9‰ and –10.1‰, respectively. Detailed sample descriptions and locations are presented in Appendix I.

Calculated Fluid Values

Fluid inclusion homogenization temperatures collected from this study (108 to 321°C) were applied to published fractionation factors (further discussed later) to calculate fluids with $\delta^{18}O_{H2O}$ values of –15.8 to 12.10‰ and $\delta^{13}C_{HCO3-}$ values of –11.8 to 14.4‰ (Figure 12). Calculated $\delta^{34}S_{H2S}$ fluid values range from –15.4 to –0.1‰ (Figure 13). When fluid inclusion data could not be directly obtained from the sample, estimates based on the literature were applied (see "Code" column, Table 2). Fluid values for

TABLE 2: STABLE ISOTOPE VALUES FOR MINERALS AND CALCULATED FLUID VALUES

SAMPLE	MINERAL	$\delta^{18}O_{mineral}$	$\delta_{13}C_{mineral}$	TEMPERATURE	CODE	$\delta^{18}O_{fluid}$	$\delta_{13}C_{HCO3-fluid}$	$\delta^{34}S_{H2S}$ mineral	$\delta^{34}S_{H2S}$ fluid
24-L-28	cc/py	17.9	-2.4	300	1	12.1	–3.6	-3.9	-5.1
25-L-113B	cc	17.3	-2.1	300	1	11.5	–3.3		
25-L-24	cc	22.1	5.5	25	13	-9.1	3.5		
26-L-13	cc/py	13.8	-2.3	230	3	5.5	-3.6	-3.8	-5.4
36-K-174	cc	7.2	-4.7	175	9	1.6	-6.0		
39-K-163B1	cc	21.4	-1.6	50	11	-4.3	-3.4		
39-K-163B1M	cc	21.6	-1.6	50	11	-4.1	-3.4		
39-K-165	cc	13.8	-3.3	50	12	-11.9	-5.1		
39-K-167	cc	23.0	-3.4	50	11	-2.7	-5.2		
A31-27-629A CC	cc	15.6	-4.6	175	8	4.3	-6.0		
AN 3 677.7	cc	16.4	-0.8	300	1	10.6	-2.0		
CC1628 1285'3"	cc	12.1	-6.3	50	13	-13.6	-8.1		
CC1628 1286'2"	cc	12.8	-6.1	50	13	-12.9	-7.9		
CR1268 1281'	cc	12.7	-2.5	200	6	2.9	-3.8		
DDHS 8-185	cc	10.5	-2.7	225	4	2.0	-4.0		
GT96-1-785R	cc	9.9	-4.0	200	6	0.2	-5.3		
UGC96-2 1779'4"	cc	16.2	-2.2	200	6	6.4	-3.5		
UGC96-2 2530'	cc	16.5	-1.9	175	8	5.5	-3.3		
UGC 97-2 1924'	cc	8.7	-3.9	225	4	0.2	-5.2		
UGC97-5 1059'6"	cc	21.9	-3.3	25	13	-9.3	-5.3		
UGC97-5 1302'	cc/py	12.6	-5.0	200	6	2.8	-6.3	-8.1	-9.9
UGC97-5 1341'3"	cc/py	12.4	-5.4	230	3	4.1	-6.6	-4.6	-6.1
UGC97-5 1348'	cc/py	12.1	-4.8	230	6	3.8	-6.1	-8.4	-10.0
UGC97-5 1399'	cc/py	12.0	-4.1	200	6	2.2	-5.4	-10.1	-11.9
UGC97-5 1491'	cc/py	12.8	-3.7	200	6	3.0	-5.0	-13.6	-15.4
UGC97-5 1497'	cc/py	15.9	-5.4	**175**	**M**	4.6	-6.8	-10.2	-12.2
UGC97-5 1565'	cc/py	12.0	-4.9	**227**	**M**	3.6	-6.2	-7.2	-8.8
UGC97-5 1582'	cc/py	10.7	-4.0	200	6	1.0	-5.3	-8.4	-10.2
UGC97-5 1592'8"	cc/py	11.5	-5.1	200	6	1.7	-6.4	-10.2	-12.0
UGC97-5 1612'10"	cc/py	12.2	-5.4	200	6	2.5	-6.8	-4.1	-5.9
UGC97-5 1724'	cc	11.0	-4.4	**184**	**M**	0.3	-5.8		
UGC97-5 1784'3"	cc	12.6	-5.2	**279**	**M**	6.2	-6.4		
UGC97-5 1854'7"	cc/py	11.5	-4.9	200	6	1.7	-6.2	-5.6	-7.4
UGC97-5 2102'7'"	cc	10.4	-4.5	**171**	**M**	-1.2	-5.8		

Notes: Minerals: cc - calcite, dol - dolomite, ank - ankerite, rh - rhodochrosite, py - pyrite, gal - galena, sp - sphalerite. Stable isotope values reported in permil. Temperature reported in degrees Celsius. Equations used in caculations are from Zheng, 1999; Ohmoto and Rye, 1979; Deines et al, 1974; and Mook et al, 1974. Code - Justifications for temperature as follows: **M** - measured; **1** - Deep Ajax/Portland samples range from 300 - 400 degrees C (Jensen, 2003, p. 696); **2** - M/ proximity to M; **3** - Average M for cc + py + base metal sulfide veins; **4** - Style of alteration associated with vein type is similar to temperatures reported by Beaty et al, 1996; **5** through **8** - Average M; **9** - Proximity to M and temperatures reported by Siebel, 1996 and Trippel, 1985; **10** - M/ proximity to M; **11** - Carbonate replacing phenocryst sites in original rock; **12** - "Sedimentarty carbonate", carbonate cement or layered sediments; **13** - Fracture surfaces/descending waters collected recently.

TABLE 2: STABLE ISOTOPE VALUES FOR MINERALS AND CALCULATED FLUID VALUES, PAGE 2

SAMPLE	MINERAL	$\delta^{18}O_{mineral}$	$\delta_{13}C_{mineral}$	TEMPERATURE	CODE	$\delta^{18}O_{fluid}$	$\delta_{13}C_{HCO3-fluid}$	$\delta^{34}S_{H2S}$ mineral	$\delta^{34}S_{H2S}$ fluid
UGC97-5 2294"	cc/py	10.3	-4.4	**193**	M	0.2	-5.7	-12.0	-13.8
UGC97-5 2410'10"	cc/py	11.6	-4.4	200	6	1.8	-5.8	-7.0	-8.8
UGC97-5 2508'4"'	cc/py	9.6	-4.4	200	6	-0.1	-5.7	-8.9	-10.7
UGC97-5 2524'4"	cc/py	11.4	-4.4	200	6	1.6	-5.8	-14.5	-16.3
UGC97-5 2553	cc	8.1	-4.3	200	6	-1.7	-5.6		
UGC97-5 2613'5"	cc/py	10.8	-4.4	200	6	1.0	-5.7	-13.1	-14.9
V-12-228	cc	17.0	-2.7	300	1	11.2	-3.9		
V-12-229	cc	9.9	-3.5	300	1	4.1	-4.7		
V-13-215	cc	15.0	-1.5	300	1	9.2	-2.7		
V6B-269	cc	10.4	-4.3	300	1	4.6	-5.5		
24-L-15	dol	13.9	-1.2	300	1	7.9	-9.4		
25-L-118	dol	10.9	-2.9	175	9	-0.6	-3.4		
25-L-21	dol	15.9	-2.6	175	9	4.3	-3.1		
25-L-38	dol	13.6	-2.9	175	9	2.1	-3.4		
36-K-209	dol	10.5	-3.4	50	12	-15.7	12.7		
37-K-248	dol	12.8	-3.0	50	12	-13.4	13.0		
39-K-141M	dol	12.1	-3.4	50	12	-14.1	12.7		
39-K-160B	dol	12.9	-4.0	50	12	-13.3	12.1		
39-K-163	dol	12.1	-4.9	50	12	-14.1	11.1		
39-K-163A1	dol	15.4	-3.9	50	12	-10.8	12.2		
39-K-163B2	dol	12.8	-4.1	50	12	-13.4	11.9		
39-K-163B2M	dol	12.2	-4.1	50	12	-14.0	11.9		
39-K-170	dol	22.2	-1.7	50	11	-4.0	14.4		
39-K-172	dol	15.4	-3.9	50	12	-10.8	12.2		
39-K-179A	dol	10.5	-3.9	50	12	-15.7	12.2		
39-K-194	dol	13.2	-3.2	50	12	-13.0	12.9		
39-K-195	dol	14.2	-3.7	50	12	-12.0	12.4		
39-K-210	dol	11.3	-4.9	50	12	-14.9	11.2		
39-K-210M	dol	10.5	-4.8	50	12	-15.7	11.2		
39-K-245	dol	11.5	-3.1	50	12	-14.7	13.0		
39-K-245M	dol	11.5	-3.0	50	12	-14.7	13.1		
39-K-248A	dol	16.9	-3.1	50	12	-9.3	13.0		
39-K-248B	dol	16.7	-3.4	50	12	-9.5	12.7		
39-K-249	dol	10.8	-4.2	50	11	5.5	11.9		
A31-27-629A DOL	dol	17.0	-4.3	175	9	5.4	-4.7		
AC96-22 223'8"	dol	7.0	-4.3	175	9	-4.6	-4.7		
AC96-23 397'9"	dol	10.1	-3.9	175	9	-1.5	-4.4		
AC96-23 418'3"	dol	10.8	-3.5	**234**	M	2.5	-8.3		

TABLE 2: STABLE ISOTOPE VALUES FOR MINERALS AND CALCULATED FLUID VALUES, PAGE 3

SAMPLE	MINERAL	$\delta^{18}O_{mineral}$	$\delta_{13}C_{mineral}$	TEMPERATURE	CODE	$\delta^{18}O_{fluid}$	$\delta_{13}C_{HCO3,\ fluid}$	$\delta^{34}S_{H2S}$ mineral	$\delta^{34}S_{H2S}$ fluid
CC1628 1281'9"	dol	14.1	-5.2	175	9	2.6	-5.6		
CC1629 458'8"	dol	14.4	-2.4	175	9	2.8	-2.9		
CC1840 1337'5"	dol	12.2	-4.3	175	9	0.6	-4.8		
CP	dol	11.9	-1.0	175	9	0.4	-1.4		
DDU-8-162	dol	15.1	-2.1	300	1	9.2	-10.3		
DOL-1	dol	13.7	-0.8	**155**	**M**	0.7	0.5		
LAMP-1	dol	15.0	-4.2	**167**	**M**	2.9	-3.9		
LAMP-2	dol	16.5	-4.8	175	9	4.9	-5.2		
UGC 96-2 2529'8"	dol	16.0	-2.3	200	9	4.4	-2.7		
36-K-7	ank	17.0	-8.6	180	7	5.8	-10.9		
CC1629 427'	ank	15.4	-3.5	180	7	4.1	-5.9		
CC1954 1165'	ank	10.7	-3.5	**185**	**M**	-4.1	-6.4		
CC2236 1131'	ank	7.4	-4.3	175	7	-4.1	-6.4		
CC2236 1137'7"	ank	7.9	-4.5	**175**	**M**	-3.7	-6.6		
CC92-61 1580'9"	ank	16.2	-1.4	180	7	4.9	-3.8		
CC92-61 1714'1"	ank/py	11.3	-3.5	180	7	0.1	-5.8	-4.1	-6.0
CC92-61 1871'2"	ank/py	11.0	-3.9	180	7	-0.2	-6.2	-6.2	-8.2
DDHS-8 553.5	ank	10.6	-3.1	50	12	-15.6	3.3		
UGC96-2 2092'5"	ank	9.4	-3.8	180	7	-1.8	-6.1		
UGC96-2 829'	ank	12.6	-1.4	180	7	1.3	-3.8		
39-K-103	rh	9.0	-4.1	210	5	-0.4	-7.8		
39-K-103B	rh	7.1	-6.0	210	5	-2.3	-9.7		
39-K-309	rh	9.8	-4.0	210	5	0.4	-7.7		
39-K-52C	rh/gal	7.1	-5.9	210	5	-2.3	-9.6	-12.2	-4.4
41-K-84	rh	12.4	-6.6	**247**	**M**	4.7	-11.8		
41-K-84A	rh	12.0	-6.4	247	2	4.2	-11.5		
41-K-89C	rh	11.5	-7.1	174	10	-0.2	-9.1		
41-K-89E	rh/gal	11.5	-6.9	**174**	**M**	-0.1	-9.0	-10.8	-0.1
RRBXHYDBX	rh	11.3	-5.5	175	10	-0.2	-7.6		
TEL-1	rh	12.4	-4.9	175	10	0.8	-7.1		
24-L-15	py			300	1			-1.1	-2.3
25-L-118	py			175	8			-6.6	-8.6
Ajax 18th	py			250	1			-1.6	-3.1
COPPER MT.	sp			200	6			-10.1	-10.5
UGC 97-5 1243'	py			200	6			-4.2	-6.0

Figure 10: Mineral Values

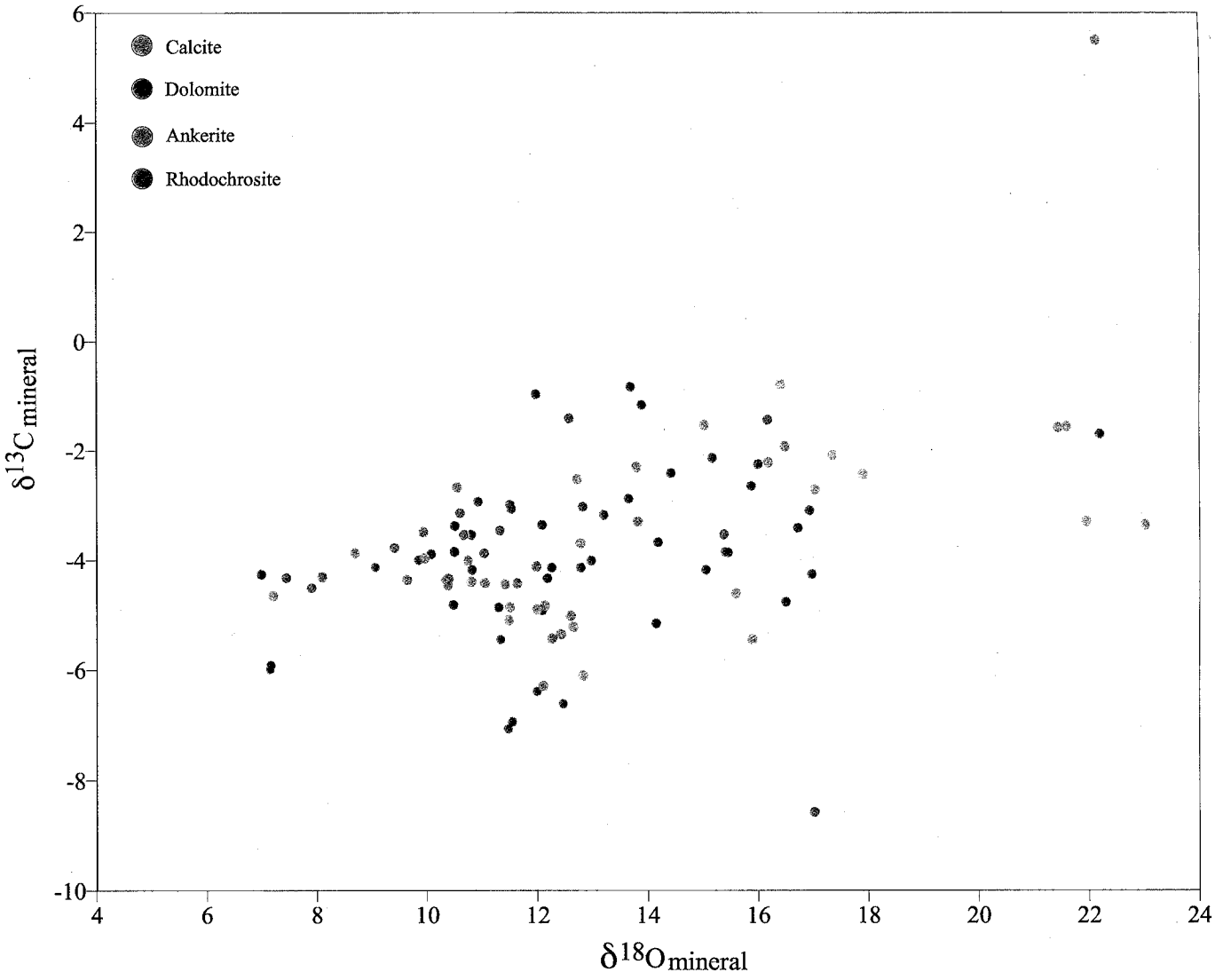

Figure 11: Histogram of $\delta^{34}S$ Mineral Values

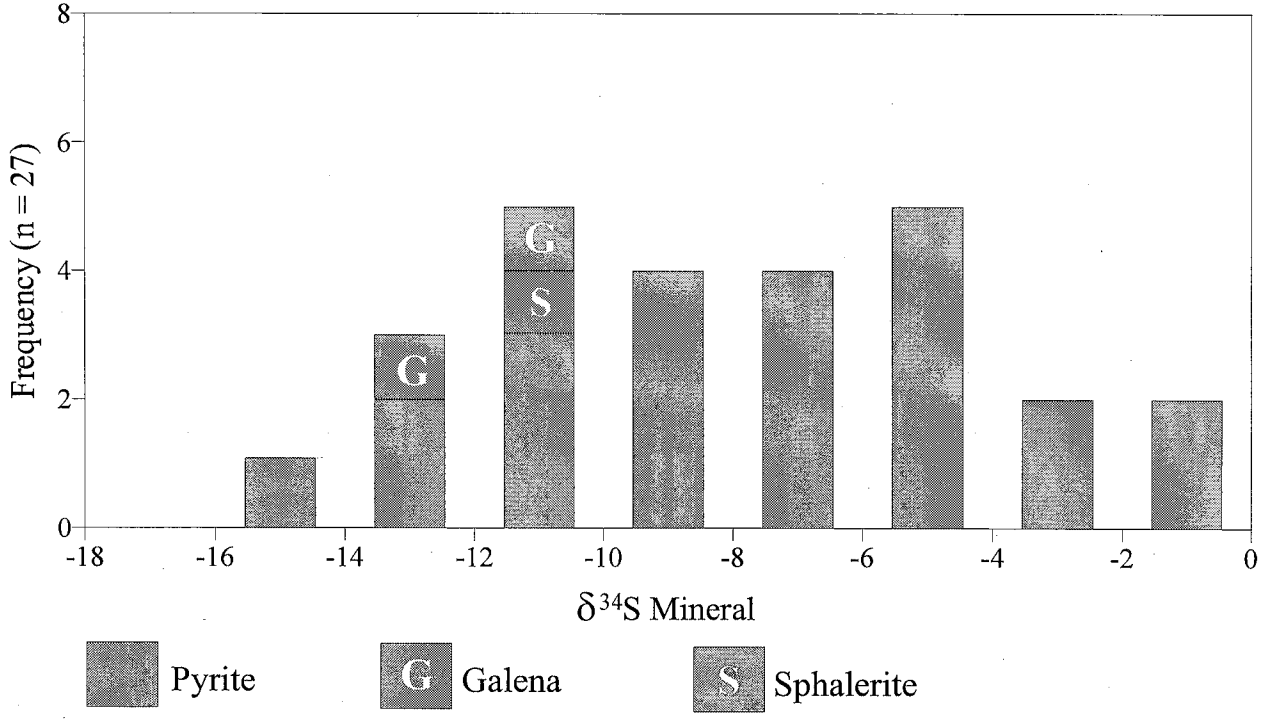

Figure 12: Calculated Fluid Values

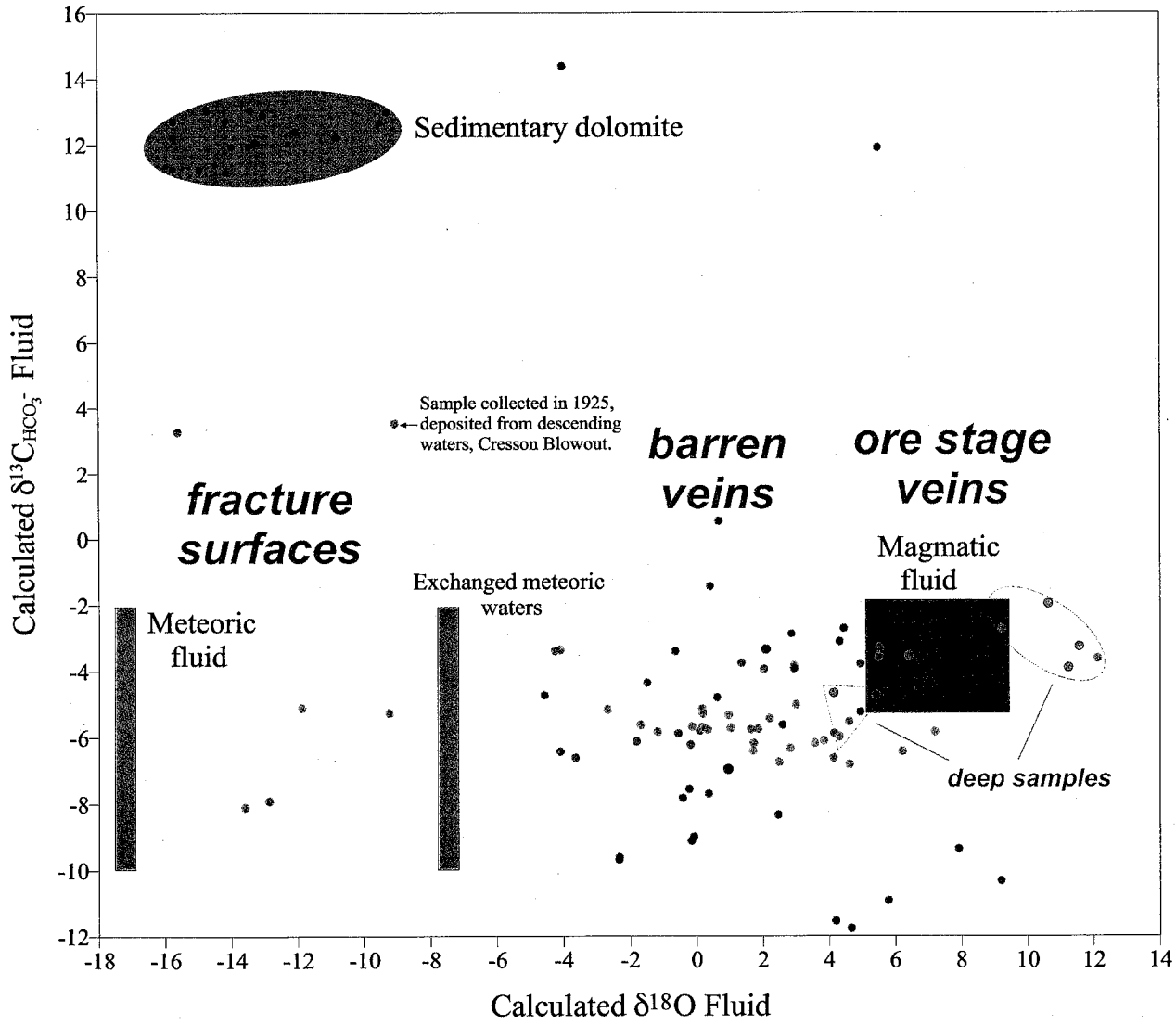

Figure 12: Fluid values calculated with temperatures listed in Table 2. Meteoric fluid field defined with values from Ohmoto and Rye, 1979 and Taylor, 1974.
Magmatic fluid field defined with values from Ohmoto and Rye, 1979 and Taylor, 1979.

- Calcite: Equations from Zheng, 1999 and Deines et al, 1974.
- Dolomite: Equations from Zheng, 1999, Ohmoto and Rye, 1979, and Mook et al, 1974.
- Ankerite calculated with dolomite equations. ≤0.7â positive shift in calculated O values.
- Rhodochrosite calculated with dolomite equations. ≤0.8â positive shift in calculated O values.
- Pre-ore stage veins
- Ore stage veins

Exchanged meteoric fluids calculated with whole rock values at 200 degrees C (Appendix C, various sources) assuming the samples are

- K-spar

Figure 13: Histogram of Calculated $\delta^{34}S_{H_2S}$ Fluid Values

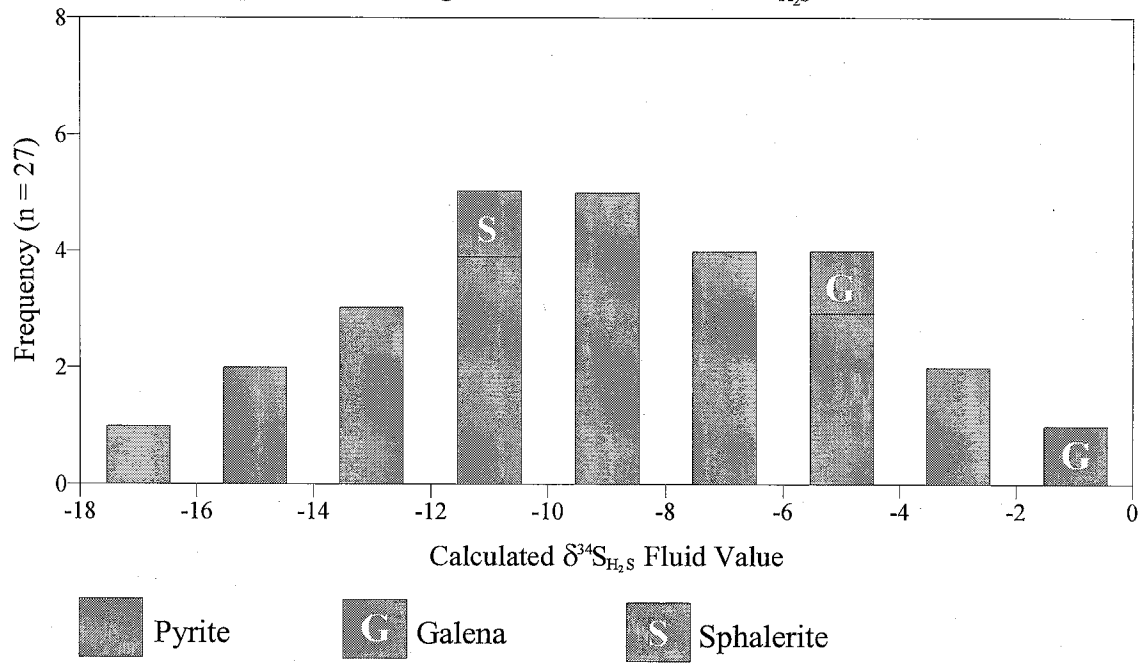

calcites on fracture surfaces or deposited from recent descending waters were calculated at 25°C, and these samples plot towards the pure meteoric end member on Figure 12.

"Sedimentary dolomite" includes rocks with fine, alternating light and dark bands that are likely water lain sediments because they exhibit soft sediment deformation features. This group also includes coarser, more clastic, arkosic sediments that also show soft sediment deformation. A temperature of 50°C was used to calculate equilibrium fluids for sedimentary dolomite, assuming diagenetic processes were responsible for its formation. In two volcaniclastic sediments and one phonolite sample, calcite is seen replacing original phenocryst sites. These were also calculated at 50°C because no other temperature constraints could be applied. Average measured T_H values from this study were used to calculate fluid values for: massive calcite veins (175°C); calcite + pyrite + base-metal sulfide veins (175°C); ankerite veins (180°C); calcite ± pyrite veins (200°C); and rhodochrosites veins and breccias (210°C). A temperature of 225°C was used for calcite veins with distinctive alteration haloes similar to those reported in the literature. Deep Ajax/Portland vein samples were calculated at 300°C based on temperatures of vein quartz reported in the literature.

X-ray Diffraction Data

Representative samples from eight different groups of carbonate were analyzed to confirm mineralogy. These include: sedimentary dolomite, calcite replacing phenocryst sites in volcaniclastic sediments, massive dolomite within lamprophyres and euhedral dolomite in vugs, yellow dolomite filling open space in breccias, sugary ankerite + fluorite veins, massive calcite (± pyrite, quartz, and base metal sulfides), massive rhodochrosite (± fluorite and base metal sulfides), and a calcite sample deposited from

recent descending waters. The eight groups fall into one of the four mineralogical categories (calcite, dolomite, ankerite and rhodochrosite) used to discuss all data in this thesis, as described above in the ***Oxygen and Carbon Isotopes (Results section)***. The sample peak pattern for each sample analyzed can be found following the sample description slide in Appendices J-M. Results are further discussed in Appendix N.

DISCUSSION

Fluid Inclusions

Fluid inclusions provide important temperature data that can be used in conjunction with stable isotopes to define fluid characteristics such as fluid source, and address interaction between different fluids.

Because this study focuses on predominantly barren carbonate veins, samples used for fluid inclusion microthermometry do not contain telluride minerals, and it is therefore unknown whether or not they are associated with the mineralizing event. Fluid inclusion measurements (107 to 321°C; 0 to 9.7 eq. wt. % NaCl) overlap the range of the low temperature (125-225°C), low salinity (< 5 wt. %) mineralizing fluids reported by previous researchers, but are up to 100°C and ~5 eq. wt. % NaCl higher. Other fluid inclusion studies (Appendix C) document temperatures ranging from 105 (Collins, 1979) to almost 510°C (Thompson, 1996), and the data presented in this study falls well within this range. Temperatures of up to 600°C have been measured, and these inclusions commonly contain daughter halite, sylvite, and opaque minerals (Rosdeutscher, 1999; Mote, 2000), and in a few instances, CO_2 (Mote, 2002; Burnett, 1995; Siebel, 1991; Collins, 1979); however, most of these inclusions are in the Precambrian rocks and do not represent the hydrothermal fluids responsible for Tertiary mineralization (Jensen, 2000).

Varying Degrees of Fill

A few samples analyzed showed varying degrees of fill amongst inclusions. In some cases this may be attributed to boiling, but in this case it is attributed to leakage or pinching off. Inclusions that had obviously leaked were observed to have varying degrees of fill at room temperature, and they did not change upon heating-freezing runs.

Because leaked inclusions give abnormally high T_H measurements, their presence makes the higher homogenization temperatures (225 to 325°C) collected in this study suspect. However, these types of inclusions were avoided during measurements, and because data in the range of 225-325°C has been documented by other studies, these higher temperatures are believed to be accurate.

Depth of Mineralization

Many lines of evidence support shallow levels for mineralization at Cripple Creek. The presence of trace fossils in the lacustrine sediments of the Eastern sub basin and tree fragments within the Cripple Creek breccia indicate that this was a near-surface environment at the time of mineralization. Because there is no direct evidence for a thick sequence of volcaniclastic or supracrustal rocks, the unconformity between Precambrian rocks and volcaniclastic and lacustrine sediments is believed to mark the paleosurface at the onset of Tertiary volcanism (Jensen, 2003).

However, when the biotite-stable alteration zones are considered, it seems likely that a few hundred meters of erosion have taken place. This type of alteration suggests temperatures of 300-450°C, which requires pressures of 100 bars to keep water liquid at ~320°C, and because these alteration assemblages are exposed at less than 100 m depth in the northern parts of the district, the paleosurface would have been several hundred meters higher than at present (Jensen, 2003). If this is the case, then it is necessary to apply a pressure correction to fluid inclusion homogenization temperatures if there is no indication that the fluids were boiling.

Because high temperatures of mineralization have been documented in previous studies, a temperature of ~400°C and a salinity of ~5% are used to estimate a pressure

correction. This temperature will reflect the highest pressure the mineralizing fluids experienced to prevent boiling. However, this is a minimum estimate, and pressures may have been even higher. Using graphs from Roedder (Figures 9.4 and 9.6, pages 262 and 274), a temperature of 400°C corresponds to a pressure of 250 bars (25 MPa). The lowest homogenization temperatures in this study need to be corrected by ~30°C and the highest temperatures by ~20°C. For example, carbonate inclusions with homogenization temperatures of 108°C may have actually been trapped (T_T) at 138°C, and higher homogenization temperatures (~320°C) may indicate trapping temperatures of 340°C. The effect this has on calculated stable isotopic fluid values will be discussed later.

Transition from Epithermal to Porphyry-Style Mineralization

Temperatures reported in the literature document the predominance of hotter fluids (300-510°C; Thompson, 1996) in the deepest levels (7000' elevation) of the Ajax and Portland mines. If the assumption can be made that fluid temperatures increase with depth, a mixing model in which hot magmatic fluids enter into deep parts of the system, ascend along structurally controlled conduits, and mix with cooler meteoric fluids at higher levels in the system may be applicable. Further evidence to support this hypothesis is the presence of high temperature (300-450°C) biotite stable alteration assemblages that are also present at deep levels in the Ajax and Portland mines and at shallower levels in the vicinity of the Mollie Kathleen mine, the Moffat Tunnel, and Globe and Ironclad Hills (Jensen, 2003; see Figure 2). Evidence for these high temperature fluids is not seen in the fluid inclusion data from present study. One explanation for this may be that the deepest sample in which inclusions were measured is from the 8061' elevation.

Stable Isotopes

Isotopic mineral values along with temperature data collected from fluid inclusions and compiled from other studies (see explanation, Table 2) were applied to fractionation equations to calculate isotopic fluid values, which rely heavily on accurate temperature data. Because a pressure correction of 20-30°C may be applied to the homogenization temperatures measured from inclusions in this study, it is important to note the effect this has on calculated fluid values. Fractionation increases with decreasing temperature so the largest shifts will be seen at lower temperatures. For example, the difference between fluids calculated at 108 and 138°C is 3‰ heavier for oxygen and .1‰ lighter for carbon, whereas the difference between 320 and 340°C is 0.5‰ for oxygen and .02‰ (negligible) for carbon.

The lack of a clearly defined paragenetic sequence limits the conclusions that can be drawn from the stable isotope data presented in this study. As discussed in the section on District Geology, it is not possible to apply a relative timing to the samples on the basis of mineralogy.

Oxygen and Carbon Isotopes

Calculated isotopic fluid values for carbonates are shown in Figure 12. Calcite and dolomite equations from Zheng (1999), Deines (1974), Ohmoto and Rye (1979), and Mook et al (1974) are used to calculate the $\delta^{18}O_{H2O}$ and $\delta^{13}C_{HCO3-}$ values for fluids that were in equilibrium with those respective minerals at the time of deposition (See introduction to appendices on disc for equations).

Because mineral-$\delta^{13}C_{HCO3-}$ equations do not exist for ankerite or rhodochrosite, fluid values calculated with mineral-$\delta^{18}O_{H2O}$ equations for ankerite and rhodochrosite

were compared to those calculated with equations for dolomite. The $\delta^{18}O$ values calculated only differ by 2‰; therefore the pair of dolomite equations was used to calculate the $\delta^{18}O_{H2O}$ and $\delta^{13}C_{HCO3-}$ values for fluids that were in equilibrium ankerite and rhodochrosite.

The fluid fields drawn on Figure 12 are defined with values from the following references: magmatic fluid field - Ohmoto and Rye, 1979 and Taylor, 1979; meteoric fluid field - Ohmoto and Rye, 1979 and Taylor, 1974. The exchanged meteoric fluid field is discussed below.

Oxygen and carbon isotopes from alkalic-type epithermal deposits generally range from 4.7 to 11.4‰ and –8 to 0‰, respectively, and overlap magmatic values (Richards, 1995). Richards (1995) identifies mixing between two fluid end members (magmatic and exchanged meteoric) as a common characteristic of alkalic-type epithermal Au-Te systems. As meteoric fluids circulate through country rocks they tend to pick up its isotopic signature, evidenced by a shift to heavier $\delta^{18}O$ values from a pure meteoric end member.

Recall that previous studies have focused on ore-stage mineralization and have documented consistent evidence to support a magmatic source for the mineralizing fluids at Cripple Creek. The $\delta^{18}O$ range of values cited in these studies is between 3 and 9‰, which overlaps magmatic composition. Ore stage veins analyzed in this study cluster around the magmatic fluid field, which is consistent with interpretations of previous studies. It is interesting to note, that the ore stage veins are included in a group of the deepest samples (10 samples total from elevations between 6716 and 7665' from the southern part of the district), which also cluster around the magmatic fluid field. This

further supports a model in which hot, magmatic fluids enter into deep parts of the system, rise along structurally controlled conduits, and mix with cooler descending meteoric fluids.

When a broader spatial and temporal view of the district is considered by looking at the range of calculated fluid values for barren carbonate veins, fracture surface carbonate mineralization, and calcite replacing phenocryst sites, a trend that suggests mixing between magmatic and exchanged meteoric fluids becomes evident. The four calcite samples that lie closest to the meteoric fluid end member are from fracture surfaces. Three samples of calcite replacing phenocryst sites plot towards the pure meteoric end member.

It is important to note that the meteoric end member (far left field, Figure 12) is a pure end member without isotopic exchange with country rocks being taken into consideration. The isotopic values of exchanged meteoric waters can be approximated using whole rock data from Beaty et al (1996) and Silberman (1992), compiled in Appendix D. The field of "exchanged meteoric water" on Figure 12 is calculated with the K-feldspar fractionation equation from Zheng, (1993b) assuming a temperature of 200°C, and that the fluid is in equilibrium with the K-feldspar in the sample. Although exact conditions of exchange are not documented, estimates provide useful information on the magnitude of shift isotopic exchange can have. The average fluid value calculated for K-feldspar at 200°C is -7.4‰, a shift of ~ 10‰ lighter. When this field is plotted on Figure 12, the mixing trend between the magmatic and exchanged meteoric fluid fields becomes more evident.

The trend can be interpreted as mixing between magmatic and exchanged

meteoric fluid end members. Further interpretations cannot be drawn due to the ambiguity in the paragenetic sequence. Carbonate commonly occurs in all stages of mineralization (Jensen, 2003; Table 5.1), but because veins seldom show all stages, or all minerals common to each stage, crosscutting relationships do not show enough information to define a clear paragenetic sequence and determining relative ages is not possible.

Sedimentary dolomite falls in a distinct field, with low $\delta^{18}O$ (-16 to –8‰) and high $\delta^{13}C$ (10 to 14‰) values relative to the ranges mentioned above for other alkalic-type epithermal deposits. Because no temperature data was obtained from this group of samples, the 50°C temperature used to calculate fluid values remains an inference based on the fact that these are water lain sediments deposited in a shallow basin, and low temperature diagenetic processes likely dominated. It is interesting to note that all of these samples came from the Eastern sub-basin, which has not been subject to the intense K-metasomatism seen throughout the rest of the district (Jensen, 2003, Figure 6.9), so these samples likely escaped a later geochemical overprint. Sedimentary dolomite was analyzed to investigate whether or not it could have been the source of C for vein carbonates, but it appears that it is not, as the values are not consistent with the rest of the data and no visible trend to suggest mixing with this reservoir is observed.

Origin of Hydrothermal Calcite

The formation of hydrothermal calcite is controlled by the concentration of aqueous carbon dioxide, pH, temperature and aqueous calcium ion activity (Simmons and Christenson, 1994). Boiling and fluid mixing are the main mechanisms that affect these parameters (Simmons and Christenson, 1994; Giggenbach and Stewart, 1982). Because

calcite has a reverse solubility, it commonly precipitates in epithermal systems as a result of cool, descending recharge waters coming into contact with hot rocks, causing slight heating (Simmons and Christenson, 1994). The occurrence of late stage barren calcite veins may be explained by this process, which typically occurs along the periphery of epithermal systems, where cooler fluids interact with hot rocks, until the collapse of the system, when cool fluids can enter what used to be the zones of upflow (Simmons and Christenson, 1994). Calcite deposited by warming, descending waters is typically coarse grained and rhombohedral, and is commonly associated with other minerals with retrograde solubilities, such as anhydrite (Moore and Norman, 1999).

Epithermal systems that experience boiling give off steam and other volatiles that condense at higher levels in the system, creating relatively dilute, slightly acidic waters with low salinities and temperatures below 240°C (Giggenbach and Stewart, 1982). These systems commonly have calcite veins deposited from steam heated groundwater, and although previous studies have documented evidence to support the occurrence of boiling in certain areas of the district, several observations from Cripple Creek are inconsistent with typical steam-heated epithermal systems.

Boiling epithermal systems typically produce an assemblage consisting of quartz + adularia + bladed calcite (Moore and Norman, 1999; Simmons and Christenson, 1994). However, no evidence for bladed calcite is seen in the Cripple Creek District. The majority of fluid inclusion homogenization temperatures presented in this study are consistent with the <240°C temperatures seen in steam heated systems, but there are some higher temperatures, and the salinities from Cripple Creek inclusions are higher than would be expected for steam heated waters. The oxygen isotope values of calcites

deposited from steam-heated waters are typically close to those of meteoric water, but the carbonates from Cripple Creek have much more magmatic values. These observations do not support the presence of common steam-heated waters reported in epithermal systems; however, the processes acting in Cripple Creek may be similar in that cooler descending groundwaters interact with rising plumes of hot magmatic waters to deposit calcite, and as the magmatic waters cool and descend, they maintain their predominantly magmatic signature, which is recorded in carbonate veins.

Sulfur Isotopes

Sulfide minerals can be used as an independent line of evidence for interpreting the source of fluids. $\delta^{34}S$ values for sulfides from epithermal Au-Ag-Te deposits range from -7.9 to 5.5‰ during the early phases of a magmatic hydrothermal system and shift to lighter values of –15 to +3 (typically less than 0‰) during later stages of evolution, reflecting the addition of exchanged meteoric waters to the system (Richards and Kerrich, 1993). Values for epithermal deposits are broader than the $\delta^{34}S$ range for porphyry-type deposits, which tend to be 0 ± 5‰ for deposits in the western U.S. (Ohmoto and Goldhaber, 1997). The $\delta^{34}S$ data from this study (-16 to 0‰; Figure 11) and studies by Jensen (2003; –20 to 2‰) and Rosdeutscher (1999; -10 to -3‰) overlap these ranges and have a few even lighter values (Figure 14). This wide range of values may represent mixing between a magmatic fluid (0‰) and another lighter end member, such as exchanged meteoric fluid; or a change in fluid fO_2 through time, with fluids characterized by lighter $\delta^{34}S$ values during later stages of mineralization. Evidence for the latter was presented in Jensen's (2003) study, with late sulfides having values of –20 to –12‰.

A mixing trend should be visible in both O and S data if mixing is the dominant

Figure 14: Compilation Histogram of $\delta^{34}S$ Mineral Values

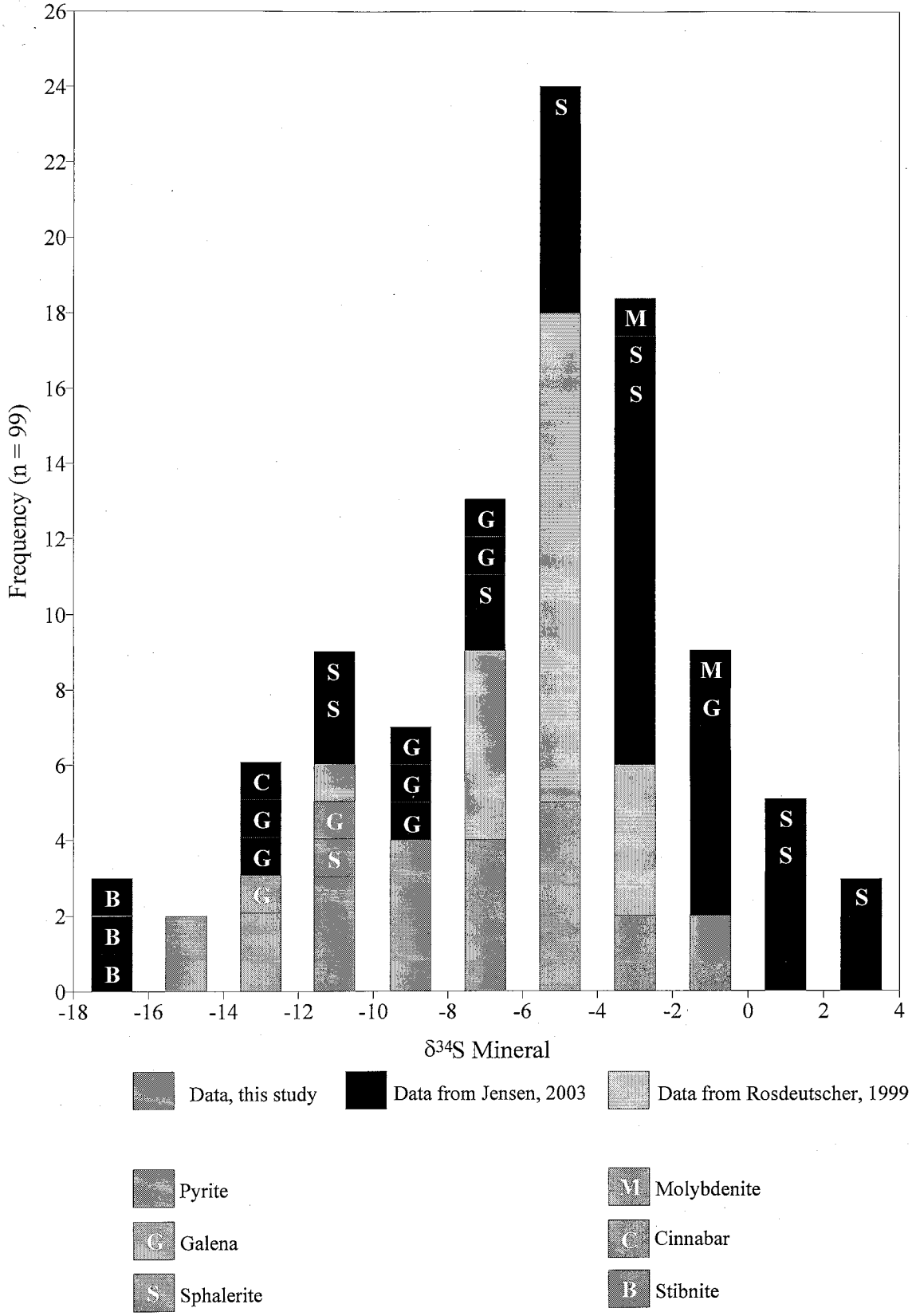

mechanism controlling isotopic values. Heavy O should correspond to heavy S (magmatic), and as meteoric fluid is introduced, values should get progressively lighter. However, when plotted, the data show no correlation (Figure 15). It is intriguing that the two samples with the heaviest S values come from the deep Ajax mine in the southern part of the district, but other than that no correlation with depth is shown (Figure 16).

An alternative explanation for such a wide variation in S values is the role of oxidation. If a magmatic source for sulfur, with $\delta^{34}S_{H2S}$ values around 0‰ undergoes oxidation, the $SO_4^{=}$ created will be heavy. The H_2S left behind will be light, therefore zones of oxidation would show light $\delta^{34}S_{H2S}$ values (Ohmoto and Goldhaber, 1997). Mechanisms such as fluid mixing, reaction with wall rocks or Fe-bearing phases, precipitation of sulfides, sulfates, and carbonates, and boiling can cause changes in the redox state of a single hydrothermal fluid (Ohmoto and Goldhaber, 1997).

Variation in Isotopes

Generally, O, C and S values reported for alkaline epithermal deposits are largely consistent with derivation from magmatic sources (Shannon et al, 1983; Richards and Kerrich, 1993; Richards, 1995; Spry and Thieben, 1998). Alkaline epithermal deposits are generally characterized by light carbon and sulfur isotopes, as mentioned above (Ahmad et al, 1987a; Richards and Kerrich, 1993; Thompson, 1998), indicating either the oxidized state of sulfur in alkaline magmatic systems, or the progressive oxidation of hydrothermal fluids (e.g. boiling; Richards and Kerrich, 1993). These ranges overlap typical magmatic values but can vary by up to 12‰, suggesting either mixing with other isotopic reservoirs such as country rocks, or the operation of redox processes during mineralization (Richards, 1995; Ohmoto and Goldhaber, 1997). Cripple Creek has a

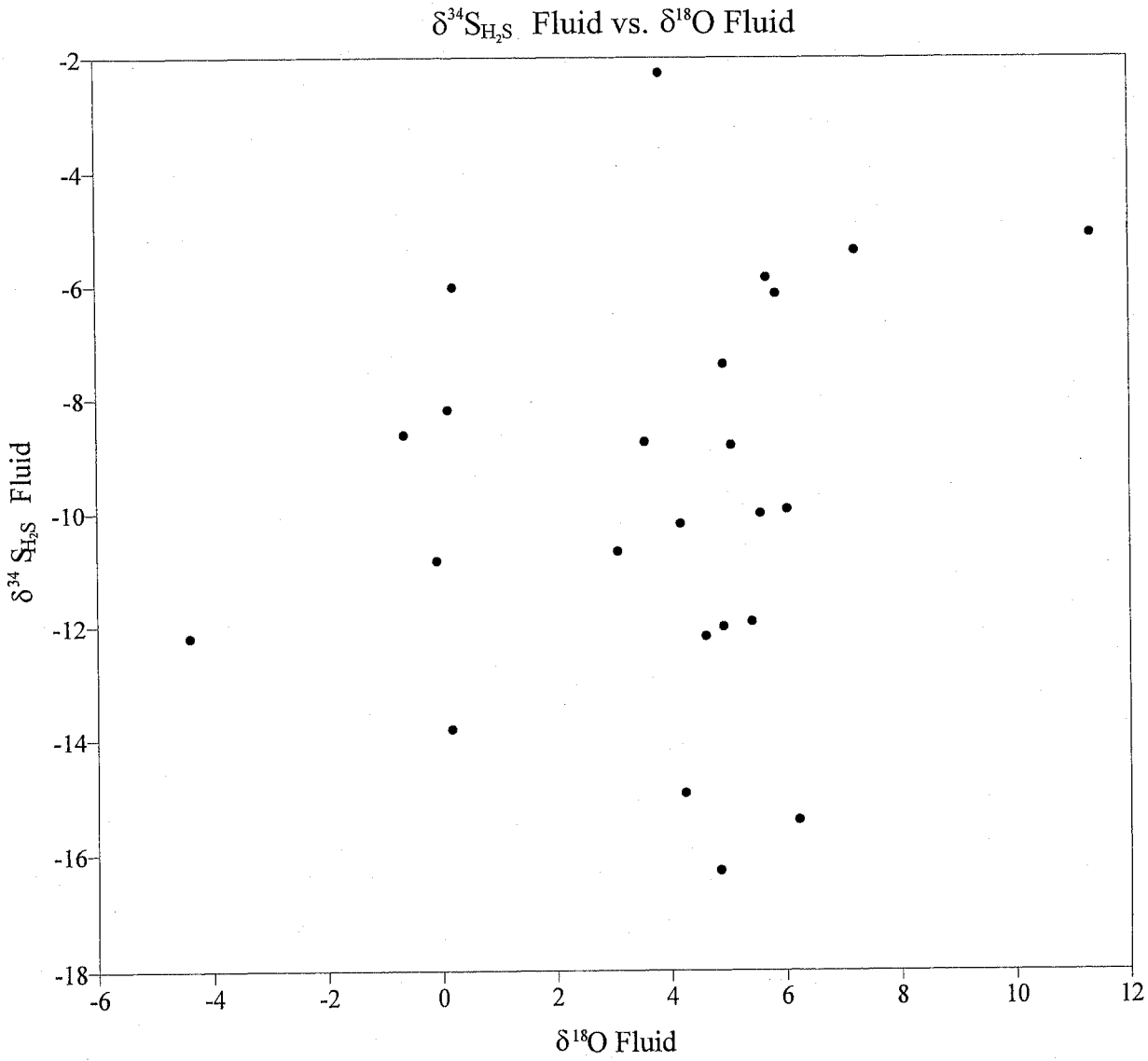

Figure 15: Oxygen vs. Sulfur Fluid Values

Figure 16: $\delta^{34}S$ Fluid Values vs. Depth

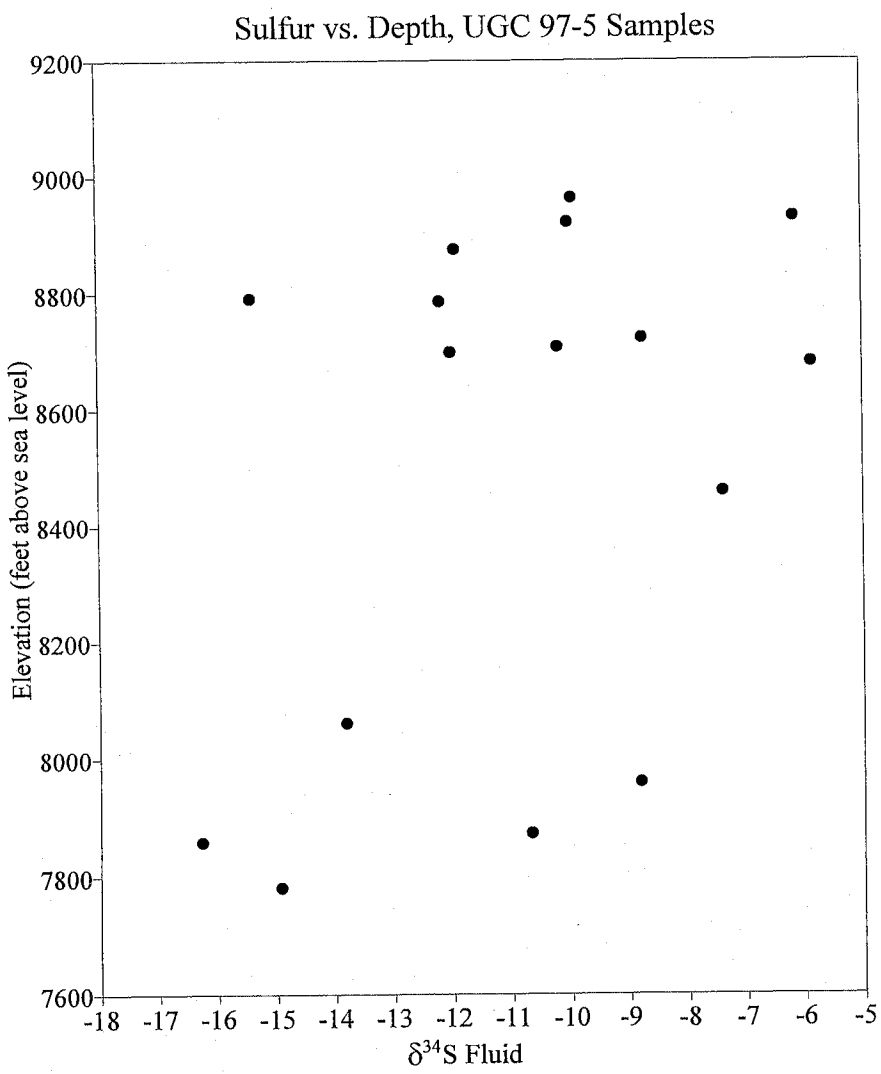

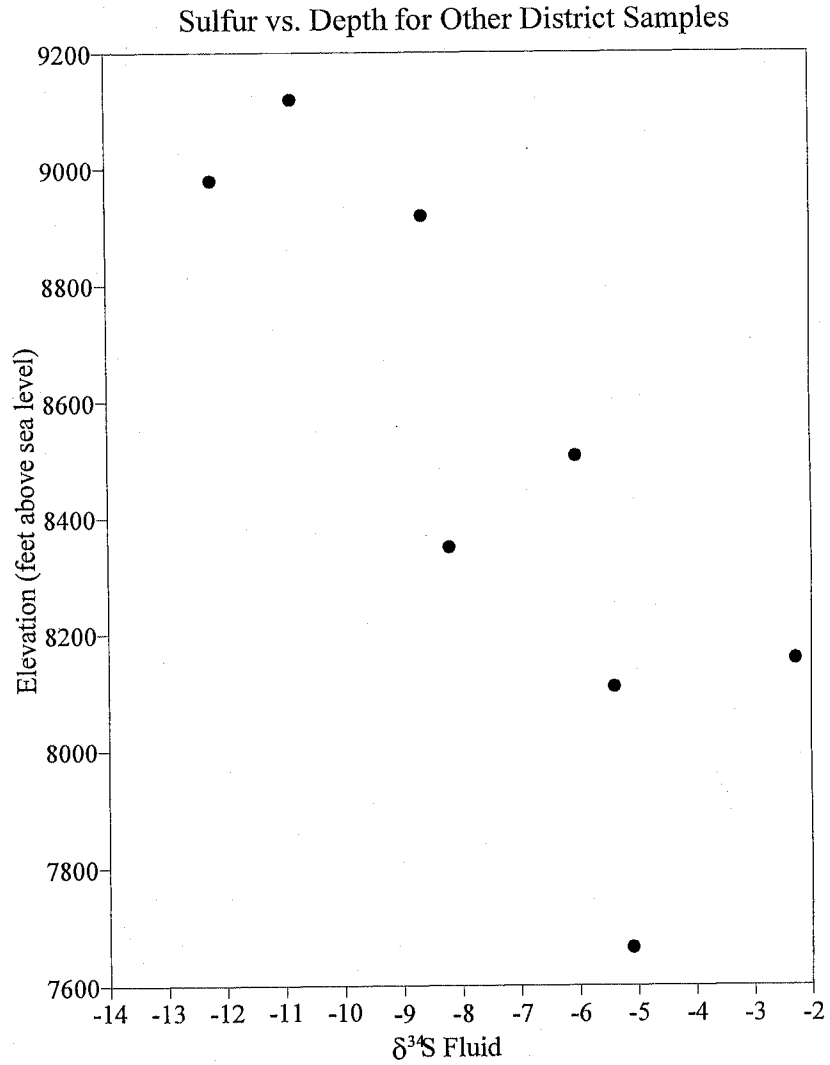

much wider range of both O and C values, and some slightly lighter S values. The generalized ranges overlap to some extent with values seen in this deposit. Mixing between magmatic and exchanged meteoric fluids may have resulted in extreme changes in fluid chemistry, causing such a wide range in isotopic values.

EXPLORATION

Stable isotope and fluid inclusion data are used to characterize the sources for mineralizing fluids in epithermal deposits. These characterizations are often applied to a simple model of an epithermal system in an attempt to explore for further mineralization. The simple model commonly used to illustrate hydrothermal plumbing in epithermal deposits shows magmatic fluids ascending in central zones and meteoric fluids descending along the margins of the hydrothermal cell and mixing with magmatic fluids (Figure 17a).

Successful exploration entails defining patterns of fluid flow and assessing mechanisms responsible for precipitation of Au-Te minerals to identify geochemical and structural environments that are favorable for mineralization. It is important to address at what scale the data needs to be examined. Many studies try to define exploration targets on the scale of a vein system, but often it is not possible to find geochemical or spatial patterns on less than a district-wide scale.

At the district scale, deposits like Cripple Creek are characterized by voluminous metasomatism, multiple magmatic and hydrothermal events, and structurally focused zones of high-grade mineralization (Jensen and Barton, 2000). Because regional structures control magmatic and hydrothermal plumbing (Figure 17b), an understanding of structural patterns, the distribution and intensity of hydrothermal alteration, and the presence of geochemical anomalies is necessary for good exploration (Jensen and Barton, 2000).

Fluid flow in the Cripple Creek district is structurally controlled. Fluids tend to exploit faults, fractures, shear zones, and contacts between rock types. Dikes are

Figure 17 a (top) and b (bottom): Schematic cross section comparing proposed models for a typical epithermal system vs. an alkalic-type system like Cripple Creek.

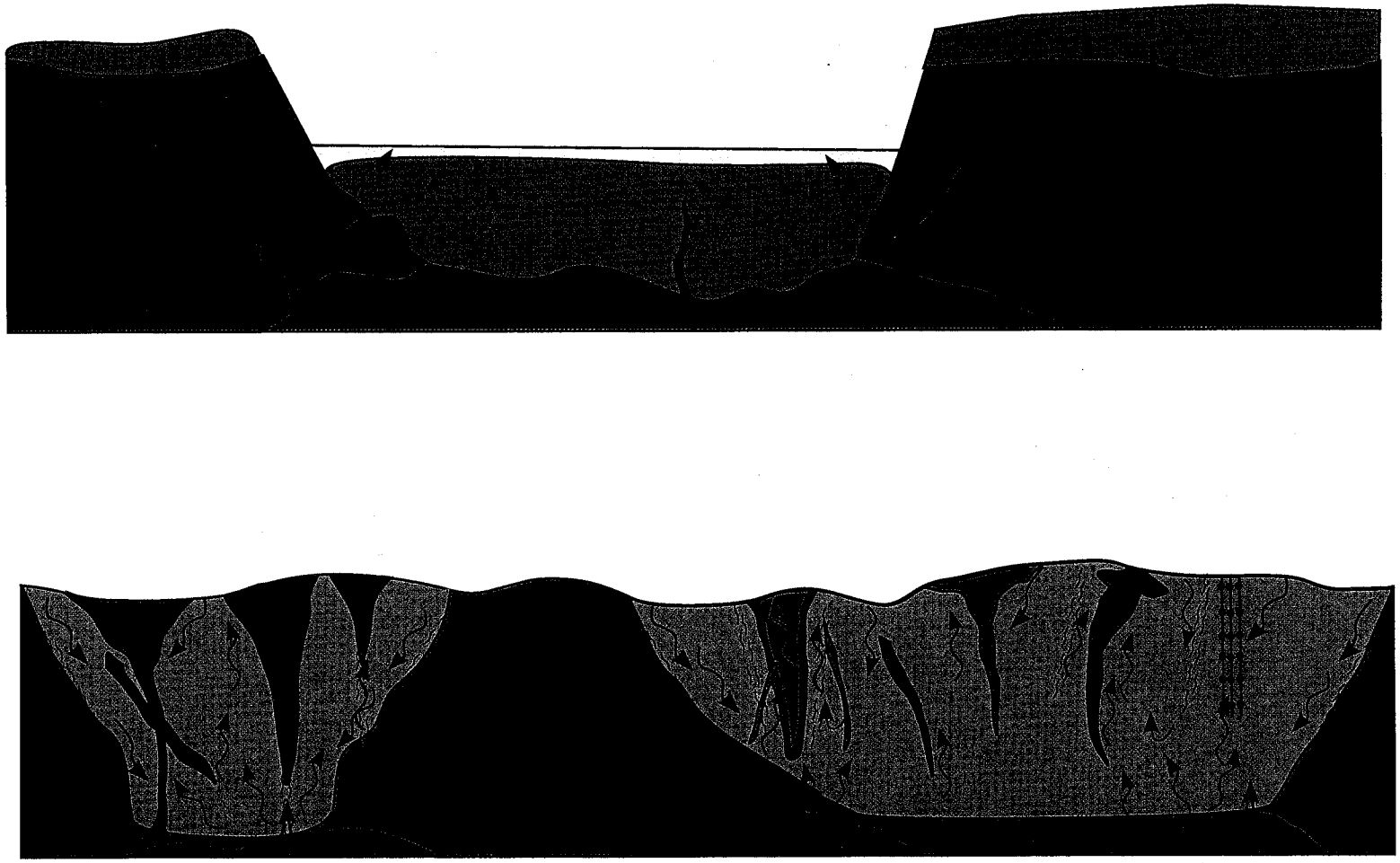

emplaced along the same trend (~N-S) as regional structures, and dike margins also function as conduits for mineralizing fluids. Evidence to support this is seen in assay data and as mineralized dike margins. Cripple Creek Breccia is often mineralized along dike margins, but the dikes themselves are barren. This suggests that fluids flow relatively more easily through the porous breccia than through dikes, and that when fluid flow is blocked by dikes or stocks, fluids pond up against the contact and are forced to flow along it.

Multiple magmatic events imply multiple source regions for fluids. Magmatic fluids likely ascend through the numerous breccia pipes so magmatic signatures would be expected in the vicinity of them and isotopic values would be expected to shift towards more meteoric values away from the pipes.

Figure 2 shows a cross section through several breccia pipes to illustrate the structural complexity of the district. Worthy of note are the Precambrian ridges (Granite Island) concealed beneath the Cripple Creek Breccia in areas of the district. These ridges divide the diatreme into sub basins, and may have blocked fluid flow between basins. If multiple breccia pipes throughout the district (located in different sub basins) each sourced fluids, it is likely that the isotopic signatures of fluids varied quite a bit on a spatial basis because the proportion of mixing between magmatic fluids and exchanged meteoric fluids could vary between the sub basins.

Figure 17 compares a simple epithermal mixing model to perhaps a more realistic scenario of hydrothermal plumbing in the structurally complex Cripple Creek District. Note the multiple "magmatic" and "meteoric" fluid sources, and the structural control on fluid flow. After considering a complex scenario for hydrothermal plumbing such as this,

the prospect of seeing small-scale isotopic patterns does not seem realistic.

This study finds that there are no discernable stable isotope patterns until a district-wide scale is considered, and the focus is broadened from ore-stage mineralization to encompass barren veins. When examined spatially (Figures 18a and b), the same data shows a broad zone, centered around the Ajax/Portland mines, characterized by a magmatic signature. Farther away from this zone, values get lighter, indicating fluids with more of a meteoric signature.

It is important to consider that this is three-dimensional data plotted in two dimensions. The deepest samples included in this study came from the southern part of the district. As a group, the deep samples include four known ore-stage samples and they have magmatic signatures (red of Figures 18a-c). Because they represent ore-stage fluids with a magmatic signature, as included in the discussion on Figure 12, areas with a magmatic signature may be promising exploration targets. It is assumed that the magmatic signature in the southern part of the district is not biased by ore stage samples because other "barren" samples with magmatic signatures are also located in the southern part of the district.

To eliminate the uncertainty in calculated values due to temperature discrepancies (pressure correction), Figures 18a and b are plots of the mineral isotope values, which exclude sedimentary dolomites, fracture surface mineralization, calcite replacing phenocryst sites, and calcite deposited by recent descending waters because they were likely deposited at low temperatures. The oxygen plot shows the clearest pattern, and the same pattern is visible in the carbon data. When oxygen fluid values are plotted (Figure 18c), the same pattern is observed, with a little less detail, indicating that the temperature

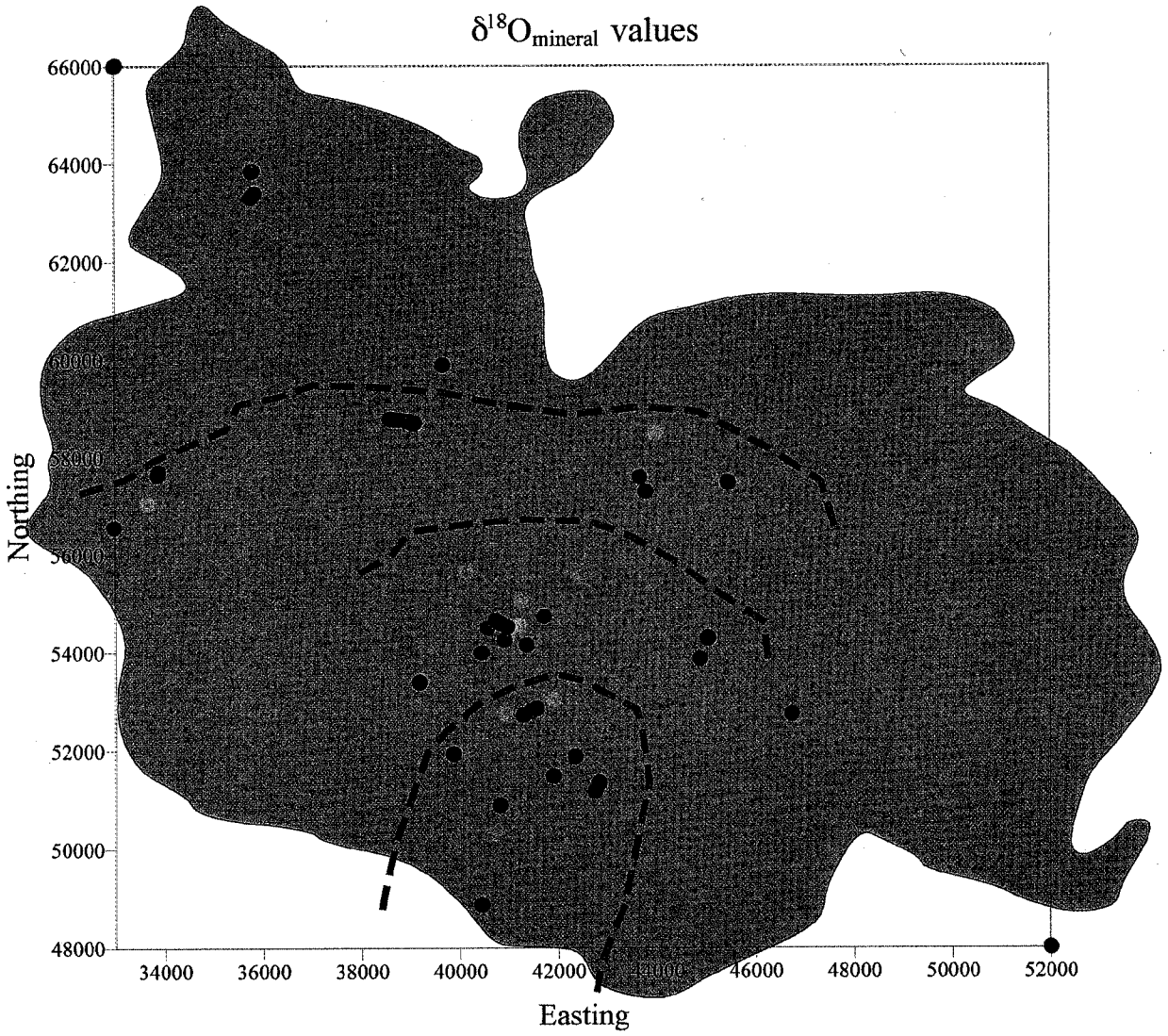

Figure 18a: Oxygen mineral values plotted spatially. Dots on the corners of the axes are for alignment only, not actual samples.

$\delta^{18}O_{mineral}$ ranges in per mil

- 15 to 18
- 12 to 14
- 9 to 11
- 6 to 8

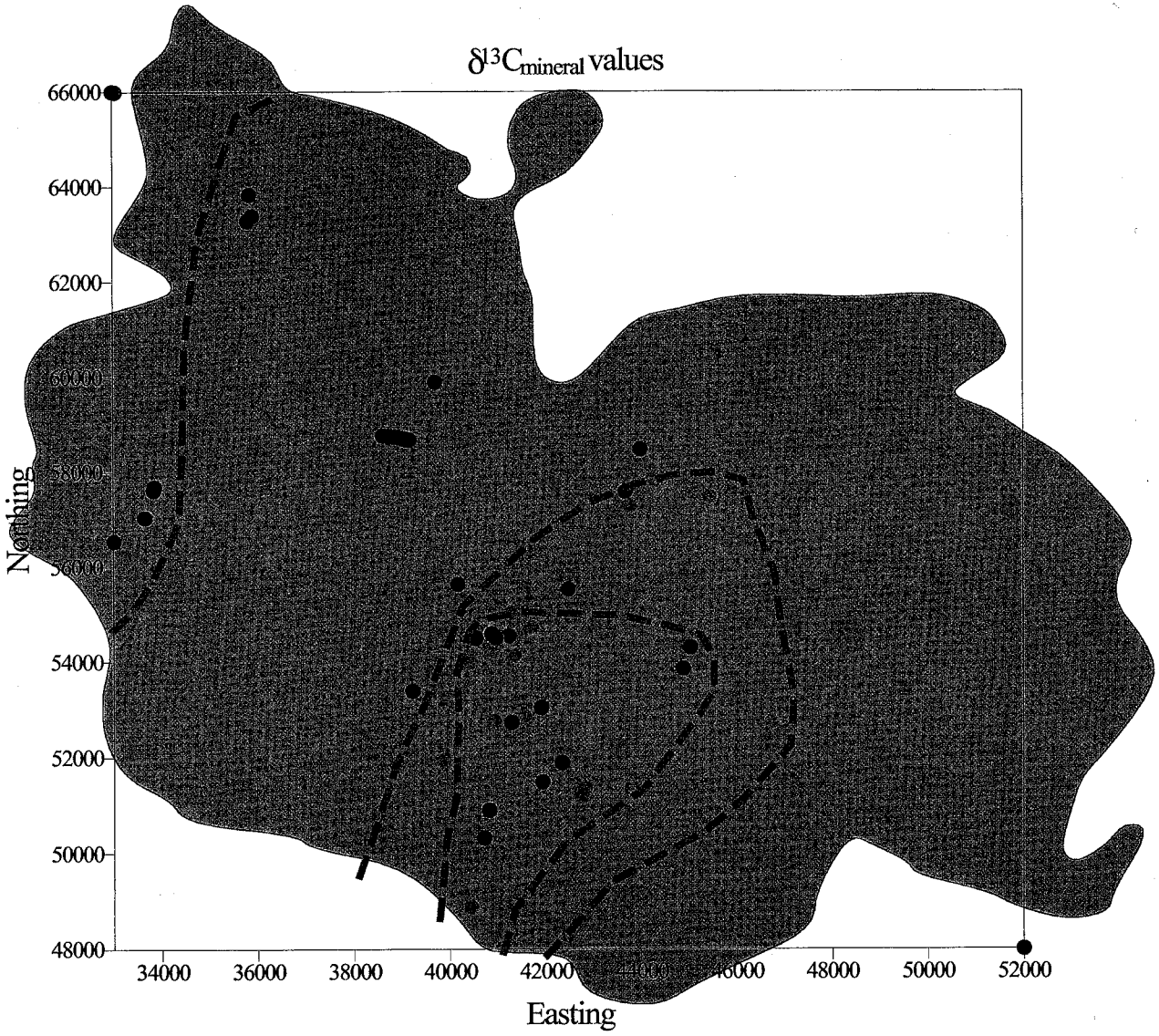

Figure 18b: Carbon mineral values plotted spatially. Dots on the corners of the axes are for alignment only, not actual samples.

$\delta^{18}O_{mineral}$ ranges in per mil

- -1 to 0
- -2 to -3
- -4 to -5
- -6 to -8

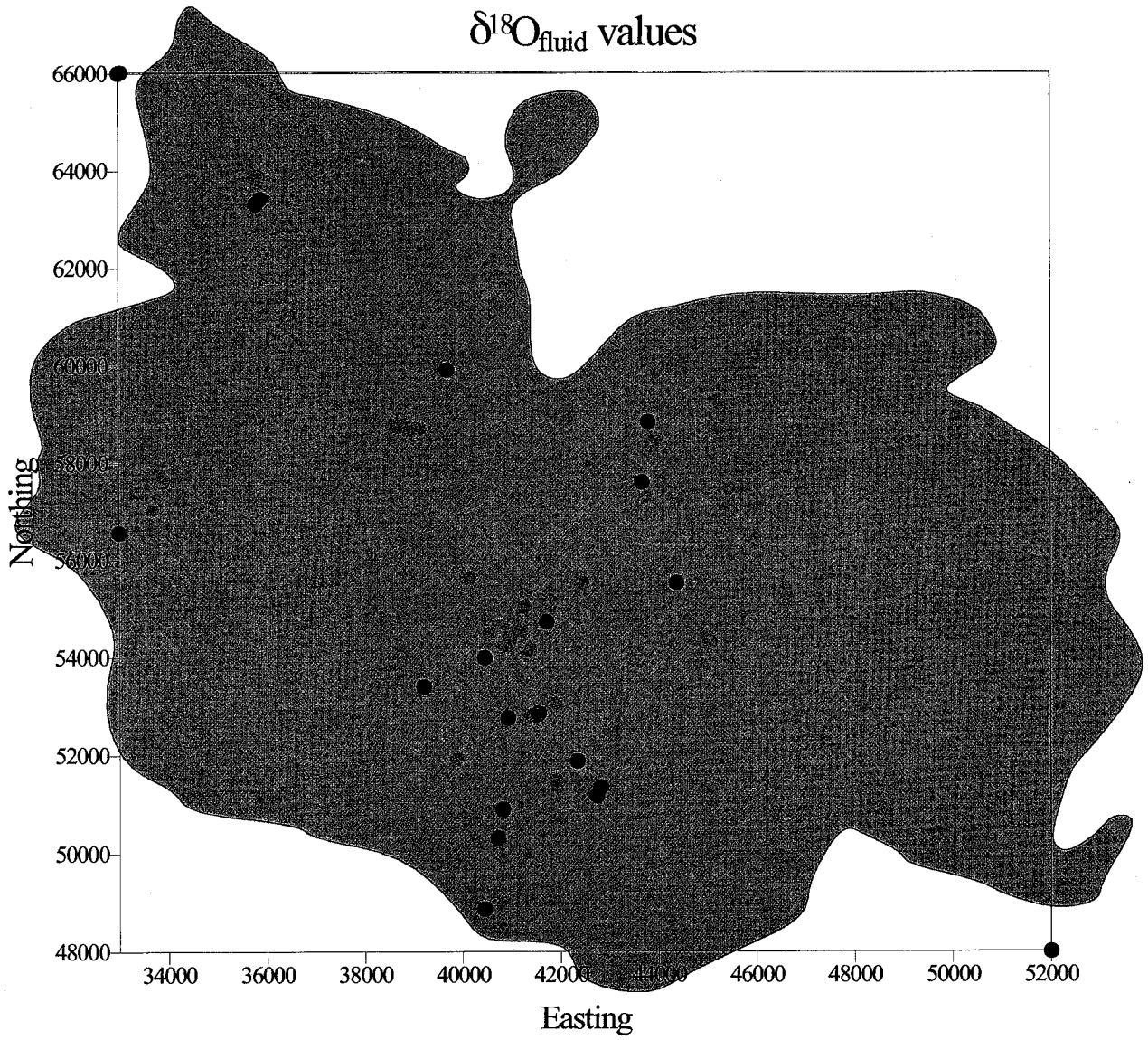

Figure 18c: Oxygen fluid values plotted spatially. Dots on the corners of the axes are for alignment only, not actual samples.

$\delta^{18}O_{fluid}$ ranges in per mil

- 6 to 13
- 1 to 5
- -5 to 0
- -13 to -6

discrepancies due to pressure correction do not have a very substantial effect. The carbon fluid values show no pattern. This may be attributed to several things: overall, the data show a narrow range of carbon values (Figure 12), so seeing relative differences between values is not as easy as with the oxygen data; and the reservoirs of carbon have larger ranges than oxygen does, making it more difficult to pinpoint a source.

All things considered, this isotopic pattern is intriguing and worthy of investigation. Based on previous research and data presented in this study, ore-stage mineralization consistently has a magmatic isotopic signature, and stable isotopic data may prove to be a valuable exploration tool.

CONCLUISONS

New stable isotope and fluid inclusion data from carbonates represent a broader spatial and temporal view of the district than previous research, which has focused on ore-stage mineralization. When this data is examined at a district scale, a geochemical trend becomes visible, suggesting mixing between magmatic and exchanged meteoric fluids. When examined spatially (Figures 18a and b), the same data shows a broad zone, centered around the Ajax/Portland mines in the southern part of the district, characterized by a magmatic signature. Farther away from this zone, values get lighter, indicating fluids with more of a meteoric signature. Because deep, ore-related samples from the Ajax/Portland mines have been shown to have magmatic signatures, areas with magmatic values may be promising exploration targets.

APPENDIX A: INTERPRETATION OF AGE DATES

Obtaining accurate age dates for rocks in the Cripple Creek District can be problematic due to the extent of hydrothermal alteration. Multiple stages of hydrothermal alteration have masked the original geochemical signatures of most rocks in the district. "Fresh", truly unaltered, rocks are rare, and although rocks may look "fresh" in hand sample, alteration may be subtle enough that it is only detectable under the electron microprobe. Samples must be carefully chosen for chemical analysis and age dating, and caution must be exercised when interpreting age dates. Alteration can "reset" argon systematics and produce apparent ages that are older than the true age. This is evidenced by lamprophyre dikes that are clearly the youngest intrusive phase based on crosscutting relationships, but give old apparent ages. The poor spectra obtained for many Ar/Ar and K/Ar analyses and lack of reproducibility of age dates is likely attributed to the effects of K-metasomatism that occurs during alteration events (Jensen, 2003). The reliability of the age data is based on correlation with observed field relationships and the extent of alteration/quality of spectra obtained. Age data are compiled in the following table for reference, but ages reported in the text are after Jensen (2003).

APPENDIX A: AGE DATA COMPILED FROM PREVIOUS STUDIES

DATE	ERROR	METHOD	SAMPLE	REFERENCE	LOCATION
31.9	1.7	Ar/Ar	N-2 tephriphonolite dike	Jensen, 2003	East Cresson
32.1	0.1	Ar/Ar	Tephriphonolite	Jensen, 2003	Vindicator
33.2	0.1	Ar/Ar	Phonolite	Jensen, 2003	Vindicator
27.8	0.3	Re/Os	Molybdenite vein	Jensen, 2003	Vindicator, 31 level
33.0	0.4	Ar/Ar	Biotite vein	Jensen, 2003	Vindicator, 31 level
33.7	0.4	Ar/Ar	Lamprophyre	Jensen, 2003	Ajax, 31 level
31.9	0.15	Ar/Ar	Tephriphonolite K-feldspar	Rampe, 2002; Table 3, thesis	
31.6	0.32	Ar/Ar	Phonolite K-feldspar	Rampe, 2002; Table 3, thesis	
31.2	0.1	Ar/Ar	Phonotephrite groundmass	Rampe, 2002; Table 3, thesis	
31.2	0.11	Ar/Ar	Phonotephrite K-feldspar	Rampe, 2002; Table 3, thesis	
31.1	0.04	Ar/Ar	N-2 tephriphonolite dike hornblende	Rampe, 2002; Table 3, thesis	
31.0	0.01	Ar/Ar	Tephriphonolite K-feldspar	Rampe, 2002; Table 3, thesis	
30.4	0.21	Ar/Ar	Lamprophyre phlogopite	Rampe, 2002; Table 3, thesis	
29.6	0.11	Ar/Ar	Phonolite groundmass	Rampe, 2002; Table 3, thesis	
29.0	0.08	Ar/Ar	Syenitoid K-feldspar	Rampe, 2002; Table 3, thesis	Beacon Hill
28.4	0.21	Ar/Ar	Cresson Pipe	Rampe, 2002; p.vi	
32.5	0.1	Ar/Ar	Sanidine in tephriphonolite	Kelley et al, 1998	
32.3	0.1	Ar/Ar	Biotite in tephriphonolite	Kelley et al, 1998	
31.8	0.2	Ar/Ar	N-2 tephriphonolite dike	Kelley et al, 1998	East Cresson
31.8	0.2	Ar/Ar	Satellite phonolite	Kelley et al, 1998	7 km outside diatreme
28.7	??	Ar/Ar	Isabella Dike	Kelley et al, 1998	East Cresson
31.8	0.2	Ar/Ar	Phonolite	Kelley et al, 1998	Vindicator
31.6	0.2	Ar/Ar	Tephriphonolite	Kelley et al, 1998	Vindicator
30.9	0.1	Ar/Ar	Sanidine in phonolite	Kelley et al, 1998	
29.6	0.1	Ar/Ar	Vein stage mineralization	Kelley et al, 1998	Vindicator
31.6	0.2	Ar/Ar	Trachyandesite	Kelley et al, 1998	Victor Pass
27.9	0.7	K/Ar	Phonolite	Wobus, 1976	
29.3	0.7	K/Ar	Phonolite	Wobus, 1976	
33.8	1.3	K/Ar	Aegerine-augite in syenite	McDowell, 1971	
33.4	1.0	K/Ar	Aegerine-augite in syenite	McDowell, 1971	

APPENDIX B: PREVIOUS WORK

Past research has documented consistent characteristics for the mineralizing fluids at Cripple Creek. Mineralization took place at relatively low temperatures (125-225°C) and salinities (< 5 wt. %), and like other alkalic-type deposits, Cripple Creek has heavy $\delta^{18}O$ values (3 - 9‰) for vein minerals and calculated fluid values, which is consistent with a magmatic source for mineralizing fluids (Jensen, 2003). This is an unusual characteristic relative to other, "classic" epithermal deposits that are dominated by meteoric fluids (O'Neil et al, 1973; O'Neil and Silberman, 1974; Taylor, 1973, 1974b; Bethke and Rye, 1979; Casedevall and Ohmoto, 1977; Criss and Taylor, 1983). Most studies on the Cripple Creek District to date acknowledge a minor shift in the stable isotope data to lighter $\delta^{18}O$ values during later stages of mineralization, suggesting that mixing with meteoric fluid may have been a factor; however, convincing data to support the presence of meteoric fluid is lacking.

Early Studies

The earliest and exceptionally detailed accounts of geology on the Cripple Creek district come from Cross and Penrose (1895) and Lindgren and Ransome (1906). These authors interpreted the deposit as a crater formed by explosive volcanic eruptions within Proterozoic rocks. Loughlin and Koschmann (1935) later realized that subsidence was largely responsible for the early formation of this deposit. Koschmann (1949) suggested that reactivation of preexisting structures controls the emplacement of intrusions and

formation of later conduits for ore fluids. Lovering and Goddard (1950) describe district geology and mineralization based on observations in active mines up to 1950.

Silberman, 1992

This study attempts to interpret the timing of mineralization and the evolution of the fluids responsible for mineralization and alteration with stable isotope and fluid inclusion data from different areas within the district. Cripple Creek shows similar temperatures to ore deposits of the Great Basin (O'Neil and Silberman, 1974), which are interpreted to have formed by epithermal circulation of predominantly meteoric water, but has enriched $\delta^{18}O$ values suggestive of a deeper origin for fluids (magmatic?).

Most temperatures reported are estimates (Reynolds, 1992) used to calculate the equilibrium ore fluid with Friedman and O'Neil's (1977) fractionation equations. Silberman proposes a mixing model in which he calculates magmatic to meteoric fluid ratios using end member compositions. Magmatic water is estimated to be 8.3‰, which falls in Taylor's (1979) range of 5.5 to 9.5‰ for magmatic water, based on average $\delta^{18}O$ of "unaltered" rocks in the district, and the value for meteoric water is –17.5 ‰ (Taylor, 1974).

Samples from quartz-pyrite veins in sericiticly altered Precambrian rocks from Grassy Valley are inferred to contain "magmatic" quartz typical of that in porphyry environments and trapping temperatures are estimated to be ~350°C (Reynolds, 1992). Calculated $\delta^{18}O$ fluid values (9.6, 5.5, and 5.0‰) are consistent with a magmatic or predominantly magmatic source. The other two samples ($\delta^{18}O$ fluid values 3.8 and 3.0‰) are interpreted to be the result of mixing 80% magmatic water with 20% meteoric.

Wild Horse: No fluid inclusion data was obtained for these samples, but based on

the assumption that the samples were deposited near surface; a temperature estimate of 180°C is used. Single samples of K-feldspar and quartz yield fluid values of –0.3 and 3.2‰, respectively. If the two minerals had formed at the same temperature, they were not in equilibrium. If they had formed from the same fluid, feldspar had to form at a higher temperature than quartz. If feldspar formed at 250°C, the fluid would be 20% meteoric, and if quartz formed at 180°C the fluid would be 33% meteoric.

Portland: Using the same estimate of 180°C, quartz yields a fluid composition of 1.8‰ and a whole rock adularia of –0.2‰, suggesting a 25% meteoric component.

Cresson: Samples taken from quartz-gold telluride, calcite-gold telluride, quartz-auriferous pyrite, adularia, and whole rock mineralization are listed in Table 1.

Table 1: Isotopic mineral values and calculated fluid values for Cresson samples.

Sample	$\delta^{18}O_{mineral}$‰	$\delta^{18}O_{fluid}$‰	**Estimated temperature and salinity**
calcite-gold telluride	17.3	6.6	165°-185°C, 4-6 eq. wt % NaCl
quartz-gold telluride	16.0	3.0	
quartz-gold telluride	17.6	4.6	
quartz-auriferous pyrite	13.6	0.6	
quartz-auriferous pyrite	18.2	5.2	
adularia	8.8	-2.0	170°-200°C for related fluorite
whole rock	10.8	0	
whole rock	12.0	1.2	
whole rock	12.2	1.4	
whole rock	10.3	-0.5	

Silberman suggests the fluid that deposited the calcite sample has a magmatic signature but is not in isotopic equilibrium with quartz at 180°C. Quartz would have been in equilibrium with a fluid that was 15-20% meteoric water. Fluids depositing quartz from auriferous pyrite samples could have 12-30%, and fluids depositing adularia may have up to 40 % meteoric water.

Altman (Gold Star Pit): Silberman cites only conclusions for this area, stating that he has a lot of detailed isotope data from a traverse across the Pharmacist vein system that leads him to believe the quartz formed from a dominantly magmatic fluid and

the K-feldspar altered wall rocks had a significant meteoric component. He interprets this as a predominantly magmatic fluid becoming diluted with meteoric water near the surface.

Based on this study, Silberman proposes a system in which magmatic waters (high, $\delta^{18}O$-enriched) move upward and mix with meteoric waters (low, $\delta^{18}O$-depleted) entering the system based on the fact that the data are not more consistent. Because the fluid inclusion temperatures are all approximately the same (< 200°C, with the exception of Grassy Valley), the fractionation effect of temperature should not affect how the data are scattered. If this was simply a cooling magmatic system, calculated fluid values should fall within a more restricted range. Mixing with meteoric water is suggested to causes the variation, and may be an important factor in triggering gold precipitation. Another way to explain the isotope values is through isotopic exchange with wall rocks, which is not addressed.

Preliminary K-Ar age data are also reported in this study (Table 2):

Table 2: K-Ar age data

Sample	**Mineral**	**Age (Ma)**
Monchiquite, Cres A-1	whole rock	29.0 ± 1.1
Vug fill, Cres A-2	adularia	31.2 ± 0.8
Drill cuttings, Cres A-3	roscoellite	28.3 ± 0.7
Breccia clasts, Cres A-4	adularia concentrate	29.3 ± 0.7
Altered volcaniclastic, Cres A-5	adularia	37.9 ± 0.1
Breccia clast, IA-1	sericite	30.8 ± 0.8
Breccia clast IA-2	sericite	32.7 ± 0.9
Altered breccia, GRA-1	sericite	35.6 ± 0.9
Altered rock, GRA-2	sericite	160 ± 3
Phonolite	sanidine	29.3 ± 0.7 (Wobus, 1976)
Phonolite	sanidine	27.9 ± 0.7 (Wobus, 1976)
Syenite	aegerine-augite	34.4 ± 1.0 (McDowell, 1971)

Based on this data, the ~1.5 km of Cripple Creek breccia had to accumulate and stop subsiding before 34 Ma, since the syenite gives the oldest age of intrusion. GRA-1,

GRA-2 and Cres A-5 appear to be anomalously old and the data need to be reexamined, but GRA-1and GRA-2 are from altered breccia so this may be interpreted as alteration that occurred before emplacement of alkaline rocks. The adularia in CresA-5 is from an altered volcaniclastic rock and may represent contamination from older feldspar. Sericite in sample IA-2 is inferred to constrain the timing of mineralization (32.7 ± 0.9 Ma) because the sericite is intergrown with quartz and fluorite containing visible gold. Sample IA-1 has sericitically altered clasts within a matrix of coarse, coxcomb quartz crystals that contain gold flakes. Sericite from the clast gives a date of 30.8 ± 0.8 Ma and is interpreted as either the age when the clast was incorporated into the quartz matrix or the age of an earlier alteration event, but in either case, Silberman suggests hydrothermal alteration occurred over at least 2 million years. Both of these dates are older than those reported in Kelley et al (1998). The whole rock Cres A-1 sample is interpreted as an intrusion age of the monchiquite (29.0 ± 1.1 Ma), which overlaps with mineralization age of Cres A-3 (28.3 ± 0.7 Ma). CresA-2 (31.2 ± 0.8 Ma) is older than the intrusion and is inferred to record a pre-monchiquite hydrothermal event.

Silberman proposes the following model based on preliminary data: The Cripple Creek volcanic center developed over 6.5 Ma, from the beginning stages of volcanic activity through the collapse of the hydrothermal system responsible for mineralization. Volcanic activity and subsidence began before 34.5 Ma, successive intrusions were emplaced until 28 Ma, and development of a hydrothermal system and mineralization followed. Silberman states that confirmation of these dates is needed, and more "well controlled" samples should be collected and dated. This study lacks well-constrained

mineralogy and paragenetic relationships, and the dates are not particularly reliable.

1996 SEG Guidebook: Pontius

Pontius (1996) presents a basic overview of the mining history, regional geology and district geology with descriptions of the rock types within the district and the occurrence of mineralization, as well as a model for formation of the district based on his own observations and data cited from Dwelley (1984) and Reynolds (1992). The model has two stages, but realistically there is probably a transition between the two. Pontius proposes that the beginning of hydrothermal activity coincided with the later stages of volcanism. Stage one involves resurgent doming and emplacement of phonolite was accompanied by high temperature (350°C), high salinity (~30 eq. wt. % NaCl) fluids responsible for widespread alteration. Stage 2 is a 2 Ma period during which cooler (160°-220°C), more dilute (<5 eq. wt. % NaCl) fluids circulated causing K-metasomatism, pyritization, and eventually depositing gold.

1996 SEG Guidebook: Beaty et al

Beaty et al (1996) studied stable isotopes of the Pharmacist vein system in the Altman area. The quartz-Au telluride-fluorite sheeted veins follow both northeast and northwest structures and are hosted primarily by phonolite, but phonotephrite and lamprophyre dikes are locally present. The richest ore occurs where veins of both trends intersect. Because mineral separates were difficult to obtain, whole rock samples of altered phonolite collected along three transects perpendicular to the northeast striking main Pharmacist vein were analyzed for oxygen isotopes and range from 7.10 to 14.31‰. Three samples of unaltered phonolite were collected from the Altman pit and another

from outside the district for comparison. Feldspar separates from a "possibly altered" phonolite yield $\delta^{18}O$ values of 10.53 and 11.19‰ and magnetite has a value of 5.44‰. Feldspar, clinopyroxene and magnetite from a fresh phonolite have $\delta^{18}O$ values of 9.41, 6.88 and 5.11‰, respectively. A whole rock value of 8.12‰ was obtained for a third phonolite. Feldspar and magnetite in phonolite from outside the district have values of 7.20 and 2.78‰. The authors assign a value of 8 to 9‰ as a pre-alteration background value of phonolite in the Altman area (Beaty et al, 1996). Presumably this is based on the whole rock value for a "fresh" phonolite. If this assumption is true, alteration increases the $\delta^{18}O$ signature by ~ 5‰ (up to 14.31‰) adjacent to the vein and the alteration halos appear to extend at least 30 m into the host rock from the vein. However, their figures show values closest to the vein increase then decrease with distance from the vein.

Phonotephrite and tephriphonolite dikes were also sampled but show no zonation around the veins. "Fresh" samples (45-55 m from the vein) have whole rock $\delta^{18}O$ values of 6.70 to 7.88‰ and altered samples (less than 10 m from vein) have values of 6.85 to 8.04‰, which is reported as no significant difference in this paper, but it is still a slight increase. In addition, three $\delta^{18}O$ values (7.91 to 9.52‰) and four $\delta^{13}C$ values (–5.48 to –4.75‰) for dolomite were obtained from these samples. The authors state that the $\delta^{18}O$ values approximate the typical range (7.9 to 9.5‰, not referenced) for igneous rocks and $\delta^{13}C$ values are similar to magmatic carbon (-2 to -5‰, Ohmoto and Rye, 1979). A dike that shows silicification gave a whole rock $\delta^{18}O$ value of 10.08‰. Two other altered rocks gave whole rock $\delta^{18}O$ values of 4.52 and 8.77 ‰. The low value of 4.52‰ is inferred to represent interaction with light meteoric water. The $\delta^{18}O$ values for four

quartz separates range from 18.01 to 23.71‰, and they represent vug quartz that post-dates mineralization. However, in the text two of these are cited as whole rock values and are inferred to indicate deposition at low temperature corresponding to increased fractionation.

A single sample of quartz-Au-telluride inferred to be part of the Pharmacist vein was analyzed for fluid inclusions. The sample shows three stages of quartz, all of which exhibit characteristics (explosion texture ?, milky?) of boiling, but they only obtained measurements from a growth zone that showed no evidence of boiling (?). Two phase, liquid dominant inclusions with no daughters or CO_2 homogenized from 177 to 257°C, with a mean of 220°C. No salinity data was obtained. The authors assume the temperature of alteration to be 200-250°C based on this data. Because the phonolite is composed predominantly of secondary feldspar the authors state that the isotopic composition of the fluid is calculated to be 4 to 7‰ using the alkali feldspar-water fractionation of O'Neil and Taylor (1967), which overlaps with Taylor's (1979) values for magmatic water. If they used reported feldspar values for these calculations there should be ~0 to 7‰ fractionation between the mineral and fluid, which means they had to use temperatures of 250°C and up.

The authors propose a model with altered phonolites adjacent to the vein having the lowest $\delta^{18}O$ values (7.10 to 14.31‰), "silicified rock from the upper levels of the hydrothermal system" (reported in their table 2 as quartz values) having intermediate values (~18‰), and the late stage vug quartz having the highest values (21 to 24‰) representing cooling of the ore fluid and increasing fractionation over time. The authors claim these results are consistent with the Altman rocks being flooded with a large

volume of heavy, $\delta^{18}O$-enriched ore fluid that mixed only locally at the margins of the deposit with light, $\delta^{18}O$-depleted meteoric water, but the conclusion cannot be proven without additional data. Because the meteoric water is represented by only one sample and the water-rock ratio is not known, they state that the composition of the light end-member fluid cannot be calculated. This study lacks well-constrained "fresh" vs. "altered" rocks and the data they base estimated temperature on is unreliable.

1996 SEG Guidebook: Thompson

Thompson (1996) includes a compilation of fluid inclusion studies done on veins throughout the district by students at the Colorado State University from 1982-1996. Some of this data has been published by Thompson and students (Thompson et al, 1985) in Economic Geology. The remainder is presented in the 1996 SEG field trip guidebook.

The Ajax mine: Mineralization in the Ajax mine occurs as sheeted zones of narrow veinlets, open space fillings, and disseminated Au-telluride mineralization in wallrock that extend up to 1000 m vertically (Thompson, 1996).

Thompson (1996) summarizes Dwelley's (1984) paragenesis (Table 3) for veins of the Ajax mine and applies it to "major veins" in the district to represent the deep environment that he later compares to the shallow environment characterized by the deposits like the Cresson diatreme and hydrothermal breccia pipes (minerals in parentheses reported in Thompson et al, 1985):

Table 3: Paragenesis after Dwelley (1984) and Thompson (1985)

Paragenesis for main stage veins

1. adularia + quartz + fluorite + dolomite + pyrite + marcasite
2. pyrite + marcasite + galena + sphalerite + chalcopyrite (+ quartz + pyrrhotite)
3. sphalerite + quartz + fluorite + pyrite + rutile (+ hematite – sphalerite)

4. quartz + pyrite + tellurides (+ rutile + acanthite)

5. vug filling quartz + chalcedony + fluorite + dolomite

Thompson (1996) reports fluid inclusions in Ajax stage 1 quartz homogenize from 234°-510°C (lower limit of 206°C, Thompson et al, 1985) and boiling is indicated by variable liquid to vapor ratios. Halite, sylvite and hematite daughters are common and salinities range from 28.1-47.8 eq. wt. % NaCl. Higher salinities occur in the upper 300 m of the vein system. He estimates true trapping temperatures to be ~200-320°C based on water-rich inclusions that yield trapping pressures of 360-400 bars (unpublished curves from Bodnar and Kuehn, not referenced). Thompson suggests ore fluid salinities dropped between stages 1 and 2, but he does not report any temperature or salinity data for stages 2 and 3 in this paper. In the 1985 paper he states stages 2 and 3 have progressively lower homogenization temperatures and salinities (0-8.3 eq. wt % NaCl). During stage 4 ore fluids were less than 200°C (reported as 105° to 159°C with a mean of 140°C in 1985 paper) with salinities from 7-9 eq. wt. % NaCl, which is much higher than the 1.4 to 3.5% range reported in the 1985 paper. Apparently higher temperatures are obtained from the Cripple Creek breccia hosted portions of the vein system (Thompson et al, 1985)

Lane (1976) measured homogenization temperatures of 168°-190°C in fluorite and 162°-266°C in barite in the El Paso mine, which correspond to Dwelley's Stage 3 for main stage veins. Burnett (1995) found filling temperatures in adularia at shallow levels in the Ajax to be 152°-262°C with salinities ~7 eq. wt. % NaCl.

Thompson et al (1985) present the following conclusions on deep, main stage veins in the 1985 paper: Ore fluids contained significant CO_2 ($CO_{2\,(L)} + CO_{2\,(V)} + H_2O$-

rich fluid) and estimated trapping pressures of 360 to 400 bars suggest first boiling would begin at a depth of 4,000 m under hydrostatic conditions but boiling occurred over the entire vertical interval of 1,050 m. As fluids boiled metal concentrations in the remaining fluid increased. Stage 1 fluids were saline and had temperatures over 300°C, indicating that chloride complexes probably transported gold. As ore fluids (less saline, below 160°C) were diluted due to meteoric influx, tellurium complexes became important and precipitation of gold was triggered by cooling.

Hydrothermal Breccias: Thompson (1996) states ore fluids responsible for mineralization in breccia pipes representing the shallower levels of the system were less saline (4-8 eq. wt. % NaCl) than veins, but have similar temperatures. Mineralization often occurs as open space filling within breccia pipes, and the various deposits have been studied in detail by Thompson's students. Paragenesis for mineralization in the hydrothermal breccias of the Ironclad and Globe Hill deposits was established by Seibel (1991). Boiling is documented in the upper portions of the Ironclad and Globe Hill hydrothermal breccias and the Cresson diatreme by Trippel (1985), Seibel (1991), Burnett (1995) and Thompson (1996).

Thompson (1996) presents the generalized version of Seibel's (1991) paragenesis (Table 4) for hydrothermal breccia hosted ores below and applies it to the Cresson diatreme:

Table 4: Paragenesis for breccia-hosted mineralization

1. adularia + quartz + apatite + pyrite/marcasite + fluorite + hematite
2. celestite + sericite + dolomite + barite + galena + sphalerite + chalcopyrite + fluorite + pyrite + quartz + rutile
3. Au-telluride + pyrite + dolomite + quartz + sericite + native gold + Fe-Mn oxides

The Ironclad deposit is a mineralized breccia pipe (90 by 150 m, extending to at least 320 m deep) that formed by cyclic brecciation, fluidization and mineralization of phonolite. Seibel (1991) classifies its formation into three events (all gold-bearing), which he summarizes in the 1996 SEG Guidebook:

1. Brecciation + precipitation of Au° + drusy quartz + chalcedony + fluorite + carbonates ± celestite (in matrix of clasts) + potassic alteration of clasts. Fluid inclusions from this stage homogenize below 186°C and some, with variable liquid to vapor ratios in individual growth bands, indicate that the fluids were boiling. Depressed melting temperatures, which give salinities less than 10 eq. wt. %, are inferred to be caused by the presence of CO_2. In addition to CO_2 other compounds must have been present in the fluids because some inclusions showed double menisci. The fluids are also interpreted to be alkaline (pH 5 – 6.5) and oxidized based on stability ranges of the mineral assemblage present.

2. Stage 2 brecciation is identified by fragments of stage 1 breccia + matrix sized material + Mn-Fe oxides (± cryptomelane) ± quartz. Fluids are inferred to be more oxidized than stage 1.

3. Stage 3, the most voluminous, contains clasts of the first two stages and occurs as both clast and matrix supported breccias as well as massive and bedded microbreccias. The bedded units display flow structures around clasts, channeling, and graded bedding parallel to host rock contact that are interpreted to have formed by repeated episodes of subsurface fluidization.

1996 SEG Guidebook: Seibel

Seibel (1996) states that oxygen isotopes from early stages of minerlaization

support a dominantly magmatic source for fluids, and speculates gold was transported as a bisulfide complex and precipitated by an increase in oxygen fugacity and pH caused by boiling, but does not cite any data. Seibel (1991) also suggests that CO_2 effervescence may have caused deposition of feldspar.

The Globe Hill ore bodies occur at the intersections of northeast and northwest or east and west trending structures just west of the Globe Hill breccia pipe, a triangular body approximately 300 m on a side (Seibel, 1996). Ore is characterized by irregular anastomosing veins of Au° ± Au-telluride ± Mn-Fe oxides ± halloysite ± fluorite in phonolite (Seibel, 1996). Trippel (1985) summarizes the development of the Globe Hill system in four events, which is described in more detail in Thompson et al, 1985:

1. Structurally controlled hydrothermal brecciation + calaverite + chalcedony + quartz + celestite + fluorite + carbonate + pyrite + anatase + monazite + sphalerite + galena + chalcopyrite + pyrrhotite + specularite + rutile + sericite + montmorillinite.

2. Development of veins with mineralogy similar to stage 1 with the absence of chalcedony, monazite and rutile.

3. Brecciation with rock flour matrix and no associated mineralization.

4. Another stage of hydrothermal brecciation resulting in an anhydrite or montmorillinite cemented breccia with the same mineral assemblage as the second stage.

Five stage 1 fluorite inclusions homogenized between 371° and 425°C and six stage 2 quartz inclusions homogenized between 198.6° and 210.6°C, and an additional one at 331.3°C (Thompson et al, 1985), but because the inclusions have variable liquid to vapor ratios suggestive of boiling they are interpreted to be trapped at temperatures below 198.6°C (Trippel, 1985).

The Cresson diatreme is a lamprophyre breccia pipe with mineralization occurring dominantly within open space between breccia clasts. Saunders (1986) and Nelson (1989) found no evidence for boiling fluids at depth in the Cresson diatreme hosted deposit. No specific data is reported for the Cresson diatreme in Thompson's 1996 paper, but Kelley et al (1998) state that mineralizing fluids were low temperature (135°-175°C), low salinity (3-9.6 eq. wt % NaCl), neutral to alkaline (pH ~5-6) and relatively oxidized (Saunders, 1986).

Saunders (1986) suggests gold telluride complexes could account for the amount of gold throughout the vertical extent of veins and that oxidation was the triggering mechanism for gold telluride precipitation followed by native gold under most oxidizing conditions. Thompson speculates gold was transported initially as chloride or bisulfide complexes and suggests other complexes were significant in an alkaline fluid under boiling conditions because bisulfide complexes would have destabilized before gold telluride deposition so paragenetically Au° would come first, which is the opposite of what is observed. Because the amount of gold remains fairly consistent throughout the vertical extent of veins (up to 1000 m) and temperatures decrease towards the surface and with time, Thompson argues that temperature was not responsible for triggering precipitation of gold, which contradicts his conclusions in the 1985 paper.

Thompson reports sulfur isotope data from galenas in the district are very light ($\delta^{34}S$ = -6.8 to –21.1‰) and in general show lightest values at shallower depths. No locations or interpretations have been given for this data. Because $\delta^{32}S$ fractionates into the vapor phase during boiling leaving behind fluids enriched in $\delta^{34}S$ (Ohmoto and Rye, 1979), these observations would be consistent with a shallow boiling horizon, where the

galenas formed from condensing H_2S. In the Ajax mine, Thompson states that fluids boiled over the entire vertical interval of 1050 m. If the S data does suggest a shallow boiling horizon, the shallower parts of the system must have experienced boiling for a lengthier amount of time relative to the deep environment.

Based on oxygen isotope data reported in Beaty et al (1996), Kelley et al (1996), and Fears (1986) and the high salinities presented in his 1996 study, Thompson supports a predominantly magmatic source for fluid, and proposes that the change over time from an H_2S dominated system to predominantly $SO4^{=}$ is a result of oxidation due to either mixing with meteoric water or boiling.

He further states trace element geochemistry links ore fluids to lamprophyre intrusions, which are also inferred to be the source of metals and $H_2\tilde{S}$ CO_2 collected from deep in the Ajax mine has $\delta^{13}C$ of –3.2‰, which approaches –3‰ for Hawaiian fumaroles and –7‰ for CO_2 dissolved in basaltic magmas, and is inferred to indicate derivation from an alkaline mafic melt.

Thompson, 1998

In his GSA abstract Thompson (1998) again reports five paragenetic stages for vein mineralization. Temperatures and salinities obtained from fluid inclusion studies are consistent with his 1996 observations. The data reported for the "bulk tonnage" deposits (hydrothermal breccias) is a combination of observations from his 1985 and 1996 papers. He states that ore fluids are magmatically derived based on fluid inclusion, stable isotope and trace element data. S data are inferred to indicate oxidation of fluid and H_2S: $SO4^{=}$ ratios. He also states Au:Ag ratios of dore produced over the past 100 years are higher (~10) in deeper levels compared to shallow levels (< 5). A correlation between Au and

K_2O, As, Te, and F in shallow level deposits is inferred, but no correlation with Ag and S is evident.

Jensen, 1998

Jensen's (1998) GSA abstract describes K-metasomatism alteration halos (adularia-pyrite- Fe, Ca, Mn, Mg carbonate-quartz-fluorite-TiO_2-tetrahedrite-sphalerite-galena-sericite ± roscoellite ± monazite ± bast (?) ± U-Th minerals) associated with high-grade Au-telluride veins. The halos are typically greater than 20 times vein width and coalesce to form broad zones of alteration that occur throughout most of the diatreme. Ore fluids are interpreted to be high in CO_2 based on the increasing carbonate:pyrite ratio outward from the veins and the lack of acid alteration. Clay and sericite alteration are pervasive in the upper 300 m of the system but become fracture controlled and more restricted with depth as do veins. Based on stable isotope and mass balance data, Jensen suggests a large volume of magmatic hydrothermal fluid is required to have entered the system syn- to post-lamprophyre time. Early, high temperature veins (biotite-pyrite-K-feldspar-fluorite-carbonate-base metal ± magnetite) present in deepest exposures but rare at shallow levels are inferred to be ore stage and are sometimes overprinted by later, low temperature Au-rich mineralization associated with deep carbonate ± base metal veins up to 2 m wide, anhydrite-celestite veins, albite-pyrite-sulfate veins and Ca-Na amphibole mineralization. Early alteration types include biotite-magnetite-K-feldspar (fracture controlled, associated with syenite), pervasive biotite-magnetite ± pyrite (deep), and pervasive K-feldspar-hematite (occurs at all levels) and are inferred to be associated with early intrusions and not related to gold mineralization.

Rosduetscher, 1998

Rosdeutscher (1998) studied stable isotopes of O, H, and S, and fluid inclusion data from quartz-adularia-pyrite-kaolinite veins hosted largely in Proterozoic granodiorite to constrain an origin for the mineralizing fluid responsible for depositing the disseminated gold in the Grassy Valley area of the district. Results are presented in a M.S. thesis and summarized in a 1998 GSA abstract. $\delta^{18}O$ and δD values for illite, kaolinite, and quartz were measured and isotopic fluid values were calculated using an average temperature of 300°C for Group 1 inclusions, described below. For ten illite samples, $\delta^{18}O$ and δD values range from 7.0 to 12.2‰ and –109 to –63‰ respectively. Nine kaolinite samples have $\delta^{18}O$ values from 13.4 to 15.9‰ and δD values from –106 to –80‰. Only four $\delta^{18}O$ values (19.2 to 22.7‰) were obtained for quartz. Calculated fluid $\delta^{18}O$ and δD values range from 3.5 to 8.7‰ and –84 to –38‰ for illite, and 7.8 to 10.3‰ and –88 to –62‰ kaolinite, respectively. Calculated fluid $\delta^{18}O$ values from quartz are 12.2 to 15.4‰. $\delta^{34}S$ values for 23 vein pyrites range from –10.4 to –3.9‰ with a mean of –5.3‰. In contrast to Thompson's (1996) statement, Rosdeutscher states no apparent relationship between depth and $\delta^{34}S$ values exist.

Eight samples of vein quartz were analyzed to obtain 24 homogenization temperatures and 10 salinity measurements. Two types of fluid inclusions can be identified. The first group consists of two-phase (L + V), liquid-rich (~90 % L) inclusions that homogenize between 228° and 432°C and have salinities from 3.3 to 6.6 eq. wt. % NaCl. The less abundant group 2 contains three-phase (L + V + NaCl) inclusions that homogenize between 407° and 467°C and have salinities ≥ 26 eq. wt. % NaCl; however, a pressure correction of 40° to 50°C (Potter, 1977) may be applied based

on Pontius's 1992 estimate that approximately 500 m of erosion have taken place since the end of volcanism in the district.

Rosdeutscher concludes that O and H isotopic values from illite and quartz suggest a magmatic origin for hydrothermal fluids, and S isotope values indicate a magmatic source for S. Mineralizing fluids were hot (~470°C) and became cooler with time as sericite precipitated followed by quartz + adularia + auriferous pyrite at around 300°C, and dickite and kaolinite at even lower temperatures. Kaolinite mineralization appears to be hypogene, but without a definite temperature estimate it is unclear whether the data indicate a supergene meteoric source at 35°C, or a magmatic fluid at 200°C.

Kelley et al, 1998

Kelley et al (1998) used a variety of techniques to investigate the timing of emplacement and mineralization and probable sources for alkalic magmas and hydrothermal fluids. Research has been published in Economic Geology and summarized in a GSA abstract. Based on trace element geochemistry, the authors propose fractional crystallization of phonotephrite creates the more felsic trachyandesite, tephriphonolite and phonolite; but, as Jensen and Barton (2000) point out, the intrusions become more mafic with time, so this model does not apply.

$\delta^{18}O$ values obtained from clinopyroxene (5.5-6.5‰ in syenites, 4.9-5.9‰ in mafic igneous rocks) and feldspar (6.6-7.6‰ in syenites, 6.6-8.0‰ in phonolites) separates overlap with values typical of unaltered mafic rocks (~ 5 to 8‰ for basalts and gabbros) according to Taylor and Sheppard (1986). Mineral values were used to calculate whole rock or "magma compositions", which range from 6.4-7.1‰ in phonotephrite and 7.7-8.4‰ in tephriphonolite, trachyandesite and phonolite. The

authors claim increasing values with differentiation throughout the suite is to be expected (Taylor and Sheppard, 1986). Based on timing relationships described above, differentiation is highly unlikely, and if it did occur at equilibrium above 900°C, the effect would be smaller than 1‰ (Taylor and Sheppard, 1986). They also state that the 1.8‰ difference between the tephriphonolite/trachyandesite (felsic, earlier), and the phonotephrite (mafic, later) and the low (<9‰) calculated "magma" values are consistent with a source in the upper mantle/lower crust, and upper crustal contamination was not significant.

Pb isotopes indicate that the source rocks for Cripple Creek magmas maintained low U/Pb ratios for a significant amount of geologic time and had average Th/Pb ratios, both of which are consistent with a source that has evolved in the lower crust after granulite metamorphism has preferentially expelled U relative to Th. Pb isotopes of galena were used to infer the source of Pb in ore fluids. Vein galena and K-feldspar are either equal to or more radiogenic than whole rock (phonolite) samples analyzed, which is interpreted as a Pb contribution to ore fluids from surrounding Proterozoic rocks. As expected, towards the periphery of the diatreme, fluids interacted to a greater degree with Proterozoic rocks and show more radiogenic values.

Sr isotope compositions of the more mafic rocks ($^{87}Sr/^{86}Sr$ = .70391-.70474) overlap with subcontinental lithospheric mantle (.7035-.7100) and oceanic island basalts (.7028-.7070) (McDonough et al, 1985) and are consistent with a metasomatized mantle source. The more radiogenic ratios of phonolites (.70600 and .71249) suggest crustal assimilation. However, one phonolite falls on the borderline with a value of .70475, and should be grouped with the mafic rocks.

Based on their observations thus far, it makes sense for the early, more felsic phonolites to have assimilated some crustal material as conduits were established during initial emplacement. With time these conduits would be coated by earlier eruptions and successive eruptions would assimilate less crustal material. This may be a reason the magmas appear more mafic and primitive with time.

$^{40}Ar/^{39}Ar$ geochronology was utilized to establish when the igneous activity in the district began. Sanidine from a tephriphonolite gives an age of 32.5 ± 0.1 Ma, and biotite from a different tephriphonolite yielded an age of 32.3 ± 0.1 Ma. These two dates are reported as statistically identical. This data negates the fractional crystallization model in which the authors propose phonotephrite is the oldest intrusive phase. Phonolite ages range from 31.8 to 30.9 Ma. Three sanidine dates reported for phonolite are 31.8 ± 0.1, 31.6 ± 0.1, and 30.9 ± 0.1 Ma and a trachyandesite age is 31.6 ± 0.2 Ma. The authors conclude tephriphonolite was emplaced first, followed by phonolite and trachyandesite. The younger phonolite date, recorded six km outside the district, is inferred to represent a second phase of phonolite emplacement.

K-feldspar and biotite from veins place an upper constraint of 31.3-29.6 Ma on gold mineralization because this is thought to be the early, high temperature form of alteration. Kelley et al (1998) calculated the composition of mineralizing fluids at the Ocean Wave mine based on $\delta^{18}O$ values for K-feldspar (7.9‰) and biotite (3.4‰) from their study and temperatures of mineralization (250°C) from Thompson (1996). Fluid $\delta^{18}O$ values (2.4 and 4.2‰) approach the range for magmatic water, but they do not address what would cause a shift toward lighter values. Two biotites gave δD values of –174 and –196‰, and again using 250°C, calculated fluids have δD values of –116 and

–138‰ if an equation for biotite-water (400-800° C; Kyser, 1987) is used. But, if Venneman and O'Neil's (1996) equation for biotite-H^+ (150-400°C) is used, fluid values of -74 and –96‰ move much closer to the magmatic range of -50 to –85‰ (Taylor, 1979).

In conclusion to their study the authors propose a timeline of events described in detail in the paper, but only briefly summarized here. They cite a change from compression to extension between 40 and 32 Ma and they suggest "postsubduction melting of the asthenosphere and subcontinental lithospeheric mantle generated alkaline, volatile-rich magmas that assimilated and mixed with lower crust and differentiated by fractional crystallization (which has already been discussed as an unlikely model above) during and/or after ascent." Felsic magmas (32.5-30.9 Ma), followed by mafic and ultramafic magmas ascended rapidly along fractures and were emplaced in the shallow crust. During the later stages of fractional crystallization, a predominantly magmatic fluid enriched in K, S, and F deposited biotite, K-feldspar, dolomite, fluorite and pyrite. Beginning ~ 31 Ma, gold and gold tellurides were deposited. Mineralization continued until 30 Ma, possibly longer.

Mote, 2000

The focus of Mote's 2000 study was to characterize the fluids responsible for vein mineralization hosted predominantly in the Precambrian granodiorite based on fluid inclusion data from deep drill hole UGC 97-5 along the margin of Granite Island. Seven samples of quartz-carbonate-sulfate-K-feldspar vein material were analyzed to obtain approximately 100 homogenization temperatures and 80 salinity measurements. Fluid

inclusions observed fall into the following four categories:

1. Moderate salinity (0.1 to 25 eq. wt. % NaCl), two phase ($H_2O_{(L)}$ + $H_2O_{(V)}$) inclusions that homogenize from 190° to 320°C.

2. Halite-bearing inclusions (salinities > 40 eq. wt. % NaCl) present at depths of 2585 to 2770 to feet. This group contains halite ± sylvite ± unknown daughter salt ($CaCl_2$?) ± opaque daughter mineral (hematite?) and homogenizes from 350° to > 500°C.

3. Inclusions that can be classified as groups 1 or 2 but also contain CO_2. This group homogenizes to temperatures from 300° to > 500°C, indicating CO_2 was trapped as a vapor phase.

4. Vapor rich inclusions present in samples at depths of 1235', 1922', and 2770' (observed but decrepitated before a measurement could be obtained). These inclusions are assumed to have low salinities because they are 60 to 80 % vapor (?). 3 inclusions homogenize from 400° to 500°C and one at 640°C.

Mote concluded that the presence of type 3 inclusions indicates a salt oversaturated fluid that may have helped in the transport of Au, the presence of type 4 inclusions indicates boiling may have occurred deep in the system, and the data observed is consistent with the presence of an intrusion at depth.

Jensen and Barton, 2000

Jensen and Barton (2000) attempt to summarize characteristics of gold deposits associated with alkaline magmatism. As a group these deposits can be characterized by:

1. Multiple intrusive phases and complex evolutionary histories. In the case of Cripple Creek, intrusions become more mafic with time and are likely derived from different sources. Most researches in Cripple Creek have tried to link gold with the

intrusive phases observed, but Jensen and Barton suggest that the intrusion responsible for introducing the gold has not yet been identified.

2. Relatively cool (< 300°C as compared to porphyry types) fluid with low salinities (< 10 eq. wt % NaCl) and moderate to high CO_2 concentrations. Cripple Creek may have formed at pressures higher than are typical of most epithermal deposits because fluid inclusions contain liquid CO_2 (Thompson et al, 1985). Fluids are inferred to be near neutral based on the widespread stability of K-feldspar and carbonate and the lack of significant hydrothermal quartz.

3. A high concentration of magmatic fluids is inferred because reported stable isotope data overlap with magmatic fluid compositions, but commonly approach lighter values during later stages of mineralization which may indicate mixing with a lighter end member fluid. However, the authors state that Cripple Creek and epithermal deposits in the Black Hills may have formed almost exclusively from magmatic fluids.

4. Alkaline epithermal deposits may transition into porphyry-type Cu (Au) deposits at depth, and this is usually evidenced by low temperature alteration overprinting higher temperature alteration, which is documented at Cripple Creek (Jensen et al, 1998).

5. Phlogopite present in deep, high temperature biotite alteration infers high oxidation states (Wones and Eugster, 1965; Beane, 1974; Guidotti, 1984), as does the presence of sulfates (Thompson et al, 1985; Saunders and May, 1986; Moyle et al, 1990; Richards and Kerrich, 1993).

6. Alkaline deposits typically have moderate to low sulfidation states and contain magnetite ± hematite, sphalerite (Fe-rich), and tetrahedrite-tennantite.

7. Because alkaline epithermal deposits are characterized by near-neutral, low

salinity, S-bearing fluids, gold is transported as a bisulfide ($Au(HS)_2^-$) complex (Seward, 1973; Romberger, 1991), whereas base metals have a low solubility. The authors state that telluro-complexing of gold suggested by previous papers (Thompson et al, 1985; Saunders and May, 1986; Richards, 1995) is not likely because gold-tellurium complexes would have to be orders of magnitude more stable than gold-sulfide complexes to transport gold.

8. Gold precipitation may be triggered by different mechanisms, several of which may be influencing fluid compositions contemporaneously: boiling, fluid mixing resulting in a change in oxidation state or dilution, cooling, and wall rock reaction (sulfidation that destabilizes gold-sulfide complexes). Evidence for wall rock reaction (sulfidation) is seen at Cripple Creek where mineralization occurs disproportionately around lamprophyres and other mafic rocks.

Jensen's current survey on S isotopes throughout the district shows clear evidence for at least two, if not multiple, fluid sources along the periphery of the diatreme. Although his O values are fairly consistent throughout the district, there is enough variation for some degree of mixing to have taken place (Jensen, written comm., 2002).

APPENDIX C: DATA COMPILED FROM PREVIOUS FLUID INCLUSION STUDIES

HOMOGENIZATION TEMPERATURE (°C)	AVERAGE T_H	LOCATION	MINERALOGY	SALINITY (EQUIVALENT WEIGHT % NaCl)	AVERAGE	REFERENCE	OBSERVATIONS
105 - 159	132	Ajax	stage 4, precious metal stage	1.4 - 3.5	2.45	Collins, 1979	weakly boiling, stage 3 - 4, internal CO2 pressure ~ 44 bars, trapping pressure ~ 360 - 400 bars) reference in Thompson, 1986
105 - 159	132	Ajax	stage 4 quartz (ore stage)	7 - 9	8	Thompson, 1985	mean T_H = 140°C
155 - 262	209	Ajax	adularia	7	7	Burnett, 1995	
200 - 350 (T_T)	275	Ajax	stage 1 quartz	28.1 - 47.8	37.95	Thompson,19 85	upper limit cited as 320°C in Thompson, 1996
206 - 510 (T_H)		Ajax	stage 1 quartz			Collins, 1979	internal CO_2 pressure ~ 27 bars, reference in Thompson, 1986
206 - 510 (T_H)		Ajax	stage 1 quartz	28.1 - 47.8	37.95	Thompson, 1995	variable liquid to vapor ratios suggest boiling; halite, sylvite and hematite daughter minerals common
234 - 510 (T_H)		Ajax	stage 1 quartz	28.1 - 47.8	37.95	Thompson, 1996	same as above
< 150	150	Ajax	main stage tellurides	1.4 - 3.5	2.45	Thompson, 1985	weakly boiling, dilute fluids
350	350	Ajax		30	30	Dwelley, 1994	reference in Pontius, 1996
131 - 175	153	Cresson diatreme	mineralized samples	< 3	3	Nelson, 1989	reference in Thompson, 1992
165 - 185	175	Cresson diatreme	fluorite			Silberman, 1992	related to adularia
170 - 200	185	Cresson diatreme	calcite + tellurides	4 - 6	5	Silberman, 1992	
162 - 266	214	El Paso	barite			Lane, 1976	correlate with Dwelley's stage 3 at Ajax
168 - 190	179	El Paso	fluorite			Lane, 1976	correlate with Dwelley's stage 3 at Ajax
198.6 - 210.6	205	Globe Hill	stage 2 quartz			Thompson, 1986	degree fill 5-50%, average T_H = 203.5°C, boiled or effervesced, true $T_T \leq 198.6$
371 - 425	398	Globe Hill	fluorite, stage 1 chalcedonic quartz			Thompson, 1986	degree fill ~ 1-50%, variable liquid to vapor ratios, true T_T < 370°C
< 198.6	198	Globe Hill				Trippel, 1985	
228 - 432	330	Grassy Valley	vein quartz, Group 2	≥ 26	26	Rosdeutscher, 1999	
228 - 467	348	Grassy Valley	vein quartz, Group 1	3.6 - 6.6	5.1	Rosdeutscher, 1999	most were not measured due to small inclusion size or metastable behavior during freezing runs
< 186	186	Ironclad breccia pipe	native gold	< 10	10	Siebel, 1996	boiling, CO_2-rich, pH 5.5-6.5
177 - 257	217	Pharmacist Vein, Altman	quartz + tellurides			Beaty et al, 1996	mean T_H = 220°C, no evidence for CO_2, 2 phase, liquid dominant, no daughters
190 - 320	255	UGC 97-5 (1235-2779 ft)	vein quartz ± (K-feldspar + carbonate + sulfide)	0.1 - 25	12.55	Mote, 2000	
350 - > 500	425	UGC 97-5 (1235-2779 ft)	vein quartz ± (K-feldspar + carbonate + sulfide)	> 40	40	Mote, 2000	halite, sylvite and unknown daughter minerals present
400 - 500 (640?)	450	UGC 97-5 (1235-2779 ft)	vein quartz ± (K-feldspar + carbonate + sulfide)			Mote, 2000	vapor rich, most decrepitated ~500°C
>500 - 600	550	UGC 97-5 (1235-2779 ft)	vein quartz ± (K-feldspar + carbonate + sulfide)			Mote, 2000	CO_2-rich
140 - 210	175		quartz + dolomite	1 - 10	5	Saunders, 1988	average T_H = 167°C for quartz and 190°C for dolomite, no evidence for boiling, gas hydrates present, dolomite → calaverite + quartz + celestite → chalcedonic quartz
160 - 220	190		telluride stage	< 5	5	Reynolds, 1992	reference in Pontius, 1996
350	350		pre-telluride stage fluids			Kelley, et al 1996	average T_H = 350°C

APPENDIX D: STABLE ISOTOPE DATA COMPILED FROM PREVIOUS STUDIES

See List of Symbols for key to rock types and lithologic descriptions

RESERVOIRS

	$\delta^{13}C$	$\delta^{18}O$	$\delta^{34}S$	δD	REFERENCE	NOTES
Meteoric water	-10 to -2				Ohmoto and Rye, 1979	
Mantle	-5		0		C (Ohmoto and Goldhaber, 1997), O (Ohmoto and Rye, 1979)	
Magmatic water	-5 to -2	5.5 to 9.5	-3 to 3		C (Ohmoto and Rye, 1979) for mantle derived rocks, O (Taylor, 1979), S (Rosdeutscher, 1999)	
Degassed magmatic CO_2	-8 to -4				C (Barnes, 1978)	
Hawaiian fumarole	-3.00				Thompson, 1996	
CO_2 dissolved in basaltic magmas	-7.00				Thompson, 1996	
Magnetite series granites			1 to 10		Ohmoto and Goldhaber, 1997	
Ilmenite series granites			-1 to -10		Ohmoto and Goldhaber, 1997	
Submarine volcanics			0 to 10		Ohmoto and Goldhaber, 1997	
Basalts (ave MORB)	-6.4		0.5		Deines, 1992	
Igneous rocks	-20 to 3		-10 to 20		Ohmoto and Goldhaber, 1997	
Organics	-25				Ohmoto and Goldhaber, 1997	
Black shales	ave -20				Ohmoto and Goldhaber, 1997	
Modern limestone	0 ± 2	30			Ohmoto and Goldhaber, 1997	
Freshwater limestone	-10 to -2				C (Ohmoto and Rye, 1979)	
Atmospheric	-7				C (Campbell, 1998)	

CARBONATES

CO_2 from deep Ajax	-3.20				Thompson, 1996	
Oligocene meteoric water in Creek		-10.00			Rosdeutscher, 1999	
Meteoric water		-17.50			Taylor, 1979	
Calcite + Au - tellurides, Cresson		17.30			Silberman, 1992	Calculated ore fluid 6.6
Dolomite + trace calcite from "fresh" basalt 150-180 ft from Pharmacist	-5.48	7.91			Beaty et al 1996	N2 whole rock $\delta^{18}O = 7.26$
Dolomite + trace calcite from more altered basalt closer to Pharmacist	-5.01	8.82			Beaty et al 1996	N1B whole rock $\delta^{18}O = 7.73$
Other dolomite from "basaltic dikes" Altman pit	-5.30				Beaty et al 1996	N1A whole rock $\delta^{18}O = 7.88$
Other dolomite from "basaltic dikes" Altman pit	-4.75	9.52			Beaty et al 1996	N1C whole rock $\delta^{18}O = 7.29$
25-L-24, calcite deposited from 1925 descending waters in Cresson blowout	5.49	22.11			Analyzed this study	
Galena (district)			-6.8 to 21.1		Thompson, 1996	
Vein pyrite, Grassy Valley			-10.4 to -3.5		Rosdeutscher, 1999	

SILICATES

QUARTZ

FXU-20, Pharmacist Vein		20.688			Jensen, 2003	
DDHS 2-198.5, Newmarket Vein System		20.064			Jensen, 2003	
CL 4063, Quartz + fluorite + calcite from Rose Nichol Mine		19.298			Jensen, 2003	
AI 5 1601, Independence Vein		18.985			Jensen, 2003	
CL 4018, Quartz + calcite from Isabella Mine		18.803			Jensen, 2003	
FXU-20, Pharmacist Vein		18.452			Jensen, 2003	
NS-PHO-VN, Quartz + telluride vein, 10050 level, Cresson Pit		18.448			Jensen, 2003	
HOC-92-1-497.5, Quartz + telluride vein, vicinity of Howard Mine		18.357			Jensen, 2003	
39-K-175, Quartz + telluride vein, 8th level Cameron Mine		17.779			Jensen, 2003	
AJX-DEX-1700, Dexter Vein, 17th level Ajax Mine		17.708			Jensen, 2003	
41-K-89A, Quartz + fluorite vein, 5th level Index Mine		17.686			Jensen, 2003	
AN 3-678.5, Newmarket vein system		17.650			Jensen, 2003	
AN 8, X-10-U-8		17.405			Jensen, 2003	
24-L-1850 SU, Mineralized Cresson Pipe, Cresson 18		17.162			Jensen, 2003	
39-K-2, Quartz + sulfide + calcite vein, Anchoria Leland 1		17.003			Jensen, 2003	
CL-4018, Quartz + calcite vein from Isabella Mine		16.799			Jensen, 2003	
CR-1023-400, Mineralized quartz + fluorite breccia, Cresson		16.756			Jensen, 2003	
37-K-90, Quartz + fluorite vein, Mary Nevin 1		16.754			Jensen, 2003	
HOC92-1-497.5, Quartz + telluride vein, vicinity of Howard Mine		16.494			Jensen, 2003	
24-L-48B, Quartz + fluorite from Dexter vein, Portland 17		16.273			Jensen, 2003	
EP 7 TILLEY, high grade vein, 7th level, El Paso		16.130			Jensen, 2003	
CL 4068, Quartz + telluride veins, Wild Horse Mine		16.096			Jensen, 2003	
41-K-74, Quartz vein, 3100 level, Carlton Tunnel		15.422			Jensen, 2003	

APPENDIX D: STABLE ISOTOPE DATA COMPILED FROM PREVIOUS STUDIES, PAGE 2

SILICATES

QUARTZ, CONTINUED

	$\delta^{13}C$	$\delta^{18}O$	$\delta^{34}S$	δD	REFERENCE	NOTES
I141-MMR-5-535, Quartz from weakly mineralized/barren veins		30.801			Jensen, 2003	
STAGE 3, Quartz from weakly mineralized/barren veins		24.126			Jensen, 2003	
STAGE 2, Quartz from weakly mineralized/barren veins		22.007			Jensen, 2003	
STAGE 1, Quartz from weakly mineralized/barren veins		19.735			Jensen, 2003	
V 35 FL, Quartz from weakly mineralized/barren veins		18.975			Jensen, 2003	
V 37 QZB, Quartz from weakly mineralized/barren veins		18.638			Jensen, 2003	
UGC 97-5 2777, Quartz from weakly mineralized/barren veins		18.493			Jensen, 2003	
V 37 QZA, Quartz from weakly mineralized/barren veins		17.946			Jensen, 2003	
AJX-DEX- 1700, Quartz from weakly mineralized/barren veins		17.708			Jensen, 2003	
I 126.SBFL, Quartz from weakly mineralized/barren veins		17.097			Jensen, 2003	
178.FLTRAIL, Quartz from weakly mineralized/barren veins		15.241			Jensen, 2003	
AN3-678-5QZ, Quartz from weakly mineralized/barren veins		14.886			Jensen, 2003	
UGC 97-3 1768, Quartz from weakly mineralized/barren veins		14.651			Jensen, 2003	
UGC 97-4 1881, Quartz from weakly mineralized/barren veins		14.325			Jensen, 2003	
I 181-CC-92-46-1256.FL, Quartz from weakly mineralized/barren veins		14.288			Jensen, 2003	
CC-92-46, Quartz from weakly mineralized/barren veins		14.155			Jensen, 2003	
DDU-2-192 LATE, Quartz from weakly mineralized/barren veins		14.123			Jensen, 2003	
I 170.FL, Quartz from weakly mineralized/barren veins		14.075			Jensen, 2003	
CR 1628-926, Quartz from weakly mineralized/barren veins		14.060			Jensen, 2003	
37-K-90-S1, Quartz from weakly mineralized/barren veins		13.854			Jensen, 2003	
24-L-74-S1, Quartz from weakly mineralized/barren veins		13.611			Jensen, 2003	
92-46-160, Quartz from weakly mineralized/barren veins		13.570			Jensen, 2003	
BANTA, Quartz from weakly mineralized/barren veins		13.318			Jensen, 2003	
FOREST QUEEN, Quartz from weakly mineralized/barren veins		10.933			Jensen, 2003	
36-K-3 S1, Quartz from weakly mineralized/barren veins		10.778			Jensen, 2003	
AJX-24-2400, Quartz from weakly mineralized/barren veins		10.377			Jensen, 2003	
UGC 5-201, Quartz from weakly mineralized/barren veins		8.913			Jensen, 2003	
AJZ 24 2400, Quartz from weakly mineralized/barren veins		8.639			Jensen, 2003	
24-L-1850 S1, Quartz from weakly mineralized/barren veins		8.084			Jensen, 2003	
CL 678, Quartz from molybdenite vein with phologopite alteration halo		9.639			Jensen, 2003	
Quartz from Xgd, Grassy Valley, GVC-1-292.5		22.7			Rosdeutscher, 1999	Calculated fluid $\delta^{18}O = 15.4$
Quartz from Xgd, Grassy Valley, GVC-1-482		19.2			Rosdeutscher, 1999	Calculated fluid $\delta^{18}O = 11.8$
Quartz from Xgd, Grassy Valley, GVC-3-473		20.2			Rosdeutscher, 1999	Calculated fluid $\delta^{18}O = 12.83$
Quartz from Gneiss, Grassy Valley, GC-8-413		19.6			Rosdeutscher, 1999	Calculated fluid $\delta^{18}O = 12.2$
Quartz veins throughout district		13.6 to 18.2			Pontius, 1992 (ref in Kelley 1996 and 1998)	
Quartz (vug) from Pharmacist vein, center outcrop trench		23.71			Beaty et al, 1996 (ref in Kelley, 1998)	
Quartz out of altered phonolite, Allman pit, 530 bench, TR-12 #09		20.72			Beaty et al, 1996	
"Other altered rocks" silicified rock, Bull Hill 880-33(A1)		18.01			Beaty et al, 1996	Elevation 10,667
"Other altered rocks" silicified rock, Bull Hill 880-33(A2)		18.41			Beaty et al, 1996	Elevation 10,667
Quartz, magmatic type, Grassy Valley		14.9			Silberman, 1992	Calculated ore fluid $\delta^{18}O = 9.6$
Quartz, early magmatic type, late epithermal, Grassy Valley		11.2			Silberman, 1992	Calculated ore fluid $\delta^{18}O = 5.9$?
Quartz, magmatic type, Grassy Valley		8.3			Silberman, 1992	Calculated ore fluid $\delta^{18}O = 3.0$
Quartz, magmatic type, Grassy Valley		10.3			Silberman, 1992	Calculated ore fluid $\delta^{18}O = 5.0$
Vuggy silica replacement (sample is mostly feldspar), Grassy Valley		7.9			Silberman, 1992	Calculated ore fluid $\delta^{18}O = 3.8$ (assuming sample is k-spar)
Quartz from Wild Horse		16.2			Silberman, 1992	Calculated ore fluid $\delta^{18}O = 3.2$
Quartz from Portland		14.8			Silberman, 1992	Calculated ore fluid $\delta^{18}O = 1.8$
Quartz, Au-Te from Cresson		16.0			Silberman, 1992	Calculated ore fluid $\delta^{18}O = 3.0$
Quartz, Au-Te from Cresson		17.6			Silberman, 1992	Calculated ore fluid $\delta^{18}O = 4.6$
Quartz, Au-pyrite from Cresson		13.6			Silberman, 1992	Calculated ore fluid $\delta^{18}O = 0.6$
Quartz, Au-pyrite from Cresson		18.2			Silberman, 1992	Calculated ore fluid $\delta^{18}O = 5.2$

K-FELDSPAR

V-17-658MT, Orthoclase vein from 3100 level Vindicator		8.020			Jensen, 2003	
L, Orthoclase vein from 3100 level Vindicator		7.386			Jensen, 2003	
L #2, Orthoclase vein from 3100 level Vindicator		7.386			Jensen, 2003	

APPENDIX D: STABLE ISOTOPE DATA COMPILED FROM PREVIOUS STUDIES, PAGE 3

SILICATES

K-FELDSPAR, CONTINUED	$\delta^{13}C$	$\delta^{18}O$	$\delta^{34}S$	δD	REFERENCE	NOTES
V-17-697, Orthoclase vein from 3100 level Vindicator		6.500			Jensen, 2003	
V-19-733, Orthoclase vein from 3100 level Vindicator		6.393			Jensen, 2003	
VIND OR, Orthoclase vein from 3100 level Vindicator		5.972			Jensen, 2003	
39-K-132, adularia from margins of veins, adjacent wallrocks		13.345			Jensen, 2003	
K-124, adularia from margins of veins, adjacent wallrocks		13.281			Jensen, 2003	
AN 3-678.5, adularia from margins of veins, adjacent wallrocks		12.711			Jensen, 2003	
CL-96-73-443, adularia from margins of veins, adjacent wallrocks		11.397			Jensen, 2003	
HOC 92-1-497.5, adularia from margins of veins, adjacent wallrocks		9.667			Jensen, 2003	
HOC 92-1-497.5,adularia from margins of veins, adjacent wallrocks		9.672			Jensen, 2003	
HOC 92-1-493, adularia from margins of veins, adjacent wallrocks		9.602			Jensen, 2003	
HOC 92-1-494, adularia from margins of veins, adjacent wallrocks		9.123			Jensen, 2003	
HOC 92-1-495, adularia from margins of veins, adjacent wallrocks		8.962			Jensen, 2003	
92-46-161, adularia from margins of veins, adjacent wallrocks		8.129			Jensen, 2003	
DDHS-8-533, adularia from margins of veins, adjacent wallrocks		7.592			Jensen, 2003	
92-46-160, adularia from margins of veins, adjacent wallrocks		7.394			Jensen, 2003	
39-K-119, adularia from margins of veins, adjacent wallrocks		6.723			Jensen, 2003	
CR-1023-400, adularia from margins of veins, adjacent wallrocks		1.826			Jensen, 2003	
Adularia from, vug filling from Cresson		8.8			Silberman, 1992	Calculated ore fluid δ18O = -2.0
K-feldspar from Wild Horse		10.5			Silberman, 1992	Calculated ore fluid δ18O = -0.3
K-feldspar veins throughout the district		8.8 to 12.2			Ponfius, 1992 (ref in Kelley 1998)	
K-feldspar from vein at Ocean Wave		7.9		-174	Kelley et al, 1998	
Adularia from pre-telluride veins		7.9			Kelley et al, 1996	
K-feldspar in altered phonolite adjacent to Au-Te vein		11.5			Kelley et al, 1996	
K-feldspar in altered phonolite adjacent to Au-Te vein		12.2			Kelley et al, 1996	
Coarse K-feldspar from "fresh" phonolite, Altman pit 89-CC-001		10.53			Beaty et al, 1996	
Fine-grained K-feldspar from "fresh" phonolite, Alt pit 89-CC-004		11.19			Beaty et al, 1996	
K-feldspar from phonolite (outside district) 89-CC-PH1		7.20			Beaty et al, 1996	
K-feldspar from phonolite ("least altered rocks from district") CCPH1		7.2			Kelley et al, 1998	
K-feldspar from phonotephrite ("least altered rocks from district") CC010		6.70			Kelley et al, 1998	
BIOTITE						
V-17-670, Biotite from veins at the 3100 level Vindicator		7.030			Jensen, 2003	
, Biotite from veins at the 3100 level Vindicator		6.157			Jensen, 2003	
V-19-697, Biotite from veins at the 3100 level Vindicator		5.979			Jensen, 2003	
V-12-366, Biotite from veins at the 3100 level Vindicator		5.773			Jensen, 2003	
VIND, Biotite from veins at the 3100 level Vindicator		5.371			Jensen, 2003	
Biotite from vein at Mollie Kathleen				-196	Kelley et al, 1998	
Biotite from vein at Ocean Wave		3.4			Kelley et al, 1998	
Biotite from pre-telluride veins		3.4			Kelley et al, 1996	
Biotite from pre-telluride veins				-174	Kelley et al, 1996	
Biotite from pre-telluride veins				-196	Kelley et al, 1996	
PLAGIOCLASE						
Plagioclase from phonolite ("least altered rocks from district") CC009		7.1			Kelley et al, 1998	
Plagioclase from trachyandesite ("least altered rocks from district") CC007		7.4			Kelley et al, 1998	
Plagioclase from phonotephrite ("least altered rocks from district") CC005		7.5			Kelley et al, 1998	
Plagioclase from phonotephrite ("least altered rocks from district") CC008		6.8			Kelley et al, 1998	
CLINOPYROXENE						
Clinopyroxene from phonolite ("least altered rocks from district") CC009		6.0			Kelley et al, 1998	
Clinopyroxene from tephriphonolite ("least altered rocks from district") CC010		6.0			Kelley et al, 1998	
Clinopyroxene from phonotephrite ("least altered rocks from district") CC005		5.8			Kelley et al, 1998	
Clinopyroxene from phonotephrite ("least altered rocks from district") CC008		5.3			Kelley et al, 1998	

APPENDIX D: STABLE ISOTOPE DATA COMPILED FROM PREVIOUS STUDIES, PAGE 4

SILICATES

KAOLINITE

	$\delta^{13}C$	$\delta^{18}O$	$\delta^{34}S$	δD	REFERENCE	NOTES
Kaolinite from Xgd, Grassy Valley, GVC-4-50		15.9		-80	Rosdeutscher, 1999	Calculated fluid $\delta^{18}O$ = 10.3, δD = -62
Kaolinite from Xgd, Grassy Valley, GVC-4-194		13.4		-106	Rosdeutscher, 1999	Calculated fluid $\delta^{18}O$= 7.8, δD = -88, sample contains both kaolinite and dickite
Kaolinite from Xgd, Grassy Valley, GVC-4-262.5		14.7		-96	Rosdeutscher, 1999	Calculated fluid $\delta^{18}O$ = 9.13, δD = -78
Kaolinite from Xgd, Grassy Valley, GVC-4-499		13.8		-86	Rosdeutscher, 1999	Calculated fluid $\delta^{18}O$ = 8.2, δD = -69
Kaolinite from gneiss, Grassy Valley, GVC-3-114.5		14.4		-84	Rosdeutscher, 1999	Calculated fluid $\delta^{18}O$ = 8.8, δD = -66
Kaolinite from Xgd, Grassy Valley, GVC-8-665		15.5		-95	Rosdeutscher, 1999	Calculated fluid $\delta^{18}O$ = 9.9, δD = -78
Kaolinite from Xgd, Grassy Valley, GVC-9-489.5		14.7		-91	Rosdeutscher, 1999	Calculated fluid $\delta^{18}O$ = 9.2, δD = -73
Kaolinite from Xgd, Grassy Valley, GVC-9-664		13.6		-100	Rosdeutscher, 1999	Calculated fluid $\delta^{18}O$ = 8.0, δD = -83
Kaolinite from Xgd, Grassy Valley, GVC-8-637.5		15.1		-88	Rosdeutscher, 1999	Calculated fluid $\delta^{18}O$ = 9.5, δD = -71, sample contains both kaolinite and dickite
Kaolinite from Xgd, Grassy Valley, GVC-9-489.5					Rosdeutscher, 1999	Calculated fluid $\delta^{18}O$ = 9.2, δD = -73
Kaolinite from Xgd, Grassy Valley, GVC-9-489.5					Rosdeutscher, 1999	Calculated fluid $\delta^{18}O$ = 9.2, δD = -73
Kaolinite from Xgd, Grassy Valley, GVC-9-489.5					Rosdeutscher, 1999	Calculated fluid $\delta^{18}O$ = 9.2, δD = -73

ILLITE

Illite from Xgd, Grassy Valley, GVC-1-519		12.2		-84	Rosdeutscher, 1999	Calculated fluid $\delta^{18}O$ = 8.7, δD = -59
Illite from Xgd, Grassy Valley, GVC-6-155.5		10.4		-81	Rosdeutscher, 1999	Calculated fluid $\delta^{18}O$ = 6.9, δD = -56
Illite from gneiss, Grassy Valley, GVC-3-128		10.8		-69	Rosdeutscher, 1999	Calculated fluid $\delta^{18}O$ = 7.3, δD = -44
Illite from gneiss, Grassy Valley, GVC-8-167		8.6		-63	Rosdeutscher, 1999	Calculated fluid $\delta^{18}O$ = 5.1, δD = -38
Illite from gneiss, Grassy Valley, GVC-8-558		10.2		-90	Rosdeutscher, 1999	Calculated fluid $\delta^{18}O$ = 6.7, δD = -38
Illite from Xgd, Grassy Valley, GVC-4-1134		7.0		-80	Rosdeutscher, 1999	Calculated fluid $\delta^{18}O$ = 3.5, δD = -65
Illite from aphanitic phonolite, Grassy Valley, GVC-1-439.5		10.5		-90	Rosdeutscher, 1999	Calculated fluid $\delta^{18}O$ = 6.9, δD = -55
Illite from Xgd, Grassy Valley, GVC-1-397		10.9		-99	Rosdeutscher, 1999	Calculated fluid $\delta^{18}O$ = 7.4, δD = -74, contains mixture of illite and plagioclase
Illite from Xgd, Grassy Valley, GVC-4-994		10.20		-100	Rosdeutscher, 1999	Calculated fluid $\delta^{18}O$ = 6.7, δD = -75, contains mixture of illite and plagioclase
Illite from porphyritic phonolite, Grassy Valley, GVC-8-31.5		11.90		-109	Rosdeutscher, 1999	Calculated fluid $\delta^{18}O$ = 8.4, δD = -84, contains mixture of illite and plagioclase

OXIDES

MAGNETITE

131 Mt, Magnetite from veins at the 3100 level, Vindicator		1.90			Jensen, 2003
VIND Mt, Magnetite from veins at the 3100 level, Vindicator		1.25			Jensen, 2003
V-17-697, Magnetite from veins at the 3100 level, Vindicator		1.21			Jensen, 2003
V-12-366, Magnetite from veins at the 3100 level, Vindicator		0.93			Jensen, 2003
L #2 Mt, Magnetite from veins at the 3100 level, Vindicator		0.22			Jensen, 2003
L # 2 Mt, Magnetite from veins at the 3100 level, Vindicator		-0.04			Jensen, 2003
L # 1 Mt, Magnetite from veins at the 3100 level, Vindicator		-0.80			Jensen, 2003
Magnetite from phonolite (outside district) 89-CC-PH1		2.78			Beaty et al, 1996
Magnetite from trachyandesite ("least altered rocks from district") CC007		2.3			Kelley et al, 1998
Magnetite from phonotephrite ("least altered rocks from district") CC005		6.0			Kelley et al, 1998
Magnetite from phonotephrite ("least altered rocks from district") CC008		5.2			Kelley et al, 1998
Magnetite from monchiquite ("least altered rocks from district") CCTM1		4.6			Kelley et al, 1998
Magnetite from monchiquite ("least altered rocks from district") CCTM1		4.9			Kelley et al, 1998
Magnetite from phonolite ("least altered rocks from district") CCPH1		2.8			Kelley et al, 1998

SULFIDES

PYRITE

UGC 97-5 2358, Ironclad, Globe Hill area			-2.70		Jensen, 2003
UGC 97-5 2777, Ironclad, Globe Hill area			-2.60		Jensen, 2003
90 DDH8-1050, Ironclad, Globe Hill area			-2.90		Jensen, 2003
90 DDH8-1050 PY, Ironclad, Globe Hill area			-2.17		Jensen, 2003
IC PY, Ironclad, Globe Hill area			-4.91		Jensen, 2003
UGC 2-1902.5, Cresson Pit			0.40		Jensen, 2003
UGC 2-2017, Cresson Pit			-0.70		Jensen, 2003
FXU-19, Cresson Pit			-1.40		Jensen, 2003
HITZ-VN PY, Cresson Pit			-4.19		Jensen, 2003
DRAB A PY, Cresson Pit			-6.10		Jensen, 2003

APPENDIX D: STABLE ISOTOPE DATA COMPILED FROM PREVIOUS STUDIES, PAGE 5

SULFIDES

PYRITE, CONTINUED	$\delta^{13}C$	$\delta^{18}O$	$\delta^{34}S$	δD	REFERENCE	NOTES
PIT PY, Cresson Pit			-4.84		Jensen, 2003	
Moffat 700 PY, Western margin of diatreme			1.63		Jensen, 2003	
KEYSTONE, Western margin of diatreme			1.70		Jensen, 2003	
154 PY, Western margin of diatreme			2.12		Jensen, 2003	
EP9B PY, Western margin of diatreme			2.91		Jensen, 2003	
WEST VEIN PY, distal base metal-rich			-2.40		Jensen, 2003	
39-K-180 PY, from sedimentary rocks, Eastern sub-basin			-3.50		Jensen, 2003	
39-K-180 PY, from sedimentary rocks, Eastern sub-basin			-3.75		Jensen, 2003	
GVC 92-79 PY, 3100 level Ajax/Vindicator Mines			-4.70		Jensen, 2003	
GVC 92-1-591, 3100 level Ajax/Vindicator Mines			-4.20		Jensen, 2003	
A 31-27-111, 3100 level Ajax/Vindicator Mines			-3.50		Jensen, 2003	
A 31-23-10.5, 3100 level Ajax/Vindicator Mines			-3.10		Jensen, 2003	
A 31-25-164.5, 3100 level Ajax/Vindicator Mines			-1.10		Jensen, 2003	
A 31-23-115, 3100 level Ajax/Vindicator Mines			-0.60		Jensen, 2003	
A 31-27-141, 3100 level Ajax/Vindicator Mines			-0.30		Jensen, 2003	
Vein pyrite from Xgd, Grassy Valley, GVC-3-473			-10.4		Rosdeutscher, 1999	Calculated fluid $\delta^{18}O$ = 12.8
Vein pyrite from gneiss, Grassy Valley, GVC-3-114.5			-4.8		Rosdeutscher, 1999	Calculated fluid $\delta^{18}O$ = 8.8, δD = -66
Vein pyrite from Xgd, Grassy Valley, GVC-9-664			-5.3		Rosdeutscher, 1999	Calculated fluid $\delta^{18}O$ = 8.0, δD = -83
Vein pyrite from Xgd, Grassy Valley, GVC-6-155.5			-4.6		Rosdeutscher, 1999	Calculated fluid $\delta^{18}O$ = 6.9, δD = -56
Vein pyrite from gneiss, Grassy Valley, GVC-8-558			-4.7		Rosdeutscher, 1999	Calculated fluid $\delta^{18}O$ = 6.7, δD = -38
Vein pyrite from schist, Grassy Valley, GVC-2-74			-5.9		Rosdeutscher, 1999	
Vein pyrite from Xgd, Grassy Valley, GVC-2-110			-3.5		Rosdeutscher, 1999	
Vein pyrite from Xgd, Grassy Valley, GVC-2-147.5			-6.2		Rosdeutscher, 1999	
Vein pyrite from gneiss, Grassy Valley, GVC-3-98			-3.7		Rosdeutscher, 1999	
Vein pyrite from gneiss, Grassy Valley, GVC-3-107			-6.8		Rosdeutscher, 1999	
Vein pyrite from porphyritic phonolite, Grassy Valley, GVC-3-233			-3.7		Rosdeutscher, 1999	
Vein pyrite from gneiss, Grassy Valley, GVC-3-284			-5.2		Rosdeutscher, 1999	
Vein pyrite from hydrothermal breccia, Grassy Valley, GVC-4-105			-6.5		Rosdeutscher, 1999	
Vein pyrite from gneiss, Grassy Valley, GVC-4-544.5			-5.8		Rosdeutscher, 1999	
Vein pyrite from aphanitic phonolite, Grassy Valley, GVC-4-662.5			-3.9		Rosdeutscher, 1999	
Vein pyrite from gneiss, Grassy Valley, GVC-4-786			-4.3		Rosdeutscher, 1999	
Vein pyrite from gneiss, Grassy Valley, GVC-5-411			-4.5		Rosdeutscher, 1999	
Vein pyrite from gneiss, Grassy Valley, GVC-7-246			-5.7		Rosdeutscher, 1999	
Vein pyrite from Xgd, Grassy Valley, GVC-7-486			-5.1		Rosdeutscher, 1999	
Vein pyrite from gneiss, Grassy Valley, GVC-8-369			-5.3		Rosdeutscher, 1999	
Vein pyrite from gneiss, Grassy Valley, GVC-8-413			-6.2		Rosdeutscher, 1999	
Vein pyrite from Xgd, Grassy Valley, GVC-12-226			-6.4		Rosdeutscher, 1999	
Vein pyrite from Cripple Creek breccia, Grassy Valley, GVC-14-131			-5.0		Rosdeutscher, 1999	
CINNABAR						
37-K-69, late-stage vein			-13.82		Jensen, 2003	
GALENA						
PIT GN, Cresson Pit			-8.21		Jensen, 2003	
PIT GN, Cresson Pit			-8.98		Jensen, 2003	
Goodwill Adit, distal base metal-rich			-13.2		Jensen, 2003	
DDH58-52 GN, deep Pointer/Index Mines			-0.42		Jensen, 2003	
41-K-115B GN, deep Pointer/Index Mines			-13.08		Jensen, 2003	
A 31 30A-74, 3100 Level Ajax/Vindicator Mines			-8.0		Jensen, 2003	
A 31-23-115, 3100 Level Ajax/Vindicator Mines			-6.9		Jensen, 2003	
A 31-27-1111, 3100 Level Ajax/Vindicator Mines			-6.6		Jensen, 2003	
MOLYBDENITE						
V-7-431.5, 3100 Level Ajax/Vindicator Mines			-2.4		Jensen, 2003	
V-4-1007.5, 3100 Level Ajax/Vindicator Mines			-1.2		Jensen, 2003	

APPENDIX D: STABLE ISOTOPE DATA COMPILED FROM PREVIOUS STUDIES, PAGE 6

SULFIDES

	$\delta^{13}C$	$\delta^{18}O$	$\delta^{34}S$	δD	REFERENCE	NOTES
SPHALERITE						
RRBX SL, Western margin of diatreme			0.05		Jensen, 2003	
BEACON SL, Western margin of diatreme			1.97		Jensen, 2003	
EP9B SL, Western margin of diatreme			2.32		Jensen, 2003	
41-K-115B SL, deep levels Pointer-Index Mines			-11.73		Jensen, 2003	
41-K-115B SL, deep levels Pointer-Index Mines			-11.41		Jensen, 2003	
A 31-24-785, 3100 leve Ajax/Vindicator Mines			-7.81		Jensen, 2003	
V-7-432, 3100 leve Ajax/Vindicator Mines			-4.7		Jensen, 2003	
A 31-29-137, 3100 leve Ajax/Vindicator Mines			-2.17		Jensen, 2003	
A 29-137.5, 3100 leve Ajax/Vindicator Mines			-2.1		Jensen, 2003	
STIBNITE						
STIBEL, Cresson Pit			-18.6		Jensen, 2003	
STIBFL, late-stage vein			-18.6		Jensen, 2003	
37-K-144 SB, late-stage vein			-16.12		Jensen, 2003	

SULFATES

ANHYDRITE						
UGC 97-5 2358, Ironclad, Globe Hill area			10.1754		Jensen, 2003	
136 (DDH 500SE), Ironclad, Globe Hill area			8.9776		Jensen, 2003	
IC SO4, Ironclad, Globe Hill area			10.5153		Jensen, 2003	
A 31-23-115, 3100 Level Ajax/Vindicator Mines			10.8483		Jensen, 2003	
A 31-23-41, 3100 Level Ajax/Vindicator Mines			11.4144		Jensen, 2003	
A 31-27-1111, 3100 Level Ajax/Vindicator Mines			11.5322		Jensen, 2003	
A 31-23-827, 3100 Level Ajax/Vindicator Mines			11.5958		Jensen, 2003	
V 7-327, 3100 Level Ajax/Vindicator Mines			12.4245		Jensen, 2003	
A 31-25-641, 3100 Level Ajax/Vindicator Mines			13.0239		Jensen, 2003	
A 31-27-500, 3100 Level Ajax/Vindicator Mines			13.048		Jensen, 2003	
A 31-25-785, 3100 Level Ajax/Vindicator Mines			13.0904		Jensen, 2003	
A 31-25-164.5, 3100 Level Ajax/Vindicator Mines			13.3342		Jensen, 2003	
A 31-27-141, 3100 Level Ajax/Vindicator Mines			14.52795		Jensen, 2003	
A 31-23-10, 3100 Level Ajax/Vindicator Mines			14.8332		Jensen, 2003	
CELESTITE						
90 DDH8-1050, Ironclad, Globe Hill area			6.8576		Jensen, 2003	
90 DDH8-1050, Ironclad, Globe Hill area			8.0733		Jensen, 2003	

WHOLE ROCK

Phonolite, near Alt pit, elev. 10,558', "fresh" in hand sample 880-34(A)		8.12			Beaty et al, 1996	
Altered phonolite, samples from east outcrop trench, CC #01		7.43			Beaty et al, 1996	
Altered phonolite, samples from east outcrop trench, CC #02		11.97			Beaty et al, 1996	
Altered phonolite, samples from east outcrop trench, CC #03		12.41			Beaty et al, 1996	
Altered phonolite, samples from center outcrop trench, CC #07		10.01			Beaty et al, 1996	Elevation 10,599'
Altered phonolite, samples from center outcrop trench, CC #07		10.37			Beaty et al, 1996	Elevation 10,599'
Altered phonolite, samples from center outcrop trench, CC #06		12.76			Beaty et al, 1996	Elevation 10,634'
Altered phonolite, samples from center outcrop trench, CC #05		11.13			Beaty et al, 1996	Elevation 10,632'
Altered phonolite, samples from center outcrop trench, CC #09		13.27			Beaty et al, 1996	Elevation 10,6389'
Altered phonolite, samples from center outcrop trench, CC #08		10.35			Beaty et al, 1996	Elevation 10,641'
Altered phonolite, samples from center outcrop trench, CC #08		10.44			Beaty et al, 1996	Elevation 10,641'
Altered phonolite, samples from center outcrop trench, CC #10		9.96			Beaty et al, 1996	Elevation 10,640'
Altered phonolite, samples from center outcrop trench, CC #03		7.15			Beaty et al, 1996	Elevation 10,638'
Altered phonolite, samples from center outcrop trench, CC #03		7.10			Beaty et al, 1996	Elevation 10,638'
Altered phonolite, Altman pit, 530 bench, TR-12 #01		9.00			Beaty et al, 1996	
Altered phonolite, Altman pit, 530 bench, TR-12 #01		9.34			Beaty et al, 1996	
Altered phonolite, Altman pit, 530 bench, TR-12 #01		9.42			Beaty et al, 1996	
Altered phonolite, Altman pit, 530 bench, TR-12 #02		9.78			Beaty et al, 1996	

APPENDIX D: STABLE ISOTOPE DATA COMPILED FROM PREVIOUS STUDIES, PAGE 7

WHOLE ROCK, CONTINUED

	$\delta^{13}C$	$\delta^{18}O$	$\delta^{34}S$	δD	REFERENCE	NOTES
Altered phonolite, Altman pit, 530 bench, TR-12 #03		11.35			Beaty et al, 1996	
Altered phonolite, Altman pit, 530 bench, TR-12 #04		9.88			Beaty et al, 1996	
Altered phonolite, Altman pit, 530 bench, TR-12 #05		11.18			Beaty et al, 1996	
Altered phonolite, Altman pit, 530 bench, TR-12 #06		9.34			Beaty et al, 1996	
Altered phonolite, Altman pit, 530 bench, TR-12 #07		14.31			Beaty et al, 1996	
Altered phonolite, Altman pit, 530 bench, TR-12 #08		13.59			Beaty et al, 1996	
Altered phonolite, Altman pit, 530 bench, TR-12 #09		10.08			Beaty et al, 1996	
Altered phonolite, Altman pit, 530 bench, TR-12 #10		11.25			Beaty et al, 1996	
Altered phonolite, Altman pit, 530 bench, TR-12 #11		12.56			Beaty et al, 1996	
Altered phonolite, Altman pit, 530 bench, TR-12 #12		13.48			Beaty et al, 1996	
Altered phonolite, Altman pit, 530 bench, TR-12 #13		12.99			Beaty et al, 1996	
Altered phonolite, Altman pit, 530 bench, TR-12 #13		13.53			Beaty et al, 1996	
Basaltic dikes, Altman pit, 530 bench N1		7.61			Beaty et al, 1996	
Basaltic dikes, Altman pit, 530 bench N1A		7.88			Beaty et al, 1996	
Basaltic dikes, Altman pit, 530 bench N1B		6.85			Beaty et al, 1996	
Basaltic dikes, Altman pit, 530 bench N1B		7.73			Beaty et al, 1996	
Basaltic dikes, Altman pit, 530 bench N1B1		8.04			Beaty et al, 1996	
Basaltic dikes, Altman pit, 530 bench N1C		7.29			Beaty et al, 1996	
Basaltic dikes, Altman pit, 530 bench N2		7.26			Beaty et al, 1996	
Basaltic dikes, Altman pit, 530 bench N2A		6.70			Beaty et al, 1996	
Basaltic dikes, Altman pit, 530 bench N2B		7.20			Beaty et al, 1996	
Basaltic dikes, Altman pit, fresh dike 622 bench, 880-36 (C2)		7.48			Beaty et al, 1996	Elevation 10,622
Basaltic dikes, Altman pit, weakly altered, 622 bench, 880-36 (B)		7.17			Beaty et al, 1996	Elevation 10,622
Basaltic dikes, Altman pit, silicified dike, 622 bench, 880-36 (C1)		10.08			Beaty et al, 1996	Elevation 10,622
"Other altered rocks" east edge of pit, 880-36(D)		8.77			Beaty et al, 1996	Elevation 10,622
"Other altered rocks" propylitic alteration, outcrop 880-35A		4.52			Beaty et al, 1996	Elevation 10,616
Whole rock, (K-spar ?) from Portland		10.6			Silberman, 1992	Calculated ore fluid $\delta^{18}O = -0.2$ (assuming sample is K-feldspar)
Whole rock, (K-spar ?) from Cresson		10.8			Silberman, 1992	Calculated ore fluid $\delta^{18}O = 0$ (assuming sample is K-feldspar)
Whole rock, (K-spar ?) from Cresson		12.0			Silberman, 1992	Calculated ore fluid $\delta^{18}O = 1.2$ (assuming sample is K-feldspar)
Whole rock, (K-spar ?) from Cresson		12.2			Silberman, 1992	Calculated ore fluid $\delta^{18}O = 1.2$ (assuming sample is K-feldspar)

APPENDIX E: METHODS

Detailed sample descriptions, photographs, and all other data collected on samples are presented in Appendices J through M (on disc). The reader is referred to the following Appendices for information on carbonates of each specific type:

Appendix J: Calcite Samples

Appendix K: Dolomite Samples

Appendix L: Ankerite Samples

Appendix M: Rhodochrosite Samples

Fluid Inclusion Microthermometry

Fluid inclusion microthermometry was conducted at the New Mexico Institute of Mining and Technology using a Linkham TH-600 heating-freezing stage and an Olympus BH2 petrographic microscope. Doubly polished fluid inclusion thick (~200 m) sections of carbonate veins were scanned and broken into chips to fit on the heating-freezing stage. To obtain accurate measurements chips with large, primary, isolated inclusions were measured to ensure no leakage or necking down had occurred. Photographs were taken prior to freezing the sample; and sizes, phases present (liquid + vapor), inclusion type (primary or psuedosecondary), and degree of fill were recorded. The rate of heating or freezing was digitally controlled, and could be dropped to 0.3°C/minute during measurements to avoid errors caused by thermal gradients.

Stable Isotopes

Stable isotope analysis was completed at The New Mexico Institute of Mining and Technology on two different systems. The majority of the carbonate (O and C) data was analyzed on the original system, a Finnigan Delta E with vacuum extraction lines.

Analytical precision, calculated from duplicate samples is ± 0.9 ‰ for O and ± 0.4 ‰ for C. 20 carbonate samples and all S samples were analyzed on a Finnigan Delta Plus XP with a Finnigan Gas Bench for carbonates and a Costech EA for sulfides. Analytical precision is ± 0.23 ‰ for O, ± 0.03 ‰ for C, ± 0.2 ‰ for S in pyrite, ± 2.33 ‰ for S in sphalerite, and ± 0.45 ‰ for S in galena.

Oxygen and Carbon Isotopes

93 carbonate vein samples taken from drill core, the Koschmann collection, and surface outcrop were coarsely crushed, sieved to an appropriate size fraction for removal of sulfides, separated, and crushed again for analysis.

Analyses done with the Finnigan Delta E with vacuum extraction lines used the following procedure: For pure carbonate samples approximately 12 mg of sample (adjusted accordingly for impure or whole rock carbonate samples) was loaded into one side of a carbonate reaction vessel for reaction with phosphoric acid loaded on the other side. Unreacted sample vessels were left open to vacuum and pumped for a minimum of four hours to remove atmospheric gasses. Sample vessels were closed and allowed to react overnight in a 50°C water bath to produce CO_2 gas for analysis. The CO_2 sample was then cleaned and extracted through a series of cold traps and analyzed for O and C on the mass spectrometer. O values were corrected using a calculated acid fractionation factor that incorporated a comparison of standard measurements to know values. C values did not require a correction.

Samples analyzed with the Finnigan Delta Plus XP used the following procedure: Approximately 0.5 to 0.6 mg of carbonate sample was measured and added to a septum-capped glass vial and flushed with helium for 3 minutes. 10 drops of phosphoric acid

was injected with a needle and samples were allowed to react at 45°C for 3 hours (calcite) to 16 hours (dolomite). The CO_2 was extracted using a helium carrier gas and analyzed by continuous flow.

Sulfur Isotopes

26 sulfide samples separated during carbonate preparation were kept for S analysis. Because some sample loss is experienced during the crushing procedure, large samples were crushed to a fine powder for analysis, but small samples were analyzed as whole grains. Pyrite, sphalerite, and galena samples of sizes 0.75, 1.2, and 3.0 mg, respectively were to be loaded in tin capsules for analysis.

X-ray Diffraction Data

Carbonate samples can be classified into eight categories (described in Results section, below) based on mineralogy and style of mineralization. Representative samples from each group were analyzed using at the New Mexico Bureau of Geology and Mineral Resources X-ray Diffraction facility to confirm mineralogy. Pure calcite and dolomite standards were also analyzed for comparison with samples. The same powdered samples used for stable isotope analysis were used for XRD. The majority of samples analyzed was obtained from clean mineral separates and generate very sharp XRD peak patterns. Groups one and two are whole rock analyses, but the carbonate peaks are still plainly visible.

Calibration of the XRD equipment was done at the beginning of each session using the silica 111 peak. All samples were scanned between 2 and 70 degrees and analyzed using JADE 6 software. The computer matched primary peaks in each pattern with minerals in the JADE database.

APPENDIX F: SALINITIES (EQUIVALENT WEIGHT PERCENT NaCl) CORRESPONDING TO MEASURED FREEZING POINT DEPRESSIONS (DEGREES CELSIUS)

FPD	0.0	0.1	0.2	0.3	0.4	0.5	0.6	0.7	0.8	0.9
0.0	0.00	0.18	0.35	0.53	0.71	0.88	1.05	1.23	1.40	1.57
1.0	1.74	1.91	2.07	2.24	2.41	2.57	2.74	2.90	3.06	3.23
2.0	3.39	3.55	3.71	3.87	4.03	4.18	4.34	4.49	4.65	4.80
3.0	4.96	5.11	5.26	5.41	5.56	5.71	5.86	6.01	6.16	6.30
4.0	6.45	6.59	6.74	6.88	7.02	7.17	7.31	7.45	7.59	7.73
5.0	7.86	8.00	8.14	8.28	8.41	8.55	8.68	8.81	8.95	9.08
6.0	9.21	9.34	9.47	9.60	9.73	9.86	9.98	10.11	10.24	10.36
7.0	10.49	10.61	10.73	10.86	10.98	11.10	11.22	11.34	11.46	11.58
8.0	11.70	11.81	11.93	12.05	12.16	12.28	12.39	12.51	12.62	12.73
9.0	12.85	12.96	13.07	13.18	13.29	13.40	13.51	13.62	13.72	13.83
10.0	13.94	14.04	14.15	14.25	14.36	14.46	14.57	14.67	14.77	14.87
11.0	14.97	15.07	15.17	15.27	15.37	15.47	15.57	15.67	15.76	15.86
12.0	15.96	16.05	16.15	16.24	16.34	16.43	16.53	16.62	16.71	16.80
13.0	16.89	16.99	17.08	17.17	17.26	17.34	17.43	17.52	17.61	17.70
14.0	17.79	17.87	17.96	18.04	18.13	18.22	18.30	18.38	18.47	18.55
15.0	18.63	18.72	18.80	18.88	18.96	19.05	19.13	19.21	19.29	19.37
16.0	19.45	19.53	19.60	19.68	19.76	19.84	19.92	19.99	20.07	20.15
17.0	20.22	20.30	20.37	20.45	20.52	20.60	20.67	20.75	20.82	20.89
18.0	20.97	21.04	21.11	21.19	21.26	21.33	21.40	21.47	21.54	21.61
19.0	21.68	21.75	21.82	21.89	21.96	22.03	22.10	22.17	22.24	22.31
20.0	22.38	22.44	22.51	22.58	22.56	22.71	22.78	22.85	22.91	22.98
21.0	23.05	23.11	23.18							

Bodnar, R.J., 1992, Revised Equation and Table for Freezing-Point Depressions of H_2O-salt fluid inclusions. PACROFI IV Abstract volume.

APPENDIX G: FLUID INCLUSION PRESENTATION

This disk contains the following PowerPoint presentations:

- Introduction to Appendices
- Appendix G: Fluid Inclusion Presentation
- Appendix J: Calcite Sample Descriptions
- Appendix K: Dolomite Sample Descriptions
- Appendix L: Ankerite Sample Descriptions
- Appendix M: Rhodochrosite Sample Descriptions

APPENDIX H: SAMPLE LOCATIONS AND LITHOLOGIC DESCRIPTIONS OF CARBONATE SAMPLES ANALYZED

SAMPLE	X (EASTING)	Y (NORTHING)	Z (ELEVATION)	MINERAL	VEIN PARAGENESIS	HOST ROCK	LOCATION
24-L-15	40720.44	50321.59	8157	Dolomite	Quartz + pyrite → euhedral quartz → euhedral Dolomite	Xgd	Level 20 Ajax
24-L-28	42829.079	51352.852	7665	Calcite	K-feldspar-pyrite alteration + trace base metal Sulfides crosscut by calcite veins	Tph	Level 26 Portland
25-L-113B	42748.43	51176.82	7387	Calcite	Tellurides → calcite → fluorite	"Basalt"	2900 level Portland
25-L-118	41701	54721	8918	Dolomite	Yellow dolomite + fluorite + pyrite + cinnabar	Tphkbx	Dante Collapse Breccia
25-L-21	39871.21	51943.27	9071	Dolomite	Yellow dolomite	Tlbx	Cresson blowout
25-L-24	39474.25	55052.6	9690	Calcite	Calcite + gypsum deposited from descending waters	Calcite crystals from vial, no host rock recorded	7th level beneath stope at NE end of the Cresson Blowout
25-L-38	40968.253	54330.971	9035	Dolomite	Tlbx clast → **dolomite** → quartz → telluride → dolomite → fluorite	Tlbx	Level 38 Cresson
26-L-13	40926.77	52760.6	8109.07	Calcite	Calcite + fluorite + galena + pyrite + sphalerite	Vein material	Cresson Lateral
36-K-7	40821.02	50899.14	8008	Ankerite	Ankerite + fluorite veins	Ttd	Level 21 Ajax, near shaft
36-K-174	42446.66	55529.72	9881	Calcite	**Calcite** → quartz → euhedral dolomite	Tsy	Level 11 Orpha May
36-K-209	43975.34	58715.5	9759	Dolomite	Dolomite cement in matrix	Tbx2, arkosic sediment	Level 10 Isabella/Golden Cycle
37-K-248	35633.18	57990.05	9459	Dolomite	Dolomite	Tbx2 (layered) shows soft sediment deformation	
39-K-52C	35857.58	63397.66	8979	Rhodochrosite	Rhodochrosite + sphalerite + galena + trace pyrite	Xgd in Tbx1L	"Silver Vein", Mollie Kathleen
39-K-103	35760	63291	9067	Rhodochrosite	Rhodochrosite breccia	Tphk in Tbx1L	Level 8 Mollie Kathleen
39-K-103B	35803.5	63845.87	9286	Rhodochrosite	Rhodochrosite breccia	Tphk in Tbx1L	Level 8 Mollie Kathleen
39-K-141M	45730.33	59511.74	9230	Dolomite	Dolomite cement in matrix	Tbx2, arkosic sediment	Level 5 Cameron
39-K-160B	45782.794	59295.496	9430	Dolomite	Dolomite cement in matrix	Tbx2, arkosic sediment	Level 4 School Section
39-K-163	45736.621	59288.964	9430	Dolomite	Dolomite	Tbx2 (layered) shows soft sediment deformation	School Section
39-K-163A1	45736.622	59288.963	9430	Dolomite	Dolomite	Tbx2 (layered) shows soft sediment deformation	School Section
39-K-163B1	45736.331	59288.606	9430	Calcite	Calcite replacing phenocryst sites	Volcaniclastic sediment	School Section
39-K-163B1M	45736.331	59288.606	9430	Calcite	Calcite replacing phenocryst sites	Volcaniclastic sediment	School Section
39-K-163B2	45736.331	59288.606	9430	Dolomite	Dolomite	Tbx2 (layered) shows soft sediment deformation	School Section
39-K-163B2M	45736.331	59288.606	9430	Dolomite	Dolomite	Tbx2 (layered) shows soft sediment deformation	School Section
39-K-165	45955.77	59051.376	9430	Calcite	Calcite in matrix	Tphk	Level 4 School Section
39-K-167	45730.31	59511.72	9230	Calcite	Calcite replacing phenocryst sites	Volcaniclastic sediment	Cameron
39-K-170	45730.34	59511.75	9230	Dolomite	Dolomite cement in matrix	Tbx2, arkosic sediment	Cameron Tunnel
39-K-172	45730.32	59511.73	9230	Dolomite	Dolomite cement in matrix	Tbx2, arkosic sediment	Level 8 winze, Cameron
39-K-179A	46005.439	59048.682	9430	Dolomite	Dolomite cement in matrix	Tbx2, arkosic sediment	Level 4 School Section
39-K-194	45929.494	59150.025	9430	Dolomite	Dolomite cement in matrix	Tbx2, arkosic sediment	School Section
39-K-195	45589.67	60238.57	9730	Dolomite	Dolomite cement in matrix	Tbx2, arkosic sediment	School Section

Notes: See List of Symbols for key to rock codes and lithologic descriptions.

APPENDIX H: SAMPLE LOCATIONS AND LITHOLOGIC DESCRIPTIONS OF CARBONATE SAMPLES ANALYZED, PAGE 2

SAMPLE	X (EASTING)	Y (NORTHING)	Z (ELEVATION)	MINERAL	VEIN PARAGENESIS	HOST ROCK	LOCATION
39-K-210	45776.22	59800.198	9730	Dolomite	Dolomite cement in matrix + specular hematite Alteration	Tbx2, arkosic sediment	Level 2 School Section
39-K-210M	45776.22	59800.198	9730	Dolomite	Dolomite cement in matrix + specular hematite alteration	Tbx2, arkosic sediment	Level 2 School Section
39-K-245	45837.408	59328.394	9430	Dolomite	Dolomite cement in matrix	Tbx2, arkosic sediment	Level 4 School Section
39-K-245M	45837.408	59328.394	9430	Dolomite	Dolomite cement in matrix	Tbx2, arkosic sediment	Level 4 School Section
39-K-248A	45900.128	59199.448	9430	Dolomite	Dolomitic dark layers	Tbx2 (layered) shows soft sediment deformation	School Section
39-K-248B	45900.128	59199.448	9430	Dolomite	Dolomitic dark layers	Tbx2 (layered) shows soft sediment deformation	School Section
39-K-249	45836.81	59325.61	9530	Dolomite	Dolomitic layers	Tbx2 (layered) shows soft sediment deformation	School Section
39-K-265	43798.93	58835.33	9865	Dolomite	Dolomite cement in matrix	Tbx2, gray, shaley sediment	Level 10 South Burns
39-K-309	35803.49	63843.85	9286	Rhodochrosite	Rhodochrosite breccia + base metal sulfides → Rhodochrosite → base metal sulfides	Tphk in Tbx1L	Mollie Kathleen
41-K-57A	44374	55529	9486	Calcite	Quartz → tellurides → colloform quartz → calcite	Tbx1L	Level 6 Hull City
41-K-84	33657	57042	9119	Rhodochrosite	Large euhedral rhodochrosite crystals with base metal sulfide-rich rims	Ycc	Level 5 Index
41-K-84A	33861	57689	9119	Rhodochrosite	Rhodochrosite	Ycc	Gilbert Vein, Level 5 Index
41-K-89C	33838.75	57621.85	9119	Rhodochrosite	Wallrock → quartz + fluorite + pyrite → rhodochrosite + sphalerite + galena → quartz + fluorite	Ycc	Level 5 Index
41-K-89E	33838.75	57621.85	9119	Rhodochrosite	Rhodochrosite	Ycc	Level 5 Index
A31-23-34	42343.85	51882.96	6990.813	Calcite	Euhedral calcite + trace fluorite + pyrite crosscutting K-feldspar-pyrite alteration	Phkbx	3100 Ajax
A31-27-629A CC	41903.39	51487.18	6985	Calcite	Rhombohedral dolomite → calcite	Vein cuts contact between Tbx1L and Tlbx	
A31-27-629A DOL	41903.39	51487.18	6985	Calcite	Rhombohedral dolomite → calcite	Vein cuts contact between Tbx1L and Tlbx	
AC96-22 223'8"	43658.08	57590.03	10469.86	Dolomite	Euhedral dolomite in vugs	Tlb	Altman
AC96-23 397'9"	43759.93	57277.35	10289.97	Dolomite	Vuggy dolomite casts after some mineral that has dissolved out	Tphk	Altman
AC96-23 418'3"	43773.65	57278.44	10275.15	Dolomite	Dolomite	Tphk	Altman
AN 3 677.7	40584.35	49638.85	6716.355	Calcite	Ore stage euhedral calcite vein	Xgd	Newmarket vein system, drilled down from 3350 level Ajax
CC1628 1281'9"	41202.87	54546.71	8583.57	Dolomite	Dolomite	Tlb	
CC1628 1285'3"	41202.87	54546.71	8579.79	Calcite	Calcite on fracture surface	Tlb	
CC1628 1286'2"	41202.87	54546.71	8578.79	Calcite	Calcite on fracture surface	Tlb	

APPENDIX H: SAMPLE LOCATIONS AND LITHOLOGIC DESCRIPTIONS OF CARBONATE SAMPLES ANALYZED, PAGE 3

SAMPLE	X (EASTING)	Y (NORTHING)	Z (ELEVATION)	MINERAL	VEIN PARAGENESIS	HOST ROCK	LOCATION
CC1629 427'	40723.96	54651.3	9471.03	Ankerite	Ankerite	Tphkd	
CC1629 458'8"	40723.96	54651.3	9453	Dolomite	Euhedral dolomite around clasts	Tlbx	
CC1840 1337'5"	40135.1	55638.01	9282.19	Dolomite	Yellow euhedral dolomite + fluorite on fracture surface	Tphk	
CC1954 1165'	40430.01	53989.34	9176.72	Ankerite	Ankerite + fluorite + quartz + trace pyrite	Tphkd	
CC2236 1131'	39179.63	53393.19	8965.84	Ankerite	Vuggy ankerite vein with boxwork developed	Tphk, stockwork developed	
CC2236 1137'7"	39181.34	53393.56	8958.95	Ankerite	Vuggy ankerite vein with boxwork developed	Tphk, stockwork developed	
CC92-61 1580'9"	41353.06	54145.67	8638.91	Ankerite	Ankerite	Tbx2	
CC92-61 1714'1"	41348.13	54143.72	8506.07	Ankerite	Ankerite + fluorite + pyrite in matrix	Tbx2	
CC92-61 1871'2"	41340.48	54140.94	8349.11	Ankerite	Sugary ankerite + pyrite + fluorite vein	Tbx2	
CP	40550	54490	9000	Dolomite	Dolomite filled vesicles	Tlbx	Cresson Pipe
CR1268 1281'	41260.45	55040.57	8957.059	Calcite	Clean calcite veins with K-feldspar-pyrite alteration halos	Contact of Tbx1L and Tlbx	
DDHS 8-185	46730.6	52737.68	9906.185	Calcite	Calcite vein with bleached halo of disseminated pyrite	Tphk	Eastern Subbasin
DDHS-8 553.5	46709.15	52492.55	9660.112	Ankerite	Ankerite	Tbx2	Eastern Subbasin
DDU-8-162	40448.29	48876.63	6977.881	Dolomite	Dolomite	Tlh	1000 level Ajax
DOL-1	40966	54503	9585	Dolomite	Dolomite	Tlbx	Cresson Pipe
GT96-1-785R	40895.18	54236.23	9360.17	Calcite	Calcite → quartz in zone of K-feldspar-pyrite Alteration	Tbx1L	
LAMP-1	40958	54524	9620	Dolomite	Dolomite	Tlh	
LAMP-2	40834	54595	9585	Dolomite	Dolomite	Tlh	
RRBXHYDBX	32950	56550	7000	Rhodochrosite	Rhodochrosite	Tlbx	Railroad Breccia
TEL-1	43975	58479	10228	Rhodochrosite	Rhodochrosite + base metal sulfides → barite → quartz + tellurides	Tphk	
UGC96-2 829'	41911.42	53039.07	9482.18	Ankerite	Hairline ankerite + fluorite veins	Tphd	
UGC96-2 1779'4"	41554.73	52859.58	8620.34	Calcite	Calcite + trace pyrite veins	Tsy, sheared	
UGC96-2 2092'5"	41440.82	52803.37	8333.36	Ankerite	Gray murky ankerite + fluorite + pyrite veins	Tsy	
UGC 96-2 2529'8"	41285.43	52724.19	7932.46	Dolomite	Euhedral dolomite around clasts	Thbx	
UGC96-2 2530'	41285.43	52724.19	7932.46	Dolomite	Calcite	Thbx	
UGC 97-2 1924'	45448.66	57473.17	9297.975	Calcite	Thin calcite vein with red halo cutting K-feldspar-pyrite alteration	Tphk	East Altman
UGC97-5 1059'6"	39228.51	58689.35	9184.97	Calcite	Pyrite veins → calcite along fracture surface	Xgd	
UGC 97-5 1221'8"	39162.43	58687.05	9037.26	Calcite	Fracture surface	Xgd	
UGC97-5 1302'	39130.59	58688.05	8963.39	Calcite	Black calcite + pyrite + quartz in 1" veins	Tph with Precambrian clasts	
UGC97-5 1341'3"	39114.94	58688.53	8929.58	Calcite	Half-inch calcite + pyrite vein with base metal sulfide-rich selvages	Tbx1L	
UGC97-5 1348'	39111.74	58688.63	8921.49	Calcite	Half-inch calcite + pyrite vein with base metal sulfide-rich selvages	Tbx1L	
UGC97-5 1399'	39090.59	58689.29	8874.5	Calcite	Hairline calcite + pyrite veins with bleached halos	Ttdd	

APPENDIX H: SAMPLE LOCATIONS AND LITHOLOGIC DESCRIPTIONS OF CARBONATE SAMPLES ANALYZED, PAGE 4

SAMPLE	X (EASTING)	Y (NORTHING)	Z (ELEVATION)	MINERAL	VEIN PARAGENESIS	HOST ROCK	LOCATION
UGC97-5 1491'	39053.54	58690.44	8791.47	Calcite	Irregular calcite + pyrite veins cutting K-feldspar-pyrite alteration and quartz veins	Syenite dike in Xgd	
UGC97-5 1497'	39051.13	58690.52	8785.86	Calcite	Biotite altered syenite → K-feldspar-pyrite alteration → calcite + pyrite	Syenite, Precambrian clasts	
UGC97-5 1565'	39023.41	58691.38	8723.74	Calcite	1" calcite + pyrite vein with trace base metal sulfides in selvages	Xgd	
UGC97-5 1582'	39016.67	58691.59	8708.1	Calcite	Yellow calcite + pyrite	Ttdd in Xgd	
UGC97-5 1592'8"	39012.53	58691.72	8698.69	Calcite	Calcite + pyrite	Ttdd	
UGC97-5 1612'10"	39005.3	58715.41	8680.63	Calcite	Calcite + pyrite	Ttdd	
UGC97-5 1724'	38959.95	58722.69	8578.77	Calcite	Calcite + pyrite with trace base metal sulfides in selvages	Xgd	
UGC97-5 1784'3"	38935.17	58726.5	8523.92	Calcite	Calcite with base metal sulfides in selvages	Xgd	
UGC97-5 1854'7"	38906.75	58731.04	8459.26	Calcite	Quarter-inch calcite + pyrite + quartz vein cutting red orthoclase veins	Xgd	
UGC97-5 2102'7"'	38804.67	58745.07	8233.71	Calcite	Calcite + quartz + trace pyrite	Xgd	
UGC97-5 2294"	38719.1	58754.79	8061.54	Calcite	Calcite with trace base metal sulfides in selvages	Vein material with Xgd clasts	
UGC97-5 2410'10"	38666.39	58760.5	7959.08	Calcite	Calcite + pyrite + fluorite + quartz	Xgd	
UGC97-5 2508'4"'	38621.77	58765.24	7873.03	Calcite	Calcite	Xgd	
UGC97-5 2524'4"	38614.42	58766.02	7858.87	Calcite	Calcite + pyrite	Xgd	
UGC97-5 2553	39670.39	59894.68	7884.849	Calcite	Calcite	Xgd	
UGC97-5 2613'5"	38574.37	58770.27	7781.64	Calcite	Calcite + pyrite + quartz	Xgd	
V6B-269	44860.31	53860.73	7047.361	Dolomite	Green dolomite + quartz + fluorite + pyrite + rhodochrosite	Tphk	3100 level Vindicator
V-12-228	45027.56	54285.46	7013.365	Calcite	Ore stage calcite + fluorite + pyrite + quartz	Tphk	1000m level Vindicator
V-12-229	45027.56	54285.46	7001.375	Calcite	Ore stage calcite vein	Tphk	deep Vindicator
V-13-215	45034.97	54297.97	7024.329	Calcite	Calcite + quartz + fluorite	Tphk	deep Vindicator

APPENDIX I: SAMPLE LOCATIONS AND LITHOLOGIC DESCRIPTIONS OF SULFIDE SAMPLES ANALYZED

SAMPLE	X (EASTING)	Y (NORTHING)	Z (ELEVATION)	MINERAL	VEIN PARAGENESIS	HOST ROCK	LOCATION
24-L-15	40720.44	50321.59	8157	Pyrite	Quartz + pyrite → euhedral quartz → euhedral	Xgd	Level 20 Ajax
24-L-28	42829.079	51352.852	7665	Pyrite	K-feldspar-pyrite alteration + trace base metal sulfides crosscut by calcite veins	Tph	Level 26 Portland
25-L-118	41701	54721	8918	Pyrite	Yellow dolomite + fluorite + pyrite + cinnabar	Tphkbx	Dante Collapse Breccia
26-L-13	40926.77	52760.6	8109.07	Pyrite	Calcite + fluorite + galena + pyrite + sphalerite	Vein material	Cresson Lateral
39-K-52C	35857.58	63397.66	8979	Pyrite	Rhodochrosite + sphalerite + galena + trace pyrite	Xgd in Tbx1L	"Silver Vein", Mollie Kathleen
41-K-89E galena	33838.75	57621.85	9119	galena	Rhodochrosite	Ycc	Level 5 Index
AJAX 18TH	41065.01	50948.17	7710	Pyrite	Quartz + pyrite	Vein material	Level 18 Ajax
CC92-61 1714'1"	41348.13	54143.72	8506.07	Pyrite	Ankerite + fluorite + pyrite in matrix	Thbx	
CC92-61 1871'2"	41340.48	54140.94	8349.11	Pyrite	Sugary ankerite + pyrite + fluorite vein	Thbx	
COPPER MT.	33880	71590	9525	sphalerite	Sphalerite + galena + quartz	Vein material	
UGC97-5 1243'	39154.24	58695.91	9017.85	Pyrite	Pyrite + quartz	Tphd	
UGC97-5 1302'	39130.59	58688.05	8963.39	Pyrite	Black calcite + pyrite + quartz in 1" veins	Tph with Precambrian clasts	
UGC97-5 1341'3"	39114.94	58688.53	8929.58	Pyrite	Half-inch calcite + pyrite vein with base metal sulfide-rich selvages	Tbx1L	
UGC97-5 1348'	39111.74	58688.63	8921.49	Pyrite	Half-inch calcite + pyrite vein with base metal sulfide-rich selvages	Tbx1L	
UGC97-5 1399'	39090.59	58689.29	8874.5	Pyrite	Hairline calcite + pyrite veins with bleached halos	Ttdd	
UGC97-5 1491'	39053.54	58690.44	8791.47	Pyrite	Irregular calcite + pyrite veins cutting K-feldspar-pyrite alteration and quartz veins	Syenite dike in Xgd	
UGC97-5 1497'	39051.13	58690.52	8785.86	Pyrite	Biotite altered syenite → K-feldspar-pyrite alteration → calcite + pyrite	Syenite w/ Precambrian clasts	
UGC97-5 1565'	39023.41	58691.38	8723.74	Pyrite	1" calcite + pyrite vein with trace base metal sulfides in selvages	Xgd	
UGC97-5 1582'	39016.67	58691.59	8708.1	Pyrite	Yellow calcite + pyrite	Ttdd in Xgd	
UGC97-5 1592'8"	39012.53	58691.72	8698.69	Pyrite	Calcite + pyrite	Ttdd	
UGC97-5 1612'10"	39005.3	58715.41	8680.63	Pyrite	Calcite + pyrite	Ttdd	
UGC97-5 1854'7"	38906.75	58731.04	8459.26	Pyrite	Quarter-inch calcite + pyrite + quartz vein cutting red orthoclase veins	Xgd	
UGC97-5 2294"	38719.1	58754.79	8061.54	Pyrite	Calcite with trace base metal sulfides in selvages	Vein material with Xgd clasts	
UGC97-5 2410'10"	38666.39	58760.5	7959.08	Pyrite	Calcite + pyrite + fluorite + quartz	Xgd	
UGC97-5 2508'4"'	38621.77	58765.24	7873.03	Pyrite	Calcite	Xgd	
UGC97-5 2524'4"	38614.42	58766.02	7858.87	Pyrite	Calcite + pyrite	Xgd	
UGC97-5 2613'5"	38574.37	58770.27	7781.64	Pyrite	Calcite + pyrite + quartz	Xgd	

Note: See List of Symbols for key to rock codes and lithologic descriptions.

APPENDIX N: X-RAY DIFFRACTION RESULTS

The sample peak pattern for each sample analyzed can be found following the sample description slide in Appendices J-M.

The first group of samples analyzed consists of lacustrine sediments of two different types. One type is dolomite-cemented arkosic sandstone (sample 39-K-245) derived from shallow lacustrine deposition of the Cripple Creek breccia. The other type (39-K-248) is fine-grained, layered sediments with alternating dark and light bands. This particular sample was drilled out of the dark layers and is dolomitic in composition.

The second group is represented by sample 39-K-163B1, a maroon, white, and green layered volcaniclastic sediment with calcite replacing original phenocryst sites.

Group 3 occurs as massive dolomite within lamprophyre intrusions (sample DOL-1), and euhedral dolomite in vugs and on fracture surfaces (CC 1840 1337'5").

Sample 25-L-21 represents a group of yellowish dolomites found as open-space filling in breccias.

The fifth group consists of sugary ankerite + fluorite veins (CC 1954 1165') or boxwork ankerite after dolomite (CC 2236 1131').

Group 6, the largest group, is made up of fairly clean, massive calcite (± pyrite, quartz, ± base metal sulfides along vein margins) veins up to two feet across, but most commonly one to three inches wide. Samples UGC 97-5 1341'3", UGC 97-5 1612'10", and UGC 97-5 2294'4" all show clean calcite peaks.

Samples 39-K-52 C and 41-K-89 E represent a group of rhodochrosites that occur

as massive veins (± fluorite ± base metal sulfides) or breccia open-space fill.

Sample 25-L-24 is a recent sample deposited from descending waters in the Cresson Blowout and consists of gypsum and calcite.

REFERENCES CITED

Barnes, I., Irwin, W.P., White, D.E., 1978, Global distribution of carbon dioxide discharges and major zones of seismicity: U.S. Geological Survey, Water-Resources Investigation, Open File Report 78-36. 12 p.

Beane, R.E., 1974, Biotite stability in the porphyry copper environment: Economic Geology, v. 69, p. 241-256.

Beaty, D.W., Kelley, K. D., Silberman, M.L., and Thompson, T.B., 1996, Oxygen isotope geochemistry of a portion of the Cripple Creek hydrothermal system: Society of Economic Geologists Guidebook Series, v. 26, p. 55-64.

Berger, B.R., and Henley, R.W., 1989, Advances in the Understanding of Epithermal Gold-Silver Deposits, with Special Reference to the Western United States, *in* Keays, R.R., Ramsay, W.R.H., and Groves, D.I., eds., The Geology of gold deposits; the perspective in 1988, Economic Geology Monographs: Lancaster, PA, Economic Geology Publishing Co., p. 405- 423.

Bethke, P.M., and Rye, R.O., 1979, Environment of ore deposition in the Creede mining district, San Jan Mountains, Colorado: Part IV. Source of fluids from oxygen, hydrogen, and carbon isotope studies: Economic Geology, v. 74, p. 1832-1851.

Burnett, W.J., 1995, Fluid Chemistry and Hydrothermal Alteration of the Cresson disseminated gold deposit, Colorado: Unpublished Colorado State University M.S. thesis, 168 p.

Campbell, A.R., and Larson, P.B., 1998, Introduction to Stable Isotope Applications in Hydrothermal Systems *in* Richards, J.P., and Larson, P.B., eds., Techniques in hydrothermal ore deposits geology, Reviews in Economic Geology, v. 10, p. 173-193.

Casedevall, T. and Ohmoto, H., 1977, Sunnyside mine, Eureka mining district, San Juan County, Colorado: Geochemistry of gold and base metal ore deposition in a volcanic environment: Economic Geology, v. 72, p. 1285-1320.

Chapin, C.E. and Cather, S.M., 1994, Tectonic Setting of the axial basins of the northern and central Rio Grande rift: Geological Society of America Special Paper 291, p. 5-25.

Collins, P.L.F., 1979, Gas hydrates in CO_2-bearing inclusions and use of freezing data for estimation of salinity: Economic Geology, v. 74, p. 1435-1444.

Criss, R.E. and Taylor, H.P. Jr., 1983, An $^{18}O/^{16}O$ and D/H study of Tertiary hydrothermal systems in the southern half of the Idaho batholith: Bulletin of the Geological Society of America, v. 94, p. 640-663.

Cross, W. and Penrose, R.A.F. Jr., 1895, Geology and mining industries of the Cripple Creek district, Colorado: U.S. Geological Survey 16th Annual Report, Part 2, p. 1-209.

Deines, P., 1992, Mantle Carbon: concentration, mode of occurrence, and isotopic composition, *in* Early Organic Evolution: Implications for Mineral and Energy Resources, Schidlowski, M., Golubic, S., Kimberley, M., McKirdy, D.M., and

Trudinger, P.A. (eds.): Heidelberg: Springer-Verlag, pp. 133-145.
Drummond, S.E., and Ohmoto, H., 1985, Chemical Evolution and Mineral Deposition in Boiling Hydrothermal Systems: Economic Geology, v. 80, p. 126-147.
Dwelley, P.C., 1984. Geology, Mineralogy and Fluid Inclusion Analysis of the Ajax Vein System, Cripple Creek Mining District, CO: Unpublished M.S. thesis, Colorado State University, 167 p.
Fears, D.W., Mutschler, F.E., and Larson, E.E., 1986, Cripple Creek Colorado- A Petrogenetic Model [abs.]: Geological Society of America Abstracts with Programs, v. 18, no. 6, p. 599.
Friedman, I. and O'Neil, J.R., 1977, Compilation of stable isotope fractionation factors of geochemical interest: U.S. Geological Survey Professional Paper 440-KK, p. KK1-KK12.
Giggenbach, W.F., and Stewart, M.K., 1982, Processes Controlling the Isotopic Composition of Steam and Water Discharges from Steam Vents and Steam-Heated Pools in Geothermal Areas: Geothermics, v. 11, no. 2, p. 71-80.
Guidotti, C.V., 1984, Micas in metamorphic rocks, in Bailey, S.W., ed., Micas: Reviews in Mineralogy, v. 13,p. 357-467.
Hedge, C.E., 1970, Whole-rock Rb-Sr age of the Pikes Peak batholith, Colorado: U.S. Geological Survey Professional Paper 700-B, p. B 86- B 89.
Hemley, J.J., and Hunt, J.P., 1992, Hydrothermal Ore-Forming Processes in the Light of Studies in Rock-Buffered Systems: II. Some General Geologic Applications: Economic Geology, v. 87, p. 23-43.
Hoefs, J., 1997, Stable Isotope Geochemistry, 4th ed: New York, Springer-Verlag, 201 p.
Jensen, E.P., 1998, Timing, Character and Significance of Late K-metasomatism and Gold Mineralization at Cripple Creek, Colorado [abs.]: Geological Society of America Abstracts with Programs, v. 30, no.7, p. 301.
--------, E.P., 2002, Written and personal communication of unpublished PhD. thesis data, University of Arizona.
Jensen, E.P., and Barton, M. D., 2000. Chapter 8: Gold Deposits Related to Alkaline Magmatism in SEG Reviews, v. 13, p. 279-314.
Karlstrom, K.E., and Humphreys, E.D., 1998, Persistent Influence of Proterozoic accretionary boundaries in the tectonic evolution of Southwestern North America: Interaction of cratonic grain and mantle modification events: Rocky Mountain Geology, v. 33, no. 2, p. 161-179.
Karlstrom, K.E., Harlan, S.S., Williams, M.L., McLelland, J., Geissman, J.W., and Ahall, K., 1999, Refining Rodinia: Geologic Evidence for the Australia-Western U.S. connection in the Proterozoic: GSA Today, v. 9, no. 10, p. 1-7.
Kelley, K.D., 1998, Geochemical and Geochronological Constraints on the Genesis of Au-Te Deposits at Cripple Creek, Colorado, USA [abs.]: Geological Society of America Abstracts with Programs, v. 30, no.7, p. 300-301.

Kelley, K.D., Romberger, S.B., Beaty, D.W., Pontius, J.A., Snee, L.W., Stein, H.J., and Thompson, T.B., 1998, Geochemical and Geochronological Constraints on the Genesis of Au-Te Deposits at Cripple Creek, Colorado: Economic Geology, 93, no. 7, p. 981-1012.

Kluth, C.F., and Coney, P.J., 1981, Plate Tectonics of the Ancestral Rocky Mountains: Geology, v. 9, p. 10-15.

Koschmann, A.H., 1949, Structural control of the gold deposits of the Cripple Creek District, Colorado: U.S. Geological Survey Bulletin 955-B, 60 p.

Kyser, T.K., 1987, Equilibrium fractionation factors for stable isotopes: Mineralogical Association of Canada Short Course, v. 13, p. 1-84.

Lane, C.A., 1976. Geology, Mineralogy and Fluid Inclusion geothermometry of the el Paso gold mine, Cripple Creek, CO: Unpublished M.S. thesis, University of Missouri-Rolla, 103 p.

Lindgren, W., and Ransome, F.L., 1906, Geology and gold deposits of the Cripple Creek district, Colorado: U.S. Geological Survey Professional Paper 54, 516 p.

Lochman-Balk, C., 1972, Cambrian system; in Mallory, W.W., ed. Geologic atlas of the Rocky Mountain region: Rocky Mountain Association of Geologists, Denver, Colorado, p. 60-75.

Loughlin, G.F. and Koschmann, A.H., 1935, Geology and ore deposits of the Cripple Creek district, Colorado: Colorado Scientific Society Proceedings, v. 13, no. 6, p. 217-435.

Lovering, T.S., and Goddard, E.N., 1950, Geology and ore deposits of the Front Range, Colorado: U.S. Geological Survey Professional Paper 223, 319 p.

McDonough, W.F., McCulloch, M.T., and Sun, S.S., 1985, Isotopic and geochemical systematics in Tertiary-Recent basalts from southeastern Australia and implications for the evolution of the sub-continental lithosphere: Geochimica et Cosmochimica Acta, v. 49, p. 2051-2067.

McDowell, F.W., 1971, K-Ar ages of igneous rocks from the western United States: Isochron West, no. 2, 16 p.

Moore, J.N., and Norman, D.I., 1999, The Thermal and Chemical Evolution of the Hydrothermal Minerals in Awibengkok 1-2, Awibengok Geothermal Field, Indonesia: Geothermal Resources Council Transactions, v. 23, p. 25-29.

Mote, A.S., 2000, Fluid Inclusion Study of Veins within Granite Island, Cripple Creek Mining District, Cripple Creek, Colorado: unpublished B.S. thesis, University of Georgia, 17 p.

Moyle, A.L., Doyle, B.J., Hoogvliet, H., and Ware, A.R., 1990, Ladolam gold deposit, Lihir Island: Australasian Institute of Mining and Metallurgy Monongraph Series, v. 14, p. 1793-1805.

Nelson, S.E., 1989, Geology, alteration and mineral deposits of the Cresson diatreme, Cripple Creek district, Colorado: unpublished M.S. thesis, Colorado State University,

Fort Collins, 147 p.
Ohmoto, H., and Goldhaber, M.B., 1997, Chapter 11: Sulfur and Carbon Isotopes in Barnes, H.L., ed., Geochemistry of hydrothermal ore deposits, 3rd ed.: New York, John Wiley and Sons, Inc., p. 517-612.
Ohmoto, H., and Rye, R.O., 1979, Isotopes of Sulfur and Carbon, *in* Barnes, H., ed., Geochemistry of hydrothermal ore deposits, 2nd ed.: New York, Rinehart and Winston, p. 509-567.
O'Neil, J.R. and Silberman, M.L., 1974, Stable isotope relations in epithermal Au-Ag deposits: Economic Geology, v. 69, p. 902-909.
O'Neil, J.R., Silberman, M.L., Fabbi, B.P., and Chesterman, C.W., 1973, Stable isotope and chemical relations during mineralization in the Bodie Mining district, Mono County, California: Economic Geology, v. 68, p. 765-784.
O'Neil, J.R. and Taylor, H.P., 1967, The oxygen isotope and cation exchange chemistry of feldspars: American Mineralogist, v. 52, p. 1414-1437.
Pontius, J.A., 1992, Gold mineralization within the Cripple Creek diatreme/volcanic complex, Cripple Creek mining district, Colorado, USA: Minexpo 92, Las Vegas, Nevada, October 18-22, Proceedings, 12 p.
Pontius, J.A., 1996, Gold Deposits of the Cripple Creek mining district, Colorado, USA: Society of Economic Geologists Guidebook Series, v. 26, p. 29-37.
Potter, II, R.W., 1977, Pressure corrections for fluid inclusion homogenization temperatures based on the volumetric properties of the system Nacl-H_2O: U.S. Geological Survey Journal of Research, v. 5, p. 603-607.
Powell, J.W., 1876, Exploration of the Colorado River of the West: Smithsonian Institution, 291 p.
Rampe, J.S., 2002, Paleomagnetic and Geochronologic Data Bearing on the Timing, Evolution, and Structure of the Cripple Creek Diatreme Complex and Related Rocks, Front Range, Colorado: unpublished M.S. Thesis, University of New Mexico, 81 p.
Reed, J.C., Bickford, M.E., Premo, W.R., Aleinikoff, J.N., and Pallister, J.S., 1987, Evolution of the Early Proterozoic Colorado Province: Constraints from U-Pb geochronology: Geology, v. 15, p. 861-865.
Reynolds, T.J., 1992, Fluid Inclusion Study of Selected Mineralized Samples from the Cripple Creek District, Colorado: Unpublished report, 6.p.
Richards, J. P. and Kerrich, R., 1993, The Porgera gold mine, Papua New Guinea: Magmatic hydrothermal to epithermal evolution of an alkalic-type precious metal deposit: Economic Geology, v. 88, p. 1017-1052.
Richards, J.P., 1995, Alkalic-type epithermal gold deposits, a review: Mineralogical Association of Canada Short Course Series, v. 23, p. 367-400.
Roedder, E., 1984, Fluid Inclusions *in* Reviews in Mineralogy, v. 12: Washington D.C., Mineralogical Society of America, 644p.
Romberger, S. B., 1991, Geochemistry of gold in hydrothermal deposits: U.S.

Geological Survey Bulletin 1857A, p. A9-A22.
Rosdeutscher, J.A., 1999, Geology and Stable Isotope Geochemistry of the Grassy Valley Au deposit, Cripple Creek Mining District, Colorado; evidence for magmatic fluids: unpublished M.S. Thesis, University of Georgia, 70 p.
Rosdeutscher, J.A., 1998, Characterization of Distal Gold Mineralization and Alteration in the Cripple Creek District, Colorado [abs.]: Geological Society of America Abstracts with Programs, v. 30, no.7, p. 301.
Rosdeutscher, J.A., Crowe, D.E., and Harris, T.D., 1998, Characterization of distal gold mineralization and alteration in the Cripple Creek District, Colorado [abs]: Geological Society of America Abstracts with Programs, v. 30, no.7, p. 301.
Sanders, R.E. and Hawkins, D.P., 1999, U-Pb Geochronology of porphyritic clasts from the Pennsylvanian Fountain Formation, Colorado Front Range: Volcanic Equivalents of the Pikes Peak Batholith [abs]: Geological Society of America Abstracts with Programs, v. 31 , no. 7 , p. A-178 .
Saunders, J.A., 1986, Petrology, mineralogy and geochemistry of representative gold telluride ores from Colorado: unpublished Colorado School of Mines PhD dissertation, 171 p.
Saunders, J.A., and May, E.R., 1986, Bessie G, a high-grade epithermal gold telluride deposit, La Plata, County, Colorado, U.S.A., *in* Macdonald, J.A., Geology of Gold Deposits: Gold '86, Toronto, Proceedings, p. 436-444.
Seibel, G.E., 1991, Geology of the Victor mine, Cripple Creek mining district, Colorado: unpublished Colorado State University M.S. thesis, 133 p.
--------, 1996, Geologic summary of the Globe Hill-Ironclad gold deposits, Cripple Creek district, Colorado: Society of Economic Geologists Guidebook Series, v. 26, p. 39-44.
Selverstone, J., Hodgins, M., Shaw, C., Aleinikoff, J.N., and Fanning, C.M., 1997, Proterozoic Tectonics of the Northern Colorado Front Range: Rocky Mountain Association of Geologists, Colorado Front Range Guidebook, p. 9-18.
Seward, T.M., 1973, Thio complexes of gold and the transport of gold in hydrothermal ore solutions: Geochimica et Cosmochimica Acta, v. 37, p. 379-399.
Seward, T.M., 1989, Advances in the Understanding of Epithermal Gold-Silver Deposits, with Special Reference to the Western United States, *in* Keays, R.R., Ramsay, W.R.H., and Groves, D.I., eds., The Geology of gold deposits; the perspective in 1988, Economic Geology Monographs: Lancaster, PA, Economic Geology Publishing Co., p. 389-404.
Silberman, M.L., 1992, Verbal and written update of oxygen isotope work on the Pharmacist vein system, Cripple Creek, CO, reference in Pontius, 1996.
Simmons, S.F. and Christenson, B.W., 1994, Origins of Calcite in a Boiling Geothermal System: American Journal of Science, v. 294, p. 361-400.
Taylor, H.P. Jr., 1979, Oxygen and hydrogen isotope relationships in hydrothermal mineral deposits, *in* Barnes, H.L., ed., Geochemistry of hydrothermal ore deposits, 2nd

ed.: New York, John Wiley and Sons, p. 236-277.
--------, H.P. Jr., 1974, The application of oxygen and hydrogen isotope studies to problems in hydrothermal alteration and ore deposition: Economic Geology, v. 69, p. 843-883.
--------, H.P. Jr., 1973, O^{18}/O^{16} evidence for meteoric-hydrothermal alteration and ore deposition in the Tonopah, Comstock Lode, and Goldfield mining districts, Nevada: Economic Geology, v. 68, p. 747-764.
Taylor, H.P. Jr., and Sheppard, M.F., 1986, Igneous Rocks: I. Processes of Isotopic fractionation and Isotope Systematics: Reviews in Mineralogy, v. 16, p. 227-271.
Thompson, T.B., 1998, Cripple Creek- a world-class gold bearing, diatreme-alkalic intrusive complex, Colorado, USA [abs]: Geological Society of America Abstracts with Programs, v. 30, no.7, p. 301.
-------, 1996, Fluid Evolution of the Cripple Creek hydrothermal system, Colorado: Society of Economic Geologists Guidebook Series, v. 26, p. 45-54.
Thompson, T.B., Trippel, A.D., and Dwelley, P.C., 1985. Mineralized Veins and Breccias of the Cripple Creek District, Colorado: Economic Geology, v. 80, p. 1669-1688.
Timmons, J.M., Karlstrom, K.E., Dehler, C.M., Geissman, J.W., and Heizler, M.T., 2001, Proterozoic multistage (ca. 1.1 and 0.8 Ga) extension recorded in the Grand Canyon Supergroup and establishment of northwest- and north-trending tectonic grains in the southwestern United States: Geological Society of America Bulletin, v. 113, no. 2, p. 163-180.
Trippel, A.D., 1985, Hydrothermal Mineralization and Alteration at the Globe Hill Deposit, Cripple Creek District, CO: Unpublished MS thesis, Colorado State University, 93 p.
Tweto, O. and Sims, R.K., 1963, Precambrian ancestry of the Colorado Mineral belt: Geological Society of America Bulletin, v. 74, p. 991-1014.
Unruh, D.M., Unpublished data, reference in Sanders, R.E., 1999, Age of the Keeton porphyry and clast lithologies within the Pennsylvanian Fountain Formation: Implications for the composition of the upper Pikes Peak batholith, Front Range, Colorado: Unpublished BA Thesis, The Colorado College, 105 p.
Venneman, R.W. and O'Neil, J.R., 1996, Hydrogen isotope exchange reactions between hydrous minerals and molecular hydrogen: I. A new approach for the determination of hydrogen isotope fractionation at moderate temperatures: Geochimica et Cosmochimica Acta, v. 60, p. 2437-2451.
Wobus, R.A., Epic, R.C., and Scott, G.R., 1976, Reconnaissance geologic map of the Cripple Creek-Pikes Peak area, Teller, Fremont and El Paso Counties, Colorado: U.S. Geological Survey Miscellaneous Field Studies Map, MF-805.
Wones, D.R. and Eugster, H.P., 1965, Stability of biotite: Experiment, theory, and application: The American Mineralogist, v. 50, p. 1228-1256.

Ye, H., Royden, L., Burchfiel, C., an Schuepbach, M., 1996, Late Paleozoic deformation of interior North America: The greater Ancestral Rocky Mountains: American Association of Petroleum Geologists Bulletin, v. 80, p. 1397-1432.